

AFCRE - 65 - 203

61(052)-490

December 1964

AD 613 593
copy 2 of 3
108pgs

FOURTH TECHNICAL ANNUAL SUMMARY REPORT

ON THE PROPAGATION OF VLF WAVES IN SOLIDS

Dr. W. Bitterlich
Innsbruck, Austria

The research reported in this document has been sponsored by
the United States Government.

Preface and contents

The three main directions of the research work conducted by the VLF team at Innsbruck during the past four years include:

1. Investigation of VLF propagation through solid media, preferably rock, and construction of the necessary measuring apparatus.
2. Measurement of the electrical conductivity σ and the dielectric constant ϵ of various rock, preferably in natural state.
3. Theoretical studies on problems of excitation and propagation of VLF waves in solid media.

In the present report, the research results of 1964 are described. For a better survey and especially for better orientation of laymen in the field of VLF propagation, a brief review shall follow.

On the first main direction (chapters 1 and 2):

In chapter 1 (Apparatus) a small, easily portable field strength meter for frequencies ranging from 1.9 to 25 kc/sec is described. The nuvistorized apparatus has a high sensitivity and a large signal-to-noise ratio. A wire-wound ferrite rod, approximately 1 m long is used as an antenna.

The studies on optimum receiving antennas for VLF signals have been terminated. The dimensioning of magnetic dipole antennas with ferrite cores is discussed in detail.

In the mine of St. Gertraudi, a new transmitting antenna with an antenna area of 1600 m² and a wire cross section of 135 mm² was set up in the immediate neighborhood of the VLF laboratory there. The distances reached with this new antenna are much larger than those reached with former antennas.

For studying the exact direction of the electromagnetic field of a VLF transmitter, a direction-finder antenna was constructed that can be freely rotated in space and fixed

in any desirable position. The results of measurement are discussed in chapter 1.

For exact angular measurements in other mines when using the portable transmitter, a small transmitting antenna was designed. Any angular adjustment becomes possible with this antenna, up to an accuracy of $\pm 2^\circ$. It is mainly used for determining the directional patterns and field directions in the neighborhood of geological interference zones.

In chapter 2, the propagation measurements in homogeneous and in inhomogeneous rock of St. Gertraudi and Bleiberg, respectively, are dealt with. A 50 W transmitter was used for measuring the propagation and the directional pattern. The attenuation values thus obtained cannot be compared with the attenuation of a remote VLF transmitter (GBR). It is shown that the great differences in attenuation are assumed to be due to the fact that one measurement was conducted in the near field, whereas the other one was made in the far field. The difference in the type of propagation and attenuation observed in the above two cases can also be derived theoretically.

The problem of near field and far field is discussed in another section giving a number of diagrams of the field strength trend as dependent on the quantities r , ρ , ω and ϵ .

Measurements in inhomogeneous media made it necessary to determine the value of the field strength at the point of reception as well as the direction of the field vector. If the rock contains inhomogeneities, the latter may be determined much more easily and accurately by measuring the field direction than by measuring only the field strength value.

On the second main direction. (chapter 3):

Measurements with direct current and with alternating current were conducted the latter in samples as well as in solid rock.

By means of measurements following the Wenner method it was empirically shown from what electrode distance onward the

III

effect of the gallery space on the result of measurement may be neglected. It can also be seen that the Wenner method is a four-electrode configuration well suited for measurements in mine galleries (section 3.1).

The sample measurements yielding a strong frequency dependence of ϵ and σ were evaluated by K.W. Wagner's dispersion theory, assuming a continuous distribution of relaxation times. The graphic method by W.A. Yager was used for the evaluation, although neither the results obtained for completely dry nor those obtained for completely damp samples can be evaluated by means of the curves calculated in his studies. The evaluable results, however, show a good agreement between experiment and theory. The dependence of the humidity constants contained in the theory was studied (section 3.2).

Furthermore the propagation resistance of electrodes in solid rock as dependent on the frequency was measured. The σ values calculated therefrom, however, could not be made consistent with the results obtained for the samples (section 3.3).

On the third main direction (chapter 4):

The theoretical part of the present annual report is mainly dedicated to one region essential for the excitation of VLF waves: Dipole radiation in a homogeneous and conducting medium. So far, dipole radiation in air or in vacuo as an elementary process of every antenna phenomenon has been treated adequately in many publications, and has been investigated in great detail. Furthermore it has been pointed out that the mathematical representation that describes the physical process when passing from vacuum to a conducting medium must be interpreted with great care, and that for certain physical standard concepts, the definitions used for processes in vacuo have to be modified for describing the processes in a conducting medium. So far, the relation between the two types of dipoles, electric and magnetic, has not been studied sufficiently as regards their energy balance. Therefore, a distinct comparison between the electric and the magnetic dipoles for VLF waves in

conducting media has been described in section (4.2).

Besides the above problems, it was our task to develop the theory of conductivity measurements by means of the potential distribution of steady currents and thus give an estimation to what an extent the experiments conducted in mine galleries below ground can be described by the usual expressions that hold for homogeneous full spaces or semispaces.

1. Apparatus

1.1 Navistorized field strength meter E4 for the VLF range

Introduction

A number of field strength meters were designed within the framework of the VLF research program, and experiments with various antenna designs were conducted (see annual reports). Owing to the range of application - measurements in mines - the common characteristics of the designs were small dimensions of the measuring device as well as the antenna, and operation independent of the mains supply.

When developing the field strength meter E4, new means of increasing the sensitivity and signal-to-noise ratio were found.

Design characteristics of the field strength meter E4

The antenna of a field strength meter for very low frequencies will in any case be small (its electric length as well as its geometrical dimensions) as compared to the wave length λ . In the measuring range of the described device, λ is about 10 to 300 km in air. Coupling of a "short" antenna to the transmitter field will be correspondingly loose. The coupling factor will be increased on the one hand by increasing the area of a frame antenna, and on the other hand by using highly permeable ferrite cores by means of which the lines of force in the antenna coil can be concentrated. The use of large frame coils as antennas had to be abandoned after several experiments, as the attainable Q values were far too low. In order to reach an induced voltage U as high as possible when using inductive antennas with ferrite cores at a given field strength E, the effective height h_{eff} which is very small for this antenna type, has to be increased (see the relation $U = h_{\text{eff}} \cdot E$). It must therefore be the aim of the investigation and development to obtain a low-loss antenna circuit which has to be coupled to an amplifier with high input impedance, as the circuit damping caused by losses is to be kept small as compared to the radiation damping caused by the radiation resistance of the antenna.

resistance. The first amplifier stage is a cascode with negative feedback. The equivalent noise resistance

$$R_e = 0.64 \cdot \frac{T_K}{T} \cdot \frac{1}{5 \cdot S} \sim 2.5/S \sim 400 \Omega$$

is determined only by the nuvistor triode whose cathode is grounded. It is negligibly small as compared to the resonant resistance R_0 which determines the noise voltage across the input: $u_Y = \sqrt{4KT\Delta f \cdot R_0}$. The cascode stage and the tuning capacitors were directly attached to the antenna rod in order to reduce screening as far as possible and avoid additional circuit damping. A multiple cable connects this antenna amplifier with the second part of the measuring device, which comprises a selective amplifier, an indicator, and current supply.

The second selective circuit was no longer built with RC networks, but with LC series resonant circuits. High Q values of the circuit can be reached by connecting these circuits between two cathode followers. The utilizable resonance rise of the signal voltage makes another amplifier stage superfluous.

Description of the circuit diagram (Fig. 1,1)

We have already mentioned that the field strength meter E4 consists of two parts:

I. The antenna part (left of the dashed line in the circuit diagram).

The ferrite rod antenna A has a number of cross coil windings which can be interconnected by means of the switch S_1 yielding the following values of inductance: in position 1 ... 2.19 H
2 ... 600 mH
3 ... 352 mH

Resonant frequencies ranging from 1.9 to 25 kc/sec can be adjusted by means of switch S_2 , the nonvariable capacitors C_1 , C_2 , C_3 and the variable capacitors C_4 , C_5 , C_6 . Range overlapping is considerably high owing to the high L-C ratio. The socket Bu_1 is used for feeding a calibration voltage, and for further experiments.

The alternating voltage induced in the antenna circuit reaches the input of a cascode amplifier that consists of the nuvistors R_{ö. 1} and R_{ö.2}. In order to reach a maximum resonance rise of the antenna circuit,

the latter is to be damped but slightly by the tube input. Measurements yielded an optimum grid bias of 1.35 V which corresponds to a maximum tube input resistance. The grid bias is produced as voltage drop at the resistors R_2 and R_4 by the common anode current. The resistor R_5 causes negative feedback. The anode circuit of the cascode is coupled with a cathode follower (Rö.3) acting as an impedance transformer via the high pass $C_{10} - R_7$ to attenuate interfering technical frequencies.

The antenna unit is pivoted on a stand and connected with the

II. measuring part

via a screened multiwire cable K. In order to keep the band width of the measuring device small, the signal is fed to another selective circuit which is constructed as a series resonant circuit. A range switch consisting of 4 switch segments serves for switching over on the one hand the inductances L_1 through L_4 , and on the other hand the capacitors C_{15} through C_{19} . In one position, the selective circuit is switched off whereby the band width of the unit is increased. The cathode follower (Rö.4) connected after the selective circuit provides low circuit damping as well as low output impedance. The adjusting potentiometer is used for amplification calibration, the socket Bu_2 serves as output (connection of an oscilloscope etc.). Amplification may be attenuated in stages (3 : 1) by means of a calibrated voltage divider and the switch S_4 . The second amplifier of the measuring device is the nuvistor stage Rö.5. The amplified output signal is fed to a voltage multiplier stage (diodes $D_1 - D_4$). A direct voltage drop proportional to the signal voltage occurs across the resistor R_{26} . This direct voltage controls the anode current and thus also the length of the luminescent band of the tuning-indicator tube Rö.6. This tube has a double task: it makes the identification of keyed transmitters and strong interferences much easier, and the instrument J calibrated in millivolt input voltage lies in its anode circuit. The nonlinear division of the scale of this instrument which facilitates the reading of small voltages, and which corresponds to the characteristics of the tube, is highly advantageous. If there is no input signal, the instrument pointer is on the right-hand side of the scale, corresponding to the maximum tube current, i.e. at the zero point or the beginning of the mv scale

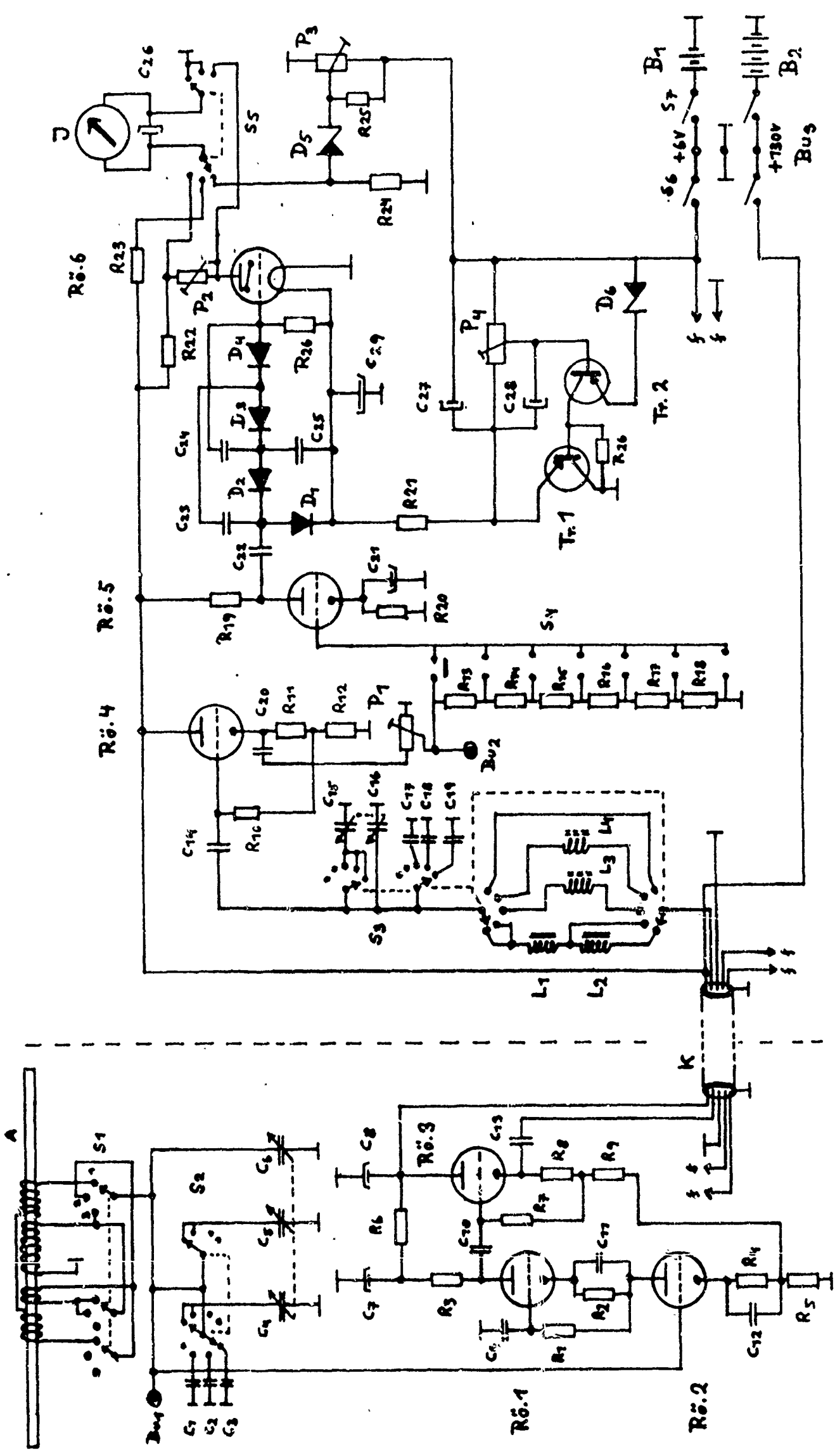


Fig. 11

(adjustment by the trimming potentiometer P_2 with the switch S_4 being in its lowest position). Overdriving of the instrument by extremely strong signals is impossible, since the instrument current will then become zero. Furthermore it is possible to use the instrument for measuring the filament voltage and the anode voltage by means of the switch S_5 . The filament voltage is indicated on an expanded scale, i.e. the zero point of the instrument is shifted to 4 v by means of the Zener diode D_5 . Thus, a slight drop in filament voltage can be read much more easily; this is of special importance for accurate field strength measurements. Another improvement of the stability is that the filament voltage of the indicator tube is kept constant by means of a stabilization circuit (transistors Tr. 1 and Tr. 2, Zener diode D_6).

A lead storage cell serves as a current source for filament voltages, and an NC battery for the anode voltages. The switches S_6 and S_7 are used as operating switches for measuring and charging. An easily portable case with the dimensions 230 x 130 x 140 mm and a weight of 5.2 kg contains the selective amplifier, indicator and current source including the battery. The small dimensions of the device also make possible measurements in difficult terrain.

Measured values

The resonance curve of the antenna unit - antenna circuit + nuvistor cascode + cathode follower, without the selective amplifier, is shown in Fig. 1,2. The solid curve holds for a resonant frequency f_0 of 10 kc/sec, the dashed line holds for 3 kc/sec. The measuring arrangement for taking the curves is shown in the block diagram. The measuring frequency f_x is produced by an RC generator and measured with a digital frequency meter. A frame coil, 30 cm in diameter, was used as transmitting antenna. The antenna stage of the field strength meter was set up at a distance of 6 meters, a precise tube voltmeter being connected to it.

Measured band width at 3 dB voltage drop:

$$b = \Delta f = d \cdot f_0 \dots \text{at } 3 \text{ kc/sec} : 10 \text{ cps} \\ \text{at } 10 \text{ kc/sec} : 75 \text{ cps}$$

This corresponds to a value $Q = 1/d = 300$ at 3 kc/sec
 = 133 at 10 kc/sec

The band width and resonance curve of the field strength meter with a selective amplifier at 10 kc/sec corresponds approximately to the 3 kc/sec curve of Fig. 1,2.

Selective amplification $V = U_0/U_e$ at 10 kc/sec : 1420-fold
 at 3 kc/sec : 1580-fold

(U_e connected to Bu_1 , U_0 is measured at Bu_2 , see Fig.1)

Smallest measurable signal voltage U_e (at Bu_1) : 5 μv (accuracy of instrument reading)

Maximum measurable signal voltage with connected selective
 amplifier : .9 mv
 without selective amplifier : 150 mv.

The background noise of the field strength meter with antenna could not be measured as there is no suitable Faraday screen for low frequencies available. A measurement in the Schwaz mine was conducted to get an idea of the height of the noise level. The site of measurement below ground was 2.2 horizontal km away from the gallery entrance. The maximum depth was 1000 m. The noise signal occurring at the output Bu_2 was measured by an oscilloscope. This noise is composed of the background noise, the local noise level, and atmospherics. Measured with the selective amplifier it was as follows:

at 10 kc/sec on average 12 μv background noise,
 atmospherics $\geq 120 \mu v_{eff}$ (peaks)
 at 3 kc/sec on average 10.8 μv background noise,
 atmospherics $\leq 20 \mu v_{eff}$ (peaks)

When the antenna was short-circuited - grid of the first cascade grounded - the voltage was 0.2 μv_{eff} (at Bu_2). The antenna was calibrated by the method described in the 1962 Annual Report. The following relation was found:

1 mv induced voltage (U_e) corresponds to $B = 1.75 \cdot 10^{-12}$ (Weber/m²). Thus, the smallest field strength measurable with the built-in instrument is $B_{min} = 8.75 \cdot 10^{-15}$ (Weber/m²). At 3 kc/sec a field strength of $E = 2 \cdot 10^{-17}$ (Weber/m²) can be measured with a microvoltmeter on the basis of the measured background noise. This is possible only if the noise level of atmospherics is very low as it is the case in the mine at great depths.

Fig. I shows the field strength meter.

Literature [1,2,3] .

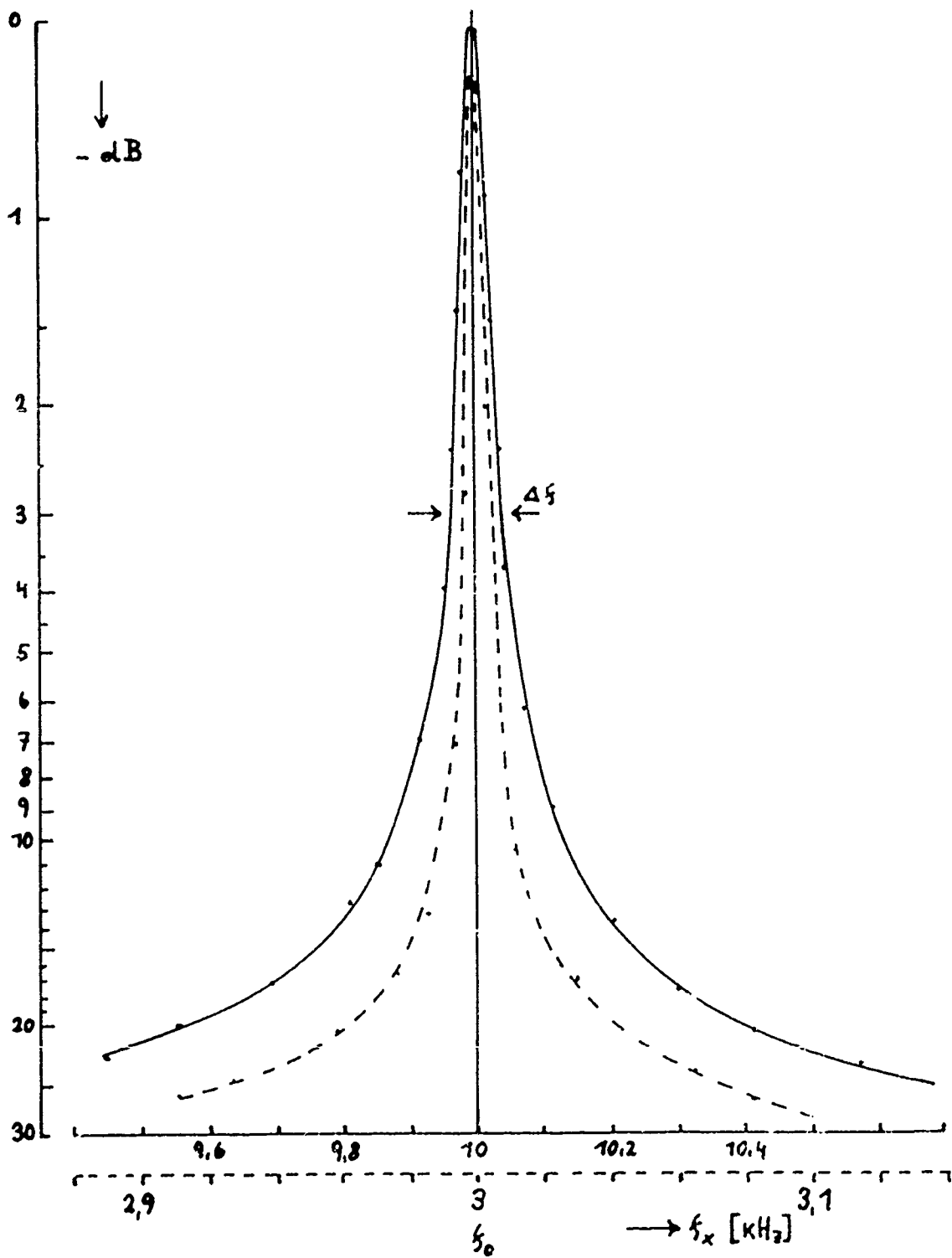
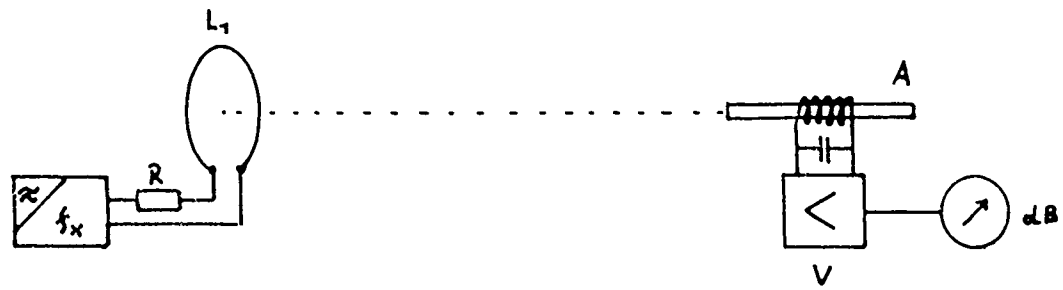


Fig. 12

1,2 Magnetic dipole antennas for receivers

Introduction:

If VLF signals are to be received in solid or liquid media, the space available for antennas is usually very limited. In the present paper the problem is to be studied what antenna type is suited best for recording electromagnetic waves of very low frequency ($f \leq 15$ kc/sec) in solid media, i.e. below ground. Another limiting condition for the antenna size is the fact that the whole receiver shall be easily portable.

1. Comparison of antennas

The above-mentioned conditions show that the electrical and geometrical length of an antenna in any case will be very small as compared to the wavelength λ of the signal. The smaller the antenna, however, the smaller its effective height and its radiation resistance, i.e. the more loosely it will be coupled with the electromagnetic field [1]. The problems lie in the fact that the damping R_v by the losses of the total antenna circuit is to be kept low as compared to radiative damping caused by the radiation resistance R_s , this means that an antenna type has to be found whose efficiency is as high as possible.

Theoretically, an electric dipole antenna of small dimensions ought to be sufficient also for the VLF region as long as it is tunable. A materializable vertical electric dipole having an effective height of 2 m for $f = 10$ kc/sec has a radiation resistance of $R_e \sim 10^{-6} \Omega$. The induced voltage at an assumed field strength of $E_{\text{eff}} = 50$ mv/m is 100 mv. The antenna impedance of a small electric dipole given mainly by its capacitive resistance, is extremely high and resonant tuning is possible only at large inductance. The useful amplifier input voltage will only be a fraction of the voltage induced in the antenna. By means of a corresponding frame antenna, an optimum adaptation and resonant tuning are easy to reach, radiation resistance and the effective antenna height, however, are very small. Electric dipoles for VLF signals are effective only in the form of long wire antennas.

2. Magnetic dipole ferrite antenna

The introduction of a magnetic material (ferrite) makes possible to concentrate the flux through a frame in a rod of much smaller dimensions.

Thus,

$$\text{eff. height} \quad h_{\text{eff}} = \frac{2\pi n F \mu_{\text{eff}}}{\lambda} \quad (1,3)$$

the radiation resistance

$$R_s = \frac{320\pi^4 n^2 F^2 \mu_{\text{eff}}^2}{\lambda^4} \quad (1,4)$$

The voltage induced in the antenna:

$$U_{\text{ind}} = 2\pi f n F B \mu_{\text{eff}} \left[v, \text{ cps, m}^2, \frac{\text{Wb}}{\text{m}^2} \right] \quad (1,5)$$

When tuning to resonance we obtain

$$U_o = U_{\text{ind}} \cdot Q = 2\pi f n F B \mu_{\text{eff}} Q \quad (1,6)$$

Dimensioning (Fig. 1,3)

The value of μ_{eff} in Eq. (1,3) depends on μ_{tor} and on the ratio A/d in Fig. 1,3 and should be as large as possible. The number of turns n is given by the inductance L necessary at a given frequency f . Fig. 1,4 shows the dependence of the inductance of a short coil ($n = 300$) on the one hand on its position on the rod and on the other hand on the rod length. Rod length $A = 32.5$ cm, curve 2; $A = 65$ cm, curve 4; $A = 97.5$ cm, curve 6.

Detailed studies of [4] have shown that it is favorable to distribute the necessary turns over a winding width of $A/2$ in the rod center. Eq. (1,6) for the voltage on the ferrite antenna is then to be multiplied with the reduction factor k , since the winding concentrates no longer at the rod center, having the permeability μ_{eff} .
 $k = 1$ for a short coil in the rod center
 $k = 0.7$ for a long coil over the whole rod.

The final form of the equation for the voltage on a tuned ferrite antenna then reads:

$$U_o = 2\pi f n F B \mu_{\text{eff}} Q k \quad (1,7)$$

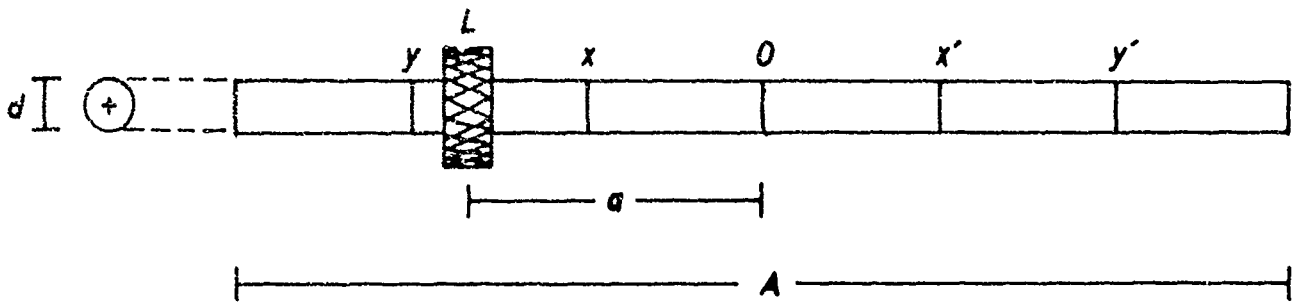


FIG. 1,3

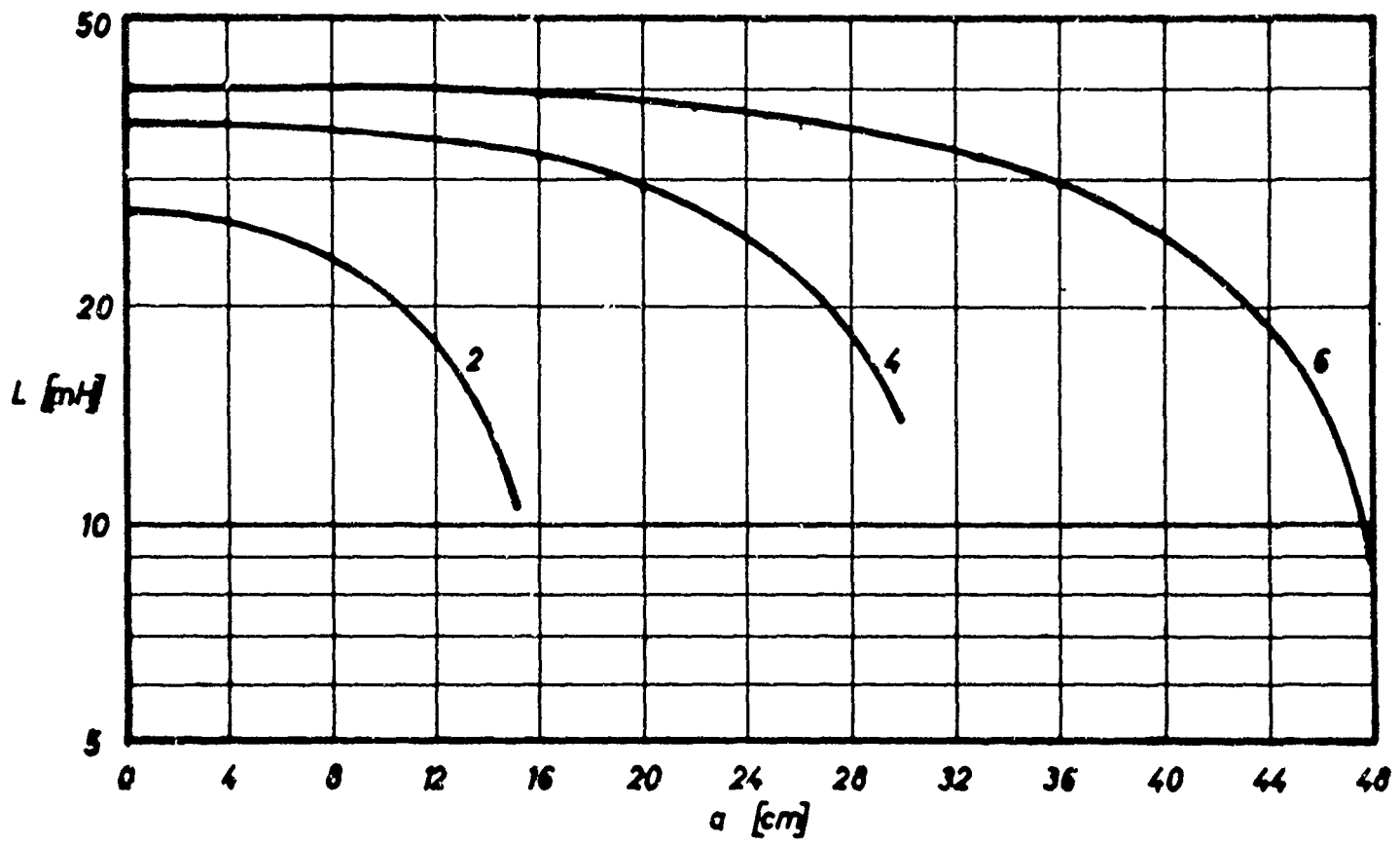
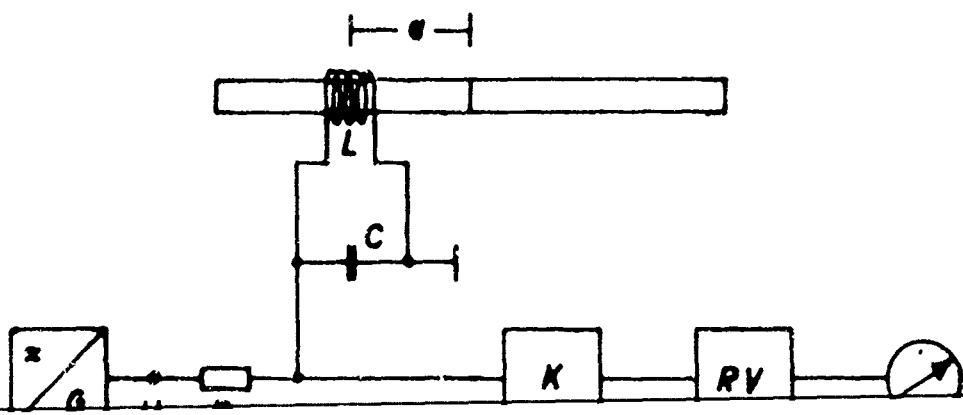


FIG. 1,4



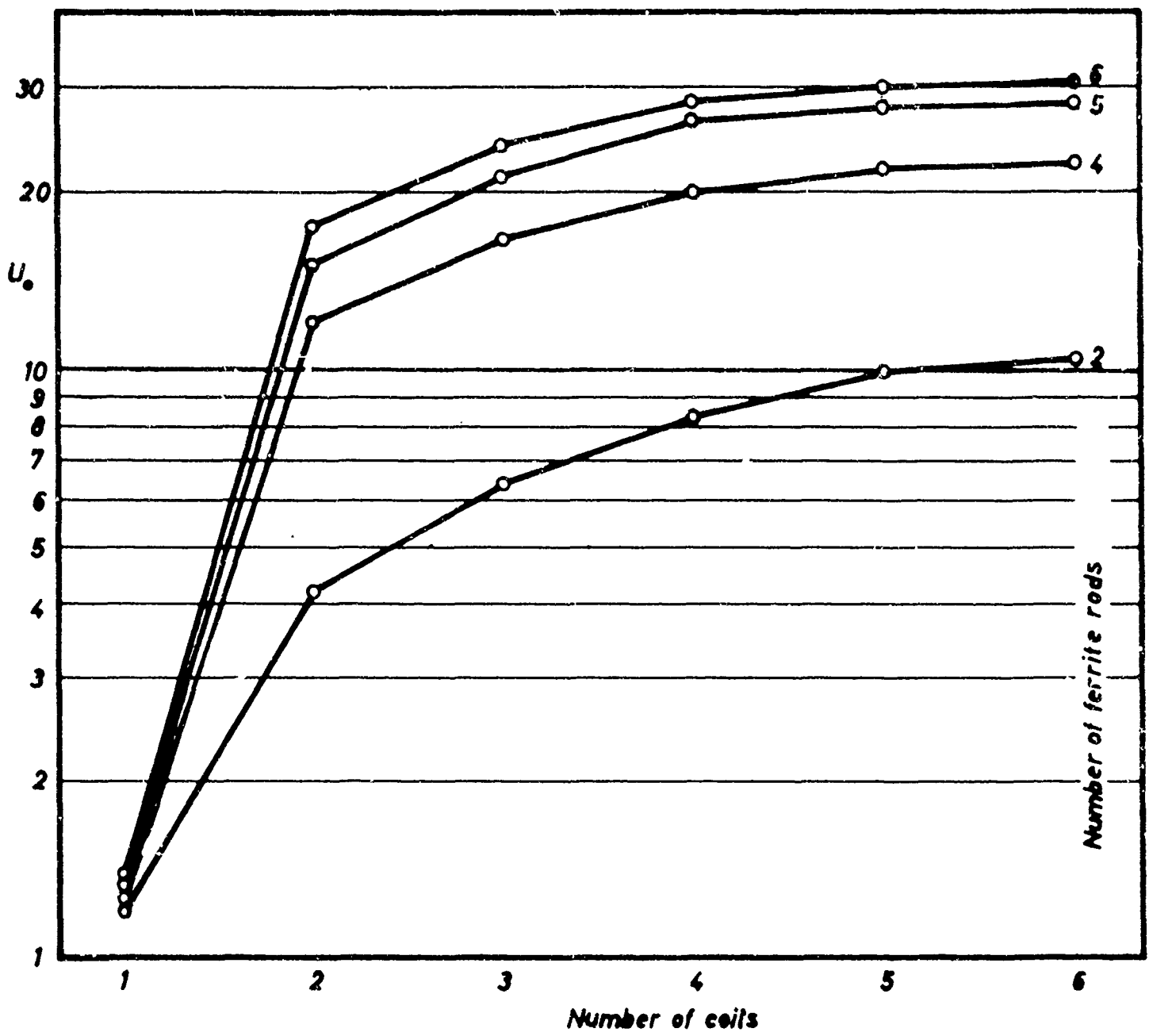
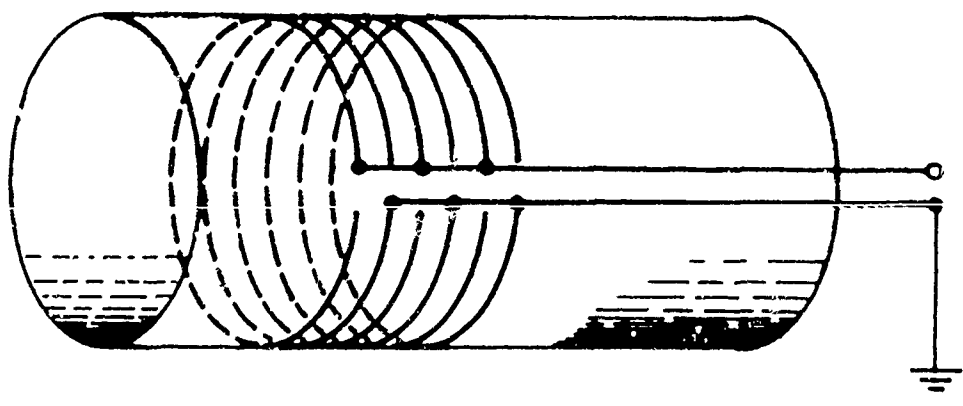


FIG. 1,5



b) Design of an optimum ferrite antenna

The core material 1100 N22 of the Siemens + Halske Co. was chosen for the reception of VLF signals in the frequency region below 20 kc/sec. Its data are the following:

$$\begin{aligned}\mu_{\text{tor}} &= 1300 \\ f_{\text{min}} &= 1 \text{ kc/sec} \\ f_{\text{max}} &= 20 \text{ kc/sec}\end{aligned}$$

The material originally intended to be used for pot cores was pressed into tube cores for antenna experiments. They have the following dimensions:

Length: A = 16 cm, outer diameter d = 19 mm
 inner " 9 mm .

Optimum rod length:

Fig. 1,4 shows that an increase in rod length to more than 98 cm at a given diameter would not be of any use. The optimum number of turns, coil shape and coil position on the core were determined by experiment. Fig. 1,5 shows the dependence of the resonant voltage U_0 on the number of individual rods (= total length) - curves 2,4,5,6 - and on the number of coils (each having $n = 300$) arranged around the rod center. An increase in rod length to more than 6 individual rods and an increase of the number of turns to more than 6 coils ($n = 1800$) does not increase the resonant voltage U_0 considerably.

The quality factor Q in Eq. (1,7) depends on the one hand on the losses in the oscillating circuit and on the other hand on the iron losses of the rod. The measurements of Q as a function of the coil position on the ferrite rod reported in various publications have proved to be incorrect at least as far as the VLF region is concerned. The reasons may be that these measurements were conducted at much higher frequencies, $f > 500 \text{ kc/sec}$, where Q is determined almost exclusively by the iron losses. The measuring device for studying the band width and the quality factor Q is shown in Fig. 1,6. The RC generator G adjustable in decades is loosely connected with the resonant circuit LC via a high-ohmic resistance R . The resonance voltage is applied to the tube voltmeter RV via a cathode follower and indicated as U_0 . Two series of measurements were made:

1. Band width $b = 2\Delta f$ as a function of the coil position on the core, number of turns = const, $f = \text{const}$.
As L decreases towards the end of the rod, the LC ratio also decreases at a constant number of turns. Result: curve b_1 of Fig. 1,7.
2. Band width $b = f(a)$. At a constant resonant frequency f , the LC ratio was also kept constant by increasing the number of turns towards the end of the rod. Result: curve b_2 of Fig. 1,7.

Measurement of b_1 : At a given frequency of 10 kc/sec, C was tuned to resonance and the generator voltage U_e was changed so far that $U_o = 100$ mv. Then f_o was changed by f until U_o was 70 mv. The indicated value Δf is $b/2$. The voltage U_e necessary for a constant U_o as a function of the coil position (curve b_1) is plotted on the right hand side of Fig. 1,7. The result shows that the band width and Q are constant over $2/3$ of the rod length. b increases only towards the end of the rod. A comparison between b_1 and b_2 in this region clearly shows the effect of the decreasing L/C ratio. Maximum Q at approximately $2/3$ of the rod length (as reported by a number of authors for higher frequencies) could not be found. An increase in Q at the expense of a decrease in resonance voltage was not observed either. A maximum number of turns distributed over $\approx \lambda/3$ left and right of the rod center will always favor optimum dimensioning at a given frequency of $\omega = \frac{1}{\sqrt{LC}}$. The coils may be shifted towards the rod ends only in case the desired band width is to be larger. Resistive damping of the antenna circuit, however, is more adequate.

3. Design of a VLF ferrite antenna for the frequency range of 1 - 20 kc/sec

In view of the test measurements, a rod (98 cm long) consisting of 6 tube cores ($d = 19$ mm) was chosen. The front planes of the individual sections were ground and the sections were pressed together (without adhesive) by an axial plexiglass rod with tightening screws. The joints between the cores (y, x, x', y' in Figs. 1,3 and 1,7) do not affect the rod quality.

The minimum cut-off frequency is to be 1 kc/sec, therefore a

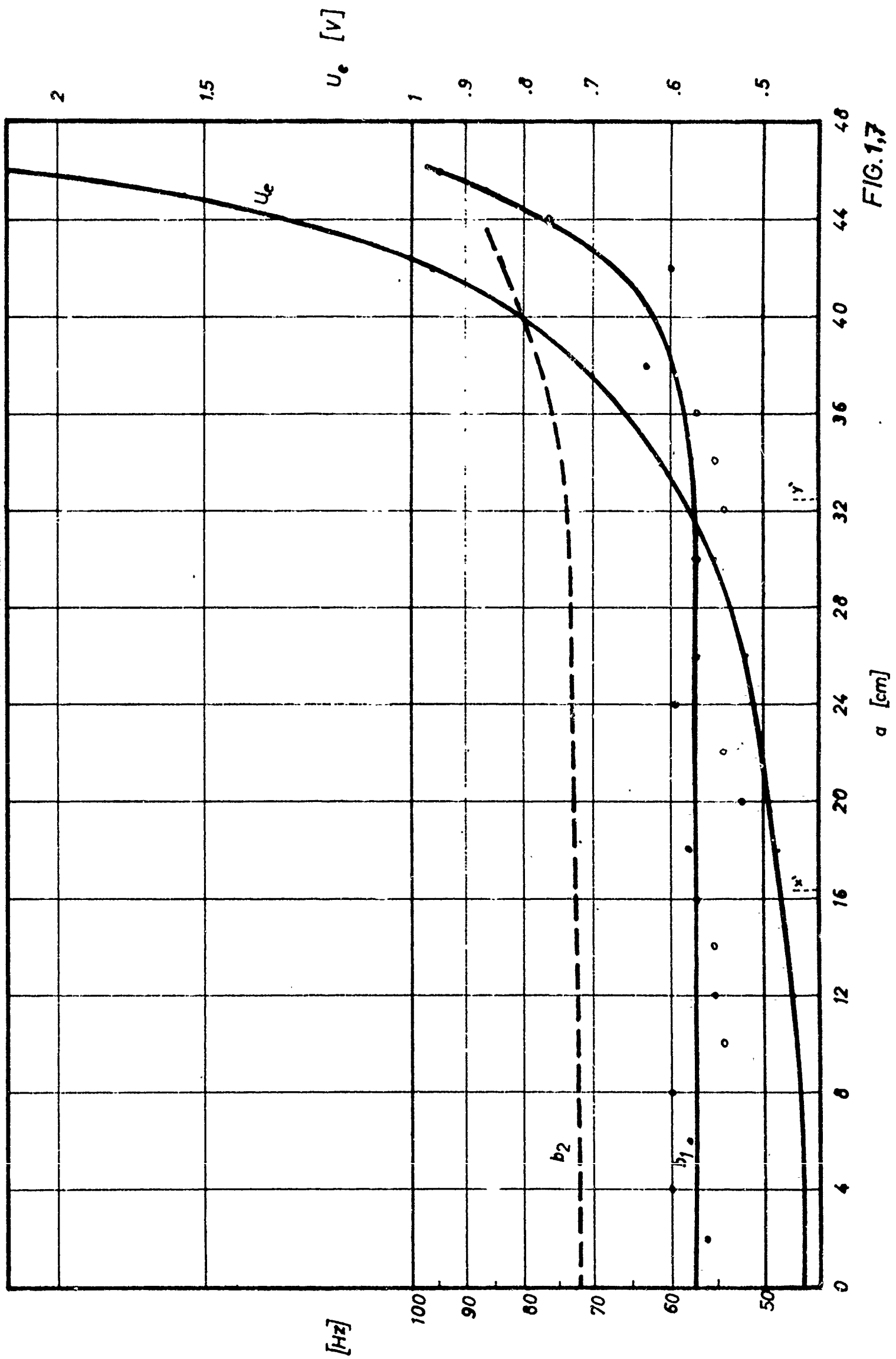


FIG. 1.7

total of 8 cross windings having 300 turns each were attached; at higher frequencies only part of the coils are used. Measurement of the band width of the antenna circuit with the same device as used for the diagram in Fig. 1,5 yielded the following values:

$f_0 = 3 \text{ kc/sec} \dots b = 10 \text{ cps}$, $f_0 = 10 \text{ kc/sec} \dots b = 75 \text{ cps}$.

A comparison of the output voltage of this optimized ferrite antenna with that of a small electric dipole at equal field strength is of great interest. For this purpose, Eq. (1,7) is written:

$$U_0 = \frac{2\pi \cdot n \cdot F \cdot E \cdot \mu_{\text{eff}} \cdot Q \cdot k}{\lambda},$$

with $n = 2400$

$F =$ cross-sectional area of the rod minus cross-sectional area of the bore

$$F = 2,2 \cdot 10^{-4} \text{ m}^2$$

$$Q = f_0/b = 133$$

$$E = 50 \text{ mv/m}$$

$$k \sim 0.8$$

$$\mu_{\text{eff}} \sim 480$$

$$\lambda = 3 \cdot 10^4 \text{ m} (= 10 \text{ kc/sec}).$$

Substituted in the above equation, these values yield an output voltage of $U_0 \sim 260 \text{ mv}$ which may be applied to the high-ohmic input of an amplifier. This voltage is much higher than that of the short antennas described above:

Short capacitive dipole $U_{\text{ind}} = 100 \text{ mv}$, but only a fraction can be used as amplifier input voltage.

Ironless frame antenna 1 m diameter: $U_{\text{ind}} \sim 0.15 \text{ mv}$

tuned: $U \sim 20 \text{ mv}$

4. Screening

In order to eliminate electric disturbances having a capacitive effect on the antenna windings, slotted aluminum or copper cylinders were tested. As the antenna is of high quality, these screens had a strongly damping effect and reduced the antenna voltage to almost 50%. Screening cylinders causing lower damping had a diameter of no less than 40 cm. Thus, the antenna was quite unhandy for solving special measuring problems in mines. A slotted screening cylinder made of a single-layer winding of an insulated copper wire - 2000 turns - 0.3 mm CuL, cylinder diameter 15 cm - yielded much better results. The wire winding was cut open and every other wire was

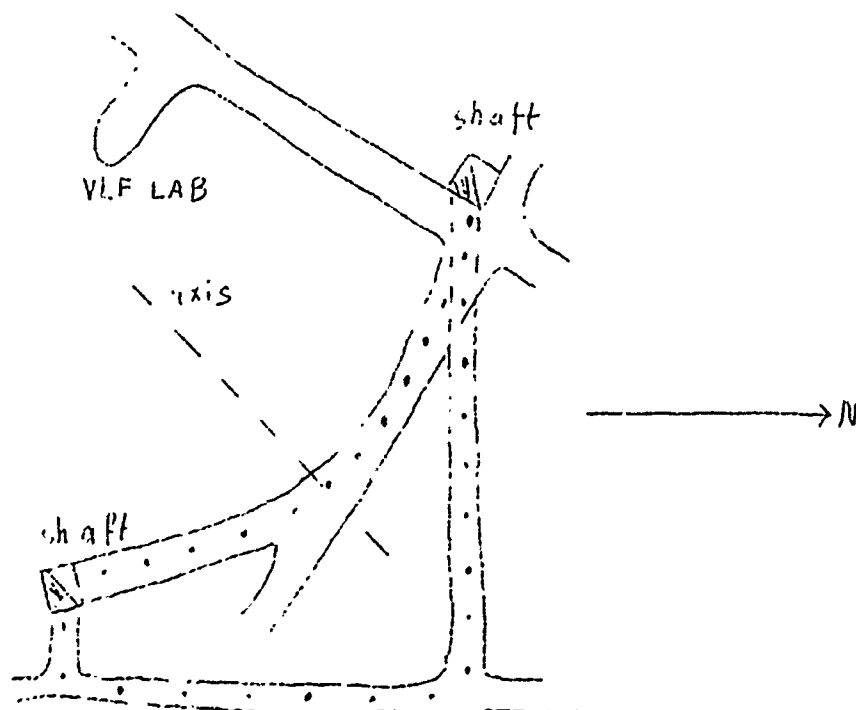
soldered to a collecting bar on either side. The principle is shown in Fig. 1,8. The capacitor thus formed yielded a frequency-dependent screen, damping mainly noise of high frequency. Damping at a much smaller cylinder diameter is low.

For detailed data on optimum ferrite antennas see our VLF report [4,5].

1.3 Transmitting antenna SAIX at St. Gertraudi

The transmitting antenna SAVIII which had already been described in the last annual report [2] and which was spanned out in a vertical plane in the mine of St. Gertraudi, was replaced by an improved and more powerful frame antenna. The antenna area (1600 m^2), however, was kept constant, but the number of turns was increased from 3 to 10. This means an increase in magnetic moment to more than the threefold as compared to the previous antenna.

As the existing galleries and shafts had to be used for building the loops, the antenna area does not exactly form a plane. However, the diagram shows that the deviations of the antenna shape from a vertical plane frame are not very large. For distances of measurement that are large as compared to the frame dimensions, this antenna acts like a horizontal magnetic dipole whose axis and the NS direction form an angle of approximately 40° .



In order to reach a large antenna current and thus also a large magnetic moment with the available transmitter whose output power is 1000 w, the resistance of the total antenna windings had to be not higher than 1 ohm. In this case an antenna current of more than 30 a occurs which is a considerable increase as compared to the former antenna. The low antenna resistance was reached by a sufficiently large wire cross section (aluminium wire being 135 mm² in diameter).

The construction of the antenna loop involved several electric and mechanical problems that had to be solved satisfactorily. In this connection the problem of insulation has to be mentioned, as it was decisive for the actual attainable antenna quality as well as for the attainable resonant current. Insulation was impaired especially by the fact that a great number of insulators were required in the narrow and windy galleries, which because of the high atmospheric humidity are covered with a thin layer of condensed water mixed with dust. If furthermore it is taken into account that the voltage across a turn may be at least 300 v under good working conditions, a maximum difference of approximately 3000 v between antenna and earth occurs. The occurring surface leakage currents deteriorate considerably the quality of the antenna circuit, thus decreasing the antenna current. Fig. II shows a section of the antenna construction; it can be seen that the insulators are large so that sufficient insulation is guaranteed also under the poor conditions in the mine. The frame is tuned to series resonance and adapted to the amplifier output in a way that has already been described in former reports.

Measurements with this transmitting antenna were conducted up to a distance of 7 km, in this case, however, part of the distance of measurement goes through air, as the St. Gertraudi mine has no galleries of the desired dimensions. These test measurements showed, however, that it is favorable to place the receiver deep below the earth's surface as thus the atmospheric noise level is attenuated and the full sensitivity of the receiver can be utilized.

1.4 Direction-finder antenna

For detailed studies on the direction of the electromagnetic field in the neighborhood of the transmitting dipole, the existing receiving antennas [2] have not been suited. Preliminary experiments showed that the deviations in field direction caused by differing rock conductivity (transition between dolomite and lead ore of better conductivity) are only a few degrees. Furthermore, the change in field direction ($\Delta\chi$) which is due to a rotation of the transmitting antenna ($\Delta\alpha$) varies according to the conductivity of the medium, which also made a more suitable receiving antenna desirable.

The new direction-finder antenna was constructed such that the axis of the receiving antenna rotates freely in space and can furthermore be fixed in any desired position; the plane of rotation of the receiving antenna can also be chosen according to the conditions of measurement. The necessity of choosing a certain plane of rotation of the receiving antenna was evident already during the measurements in the mines of Bleiberg [7] where the directional pattern of the transmitting antenna along a steep ore body was measured. The antenna is set up in such a way that the base plate which simultaneously serves as a plane of reference, is fixed horizontally at the beginning of a measurement, then the antenna axis is adjusted in north-south direction (Fig. 1.9). This position serves as the starting position relative to which a field direction or a change in field direction can be measured with an accuracy of $\pm 1^\circ$.

Fig. 1.9 shows the direction-finder antenna and the arrangement of the circular scales in a schematic diagram. The antenna circuit on the whole agrees with that of former receiving antennas. The ferrite rod is approximately 50 cm long, the coils being arranged at its center. The resulting resonance elevation of the receiving voltage can be fully utilized by adapting the high resonance resistance of the parallel resonant circuit to the low-ohmic input of the meter by means of a suited impedance transformer. The circuit of this

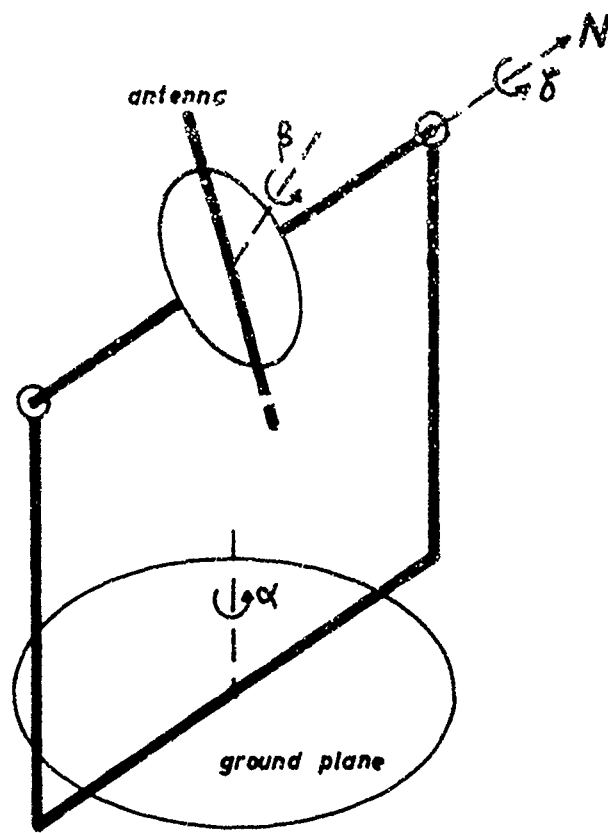


FIG.19

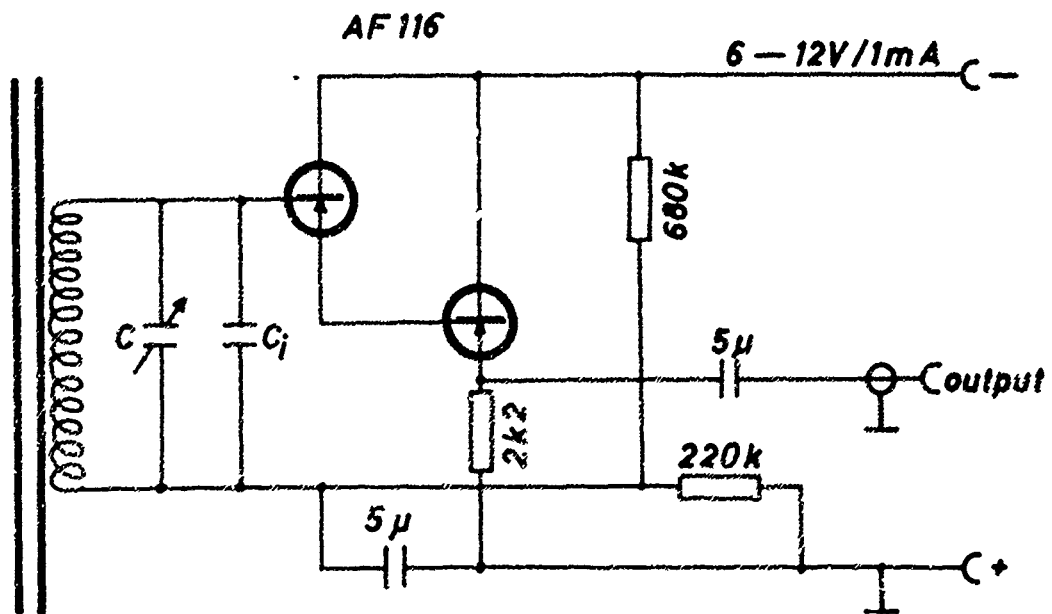


FIG. 1.10

impedance transformer which has an input impedance of approximately 10 megohms is shown in Fig. 1.10. Such a high input resistance can be reached by the simple method of a double collector base circuit equipped with two transistors of high current amplification. The frequency dependence may be largely neglected, since the circuit shows a constant amplification factor ($v = 0.95$) and a constant input impedance (10 megohms) up to 600 kc/sec. The current (6 - 12 v, 1 mA) is supplied by the indicator.

The impedance transformer and the resonance tuner together with the receiving antenna form one unit so that the connecting cables can be made as short as possible. For measurements in other mines where there is no powerful stationary transmitter available, the 50 w amplifier described previously is used. As far as a well-known and reproducible angle \mathcal{L} is required for such measurements, a coil whose axis can be adjusted into a given direction with an accuracy of approximately $\pm 2^\circ$ is used as a transmitting antenna. The transmitting antenna is aligned in the usual manner by means of a compass and mine map. The angle is based on $\mathcal{L} = 0^\circ$ and can be chosen arbitrarily in order to study the transmitting antenna or the dependence of the field direction (χ) on the alignment of the transmitting antenna (\mathcal{L}) (see 2.3). In contrast to former transmitting antennas, this new design makes possible to rotate the antenna axis also in vertical direction. This represents a considerable improvement as numerous measurements frequently have to be conducted along a steep ore body, i.e. passing from a higher to a lower floor [7].

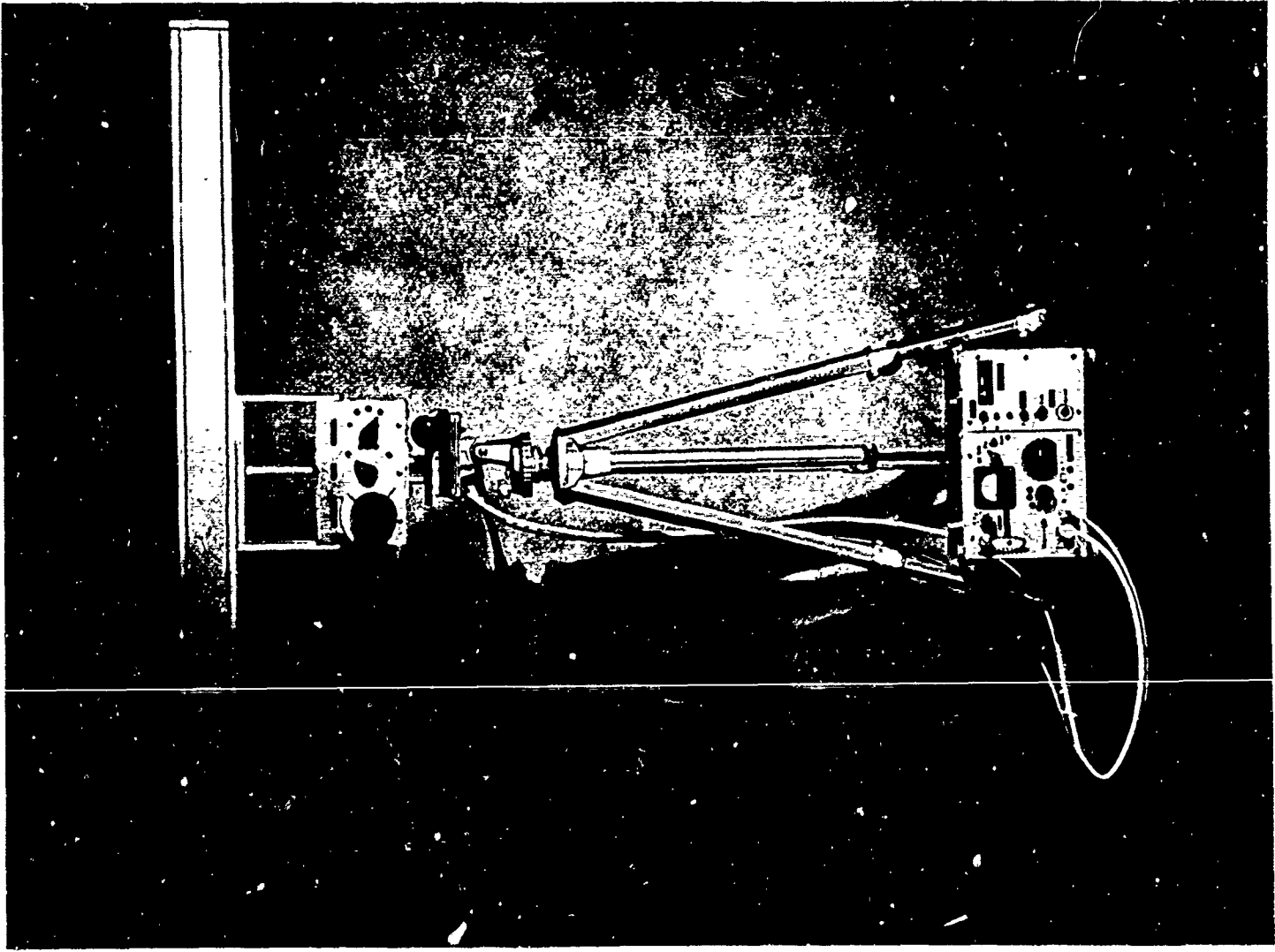


Fig. 1

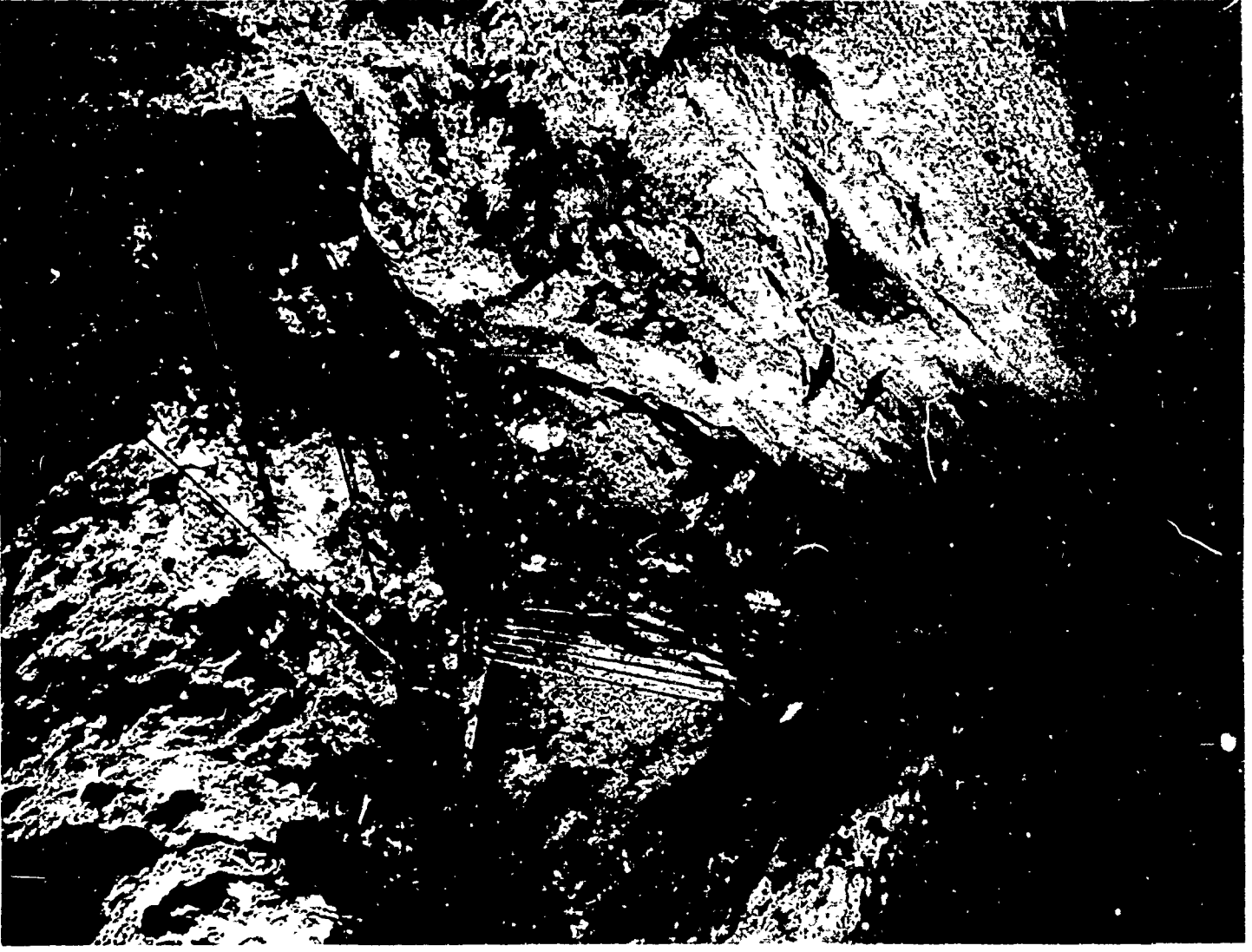


Fig. 2

2. Propagation measurements

Review

In our third annual report, measurements in several mines and different types of rock have been described. The studies conducted in a potassium and salt mine, various iron ore mines and a coal mine were treated in detail. The results obtained were of great interest, showing that the methods of measurement developed in the Tyrollean mines of St. Gertraudi, Schwaz and Lafatsch are applicable also to other types of rock, yielding good results. Furthermore, the obtained results of measurements were compared with the existing results; thus, facts were obtained that hold for a general theory of propagation in different types of rock.

The most important points that result from the measurements conducted in Northern Germany in 1963 shall now be summarized in brief. The program of measurement of the 1964 report is based on them.

1. The measurements were conducted in rock having a strongly changing conductivity (Konrad I having approximately 10^{-1} mhos/m and Hansa III approximately 10^{-8} mhos/m). In these cases the conditions of propagation were as expected, in the second case a very strong attenuation occurred, with transition from the pure near field to the far field being observed at 20 m; attenuation in the second case was very small and was related with a very great expansion of the near field which extended even beyond the remotest points of measurement. If the conductivities are so small and the frequencies are below 10 kc/sec, the pure near field of the transmitting antenna may be several kilometers.

2. Almost all measurements were made in very inhomogeneous rock. The mineralization on the whole was concentrated to a very small section of the range of measurement having approximately the shape of a vertical ore layer 10 to 20 m thick. As the conditions of measurement as well as the geometrical conditions were too complicated to be accurately evaluable

by theory, a great number of measurements had to be made. A comparison with the results obtained under homogeneous conditions enabled us to determine the effect of inhomogeneities from the above results. For this method, however, very comprehensive data of measurements are required in order to evaluate unknown conditions of propagation.

3. Measurements of the received field strength of the GBR transmitter that were conducted in Tyrolean mines as well as in mines of Northern Germany showed different attenuation in horizontal and in vertical direction. Attempts of explaining this phenomenon have already been made in [2] and in [6], yet there still exist doubts as to the correctness of these explanations. A repetition of the measurement in a mine was very desirable, where field strength measurements in horizontal galleries and in vertical shafts were possible beginning at the earth's surface.

2.1 Measurements at Bleiberg

In order to complete the above program of measurements, an excursion was made into the lead mines of Bleiberg (Kärnten). The measurements conducted there can be summarized as follows:

1. Propagation measurements through homogeneous or weakly inhomogeneous rock.
2. Measurement of the directional pattern of the transmitting antenna and determination of the rock conductivity. These measurements also made possible statements on the near field and on the far field.
3. Measurement of the decrease in field strength of the GBR transmitter in rock in horizontal and vertical direction.

This program was intended to serve as a supplement to the above studies and to yield explanations of unknown phenomena such as the difference in attenuation of GBR signals in vertical and horizontal direction. This was the first measurement in a large and strongly mineralized lead mine.

ad 1) The propagation measurements were made at a frequency of 3 kc/sec. The rock lying between transmitter and receiver mainly consisted of Wetterstein limestone, at individual points, however, mineralization in the form of lead sulfide and sphalerite was found. These ore inclusions were only small as compared to the total distance of measurement (20 - 30 m mineralization as compared to 400 - 800 m of measurement). Therefore the effect of this mineralization could not be seen in the measured curve. Figur 2.1 shows the curve of the Bleiberg measurements (curve 1 and Table 2.1).

Table 2.1

m	δ°	Ue [μ V]
90	85	2400
192	20	400
250	20	190
320	15	110
385	18	63
400	8	51
440	3	36
650	3	8
860	2	3

At a distance of approximately 400 m, attenuation proved to increase owing to a change in rock. For reasons of comparison, a curve calculated for 10^{-4} mhos/m conductivity was plotted as a dashed line. This shows that up to a distance of 400 m the conductivity was smaller than 10^{-4} mhos/m, whereas at greater distances it was higher than the assumed value. If the dashed curve is assumed to be a mean value, which may be done for approximation, the attenuation factor for the first kilometer, beginning at the transmitting antenna, is approximately 66 db. At the first glance, this value seems to be rather high, but it must be taken into account that this value only holds for the immediate near field of the transmitting antenna. The greater the distance of measurement in the far field of the transmitting antenna, the lower becomes the value of attenuation per kilometer. This shows that the attenuation depends on the distance from the transmitting antenna and it is

only in the far field that attenuation per kilometer becomes constant. Yet, the above value is quite important, as will be explained in detail in chapter 2.2 in connection with the near field and the far field. The curves 2, 2a and 3 plotted in Fig. 2.1 show the effect of the different attenuations in the far field and in the near field. Curves 2 and 2a give the decrease in field strength of the GBR transmitter during the horizontal penetration into the earth's surface. The two curves only differ by the fact that the distance from the shaft mouth (m) is plotted in curve 2, whereas in curve 2a the depth (m^*), i.e. the shortest distance between the site of measurement and the earth's surface are plotted. Curve 3, however, gives the decrease in field strength in vertical direction.

Table 2.2

horizontal measurement

m	m^*	$U_e[\mu V]$
560	150	64
650	175	44
750	205	40
850	240	31
920	260	28

Table 2.3

vertical measurement

m	$U_e[\mu V]$
0	400
50	70
100	30
200	15
300	15
400	12.5
450	11
500	7.6
600	5.6
650	5.0

In contrast to the results of measurements in the mines of Northern Germany [2], both curves show approximately equal attenuation. By means of extrapolation, the attenuation of the GBR transmitter (16 kc/sec) in rock having a conductivity

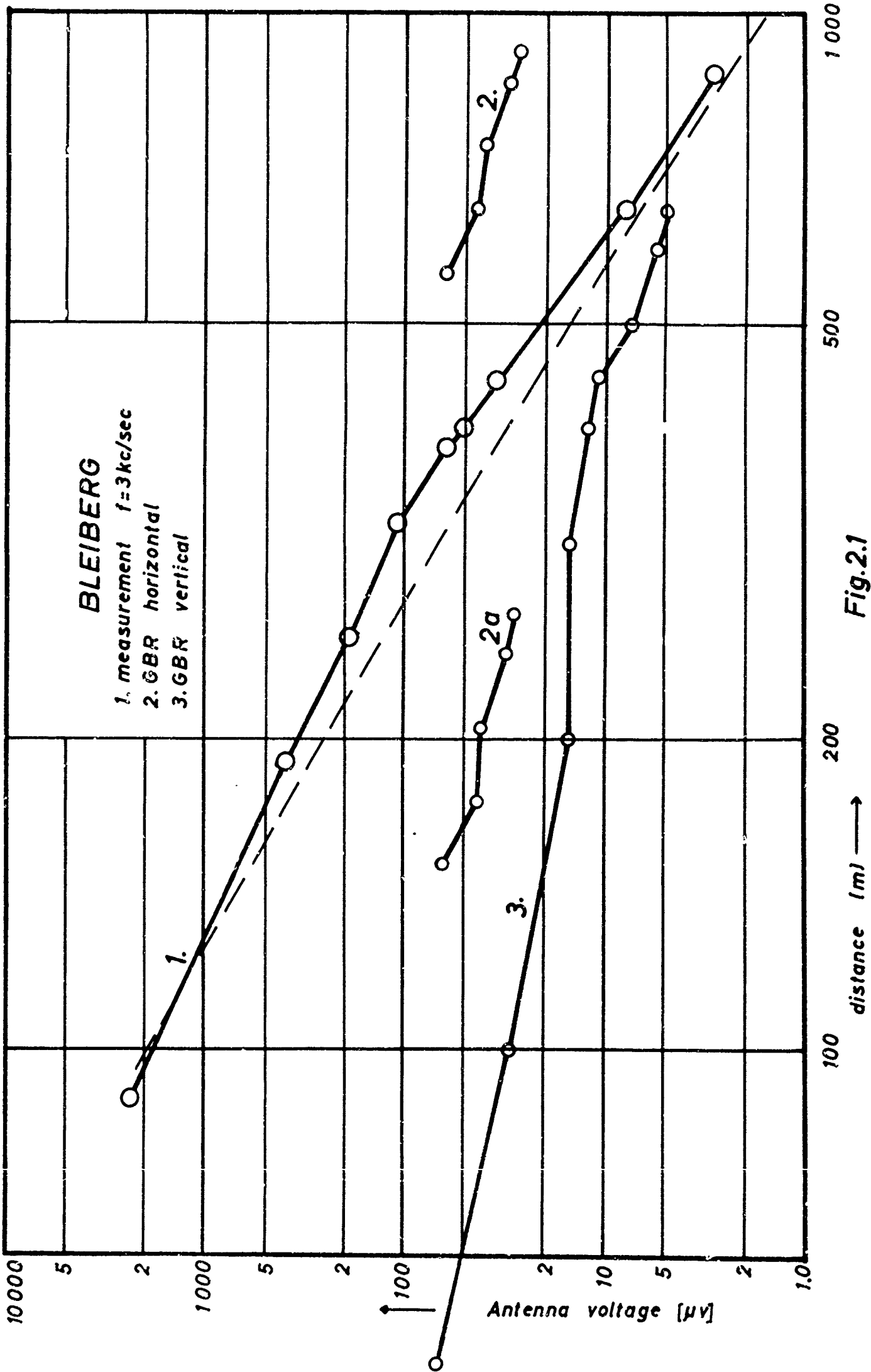


Fig. 2.1

of $5 \cdot 10^{-3}$ mhos/m, was found to be approximately 22 db. In order to explain this discrepancy between the values of attenuation obtained from propagation measurements with the transmitter set up in the mine and those obtained from measurements of the GBR transmitter, we may state the fact that in one case the attenuation in the near field was measured, and in the other case in the far field. At what distance the far field begins and in how far the distance depends on the conductivity of the medium and on the frequency is shown on the one hand by measurements of the radiation pattern of the transmitting antenna (chapter 2.4) and on the other hand by theoretical considerations discussed in the next chapter.

Besides the studies on the above problem, the conductivity of rock was also determined in the mines of Bleiberg by measuring the directional pattern of the transmitting antenna by means of the function $\varphi(r,k)$. Figur 2.2 shows a graphic representation of the function $\varphi(r,k)$ for several conductivity values and for a frequency of 3 kc/sec. The values of measurement in Table 2.4 are also plotted and make possible to determine the electrical conductivity. Since, however, the different points of measurement were made in rock of changing ore content, the results show an adequate straying. For dead rock, the mean value of conductivity may be assumed to be 10^{-4} mhos/m, whereas for more strongly mineralized rock this value increases somewhat, being approximately $5 \cdot 10^{-4}$ mhos/m, as was shown by measurements of the four-electrode configuration. How far this method of determining $\varphi(r,k)$ makes possible to prove spatially confined inhomogeneities is discussed in detail in [7].

Table 2.4

Frequency of measurement
3 kc/sec

<u>m</u>	<u>$\varphi(r,k)$</u>
192	1.55
385	0.80
100	1.80
101	1.97
150	1.93
191	1.11

2.2 Near field - far field

For a better understanding of the experimental results it is important to know whether a measurement is conducted in the near field or in the far field of the transmitting antenna. The conditions of propagation differ decisively for these two cases. Whereas the near field is characterized by the fact that the H_r component of the electromagnetic field prevails as compared to the H_θ component, this relation of components is reverse as the distance of measurement increases, i.e. at the transition from a pure near field to the far field. If the measurement is made at a great distance from the transmitter or more precisely at a distance from the transmitting antenna that is large as compared to the antenna dimensions and the wavelength, only the H_θ component of the magnetic field vector is left over. In propagation measurements in the high-frequency region, this case alone is considered. At the short wavelength usually studied, the effect of the near field of the transmitting antenna may be largely neglected, as it is too small as compared to the total range of measurement. If the propagation conditions of VLF waves are to be studied, this otherwise neglected range is of main interest. Considering that the wavelength in a medium of average conductivity ($5 \cdot 10^{-4}$ mhos/m, i.e. dolomite, for example), is approximately 4 km at a frequency of 3 kc/sec, the near field extends over a range of at least 10 km. Then the transition zone begins which at distances larger than that goes over into the actual far field. An increase in frequency or conductivity causes a decrease in the near zone, which must not be neglected, not even in this case.

A principal point which has already been pointed out (chapter 2.1) is the fact that the attenuation of an electromagnetic wave in a conducting medium is much larger in the near field than in the far field. This becomes evident from

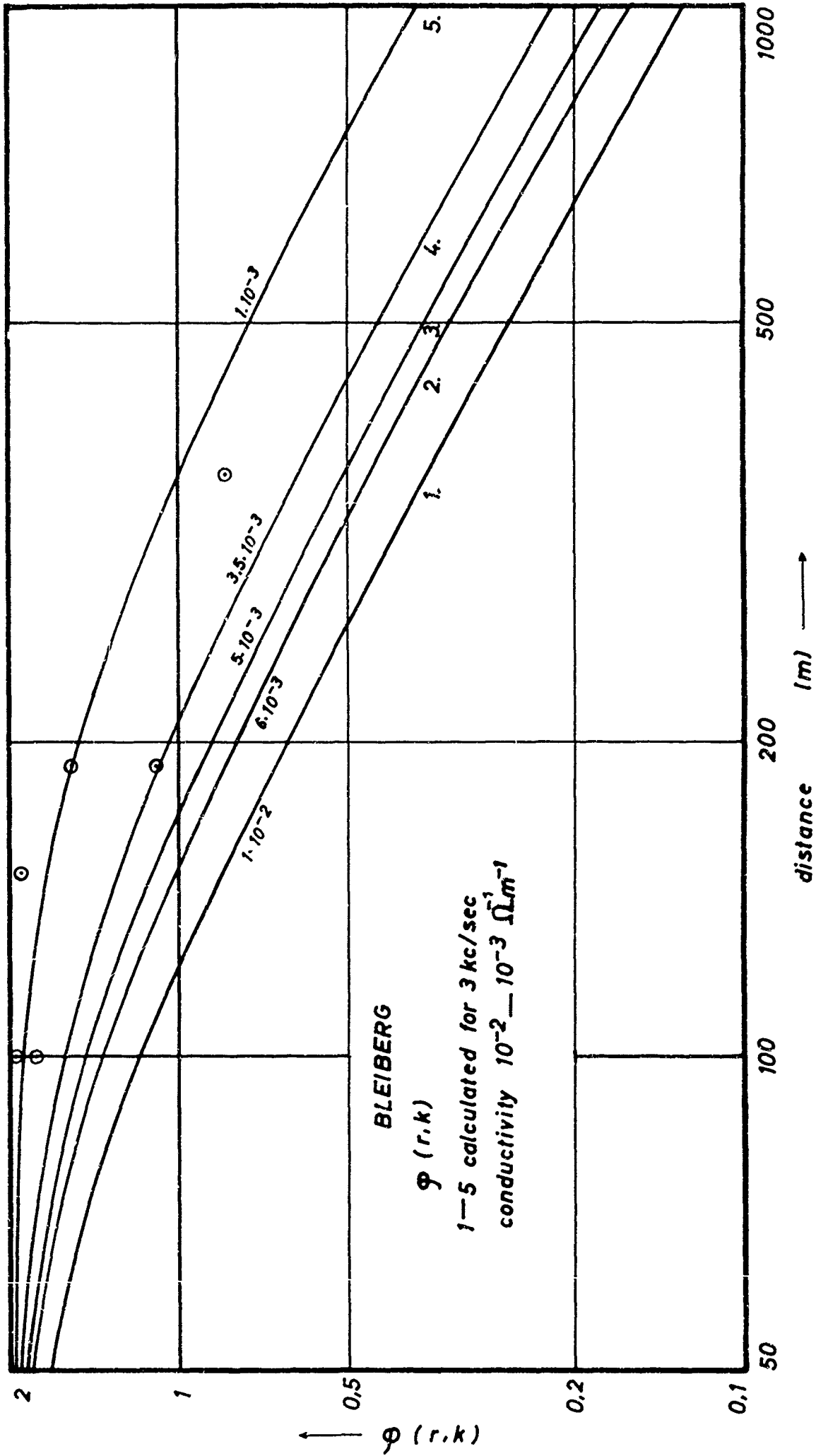


Fig. 2.2

the expression (2.1) in chapter 2.3 for the magnetic field strength of a radiating dipole in a conducting medium.

At small distances r , the first terms with high powers of r give the main portion of the field strength. At very large distances, however, the exponential factor is decisive, whereas the parenthetical expression assumes a constant value determined by the conductivity.

Furthermore, the equation shows that at $\vartheta = 0^\circ$, which corresponds to the H_r component, the field strength decreases much faster towards zero than at $\vartheta = 90^\circ$. In order to illustrate this behavior the magnetic field strength $|H|$ was calculated for several frequencies beginning at 1 kc/sec up to 100 kc/sec. Figs. 2.3 through 2.10 give a representation of the field strength trend as dependent on the distance of measurement r . The curves $\vartheta = 0^\circ$ and $\vartheta = 90^\circ$ were calculated and plotted always for one frequency. Thus, a comparison of the H_r and H_ϑ components is possible at otherwise constant parameters. It can be seen that the families of curves are almost consistent even at larger distances (5 - 10 km). Especially at 3 kc/sec we may not speak of a pure far field at distances of up to 10 km. Even at higher frequencies, e.g. 100 kc/sec, an essential quantitative difference between the two field components H_r and H_ϑ becomes effective only at a distance of several kilometers, which corresponds to a distance of measurement of at least 10 wave lengths. At the first glance, this result may be surprising, but it can easily be confirmed by experiment (see section 2.4).

The fact that the examination of the near field yields interesting and useful results shall be shown by means of Fig. 2.10. It shows how the attenuation of electromagnetic waves depends on the distance, furthermore it shows attenuation to assume a comparatively small, constant value within a certain range. This behavior may be interpreted by the fact that a certain frequency at a given underground path of trans-

mission yields the most favorable field strength at the point of reception. This shows that not every frequency may be used, but that the applied frequency has to be determined in accordance with the electrical properties of the rock and also with the distance of every individual measurement. For transmission below ground, the most favorable frequency of transmission has therefore to be determined in accordance with the conditions of propagation.

In the part that follows, another item confirming the difference of propagation conditions in the near field and in the far field shall be discussed. In chapter 2.1, the rather high value of 66 db was determined for "attenuation value/km", which holds for the immediate near zone of the transmitting antenna. In contrast to this value, there is that of 22 db for the attenuation of the GBR transmitter measured in the same mine under equal environmental conditions, despite the much higher frequency (16 kc/sec as compared to 3 kc/sec). These two results may be looked upon as being reliable, as they were obtained in several different mines as well as in different types of rock. It has already been mentioned in chapter 2.1 that this discrepancy in attenuation of the electromagnetic wave may be explained by the fact that one measurement was made in the near field and the other one in the far field of the transmitting antenna. Considering expression (2.1) of chapter 2.3 we find that the terms decisive for the near field decrease with the third and fourth power of r . In contrast to it, attenuation in the far field is determined only by the factor e^{-kr}/r .

2.3 Measurement of the direction of the magnetic field strength

In the propagation measurements conducted and described so far, the direction of field strength is not taken into account, only the amount of the field strength being measured.

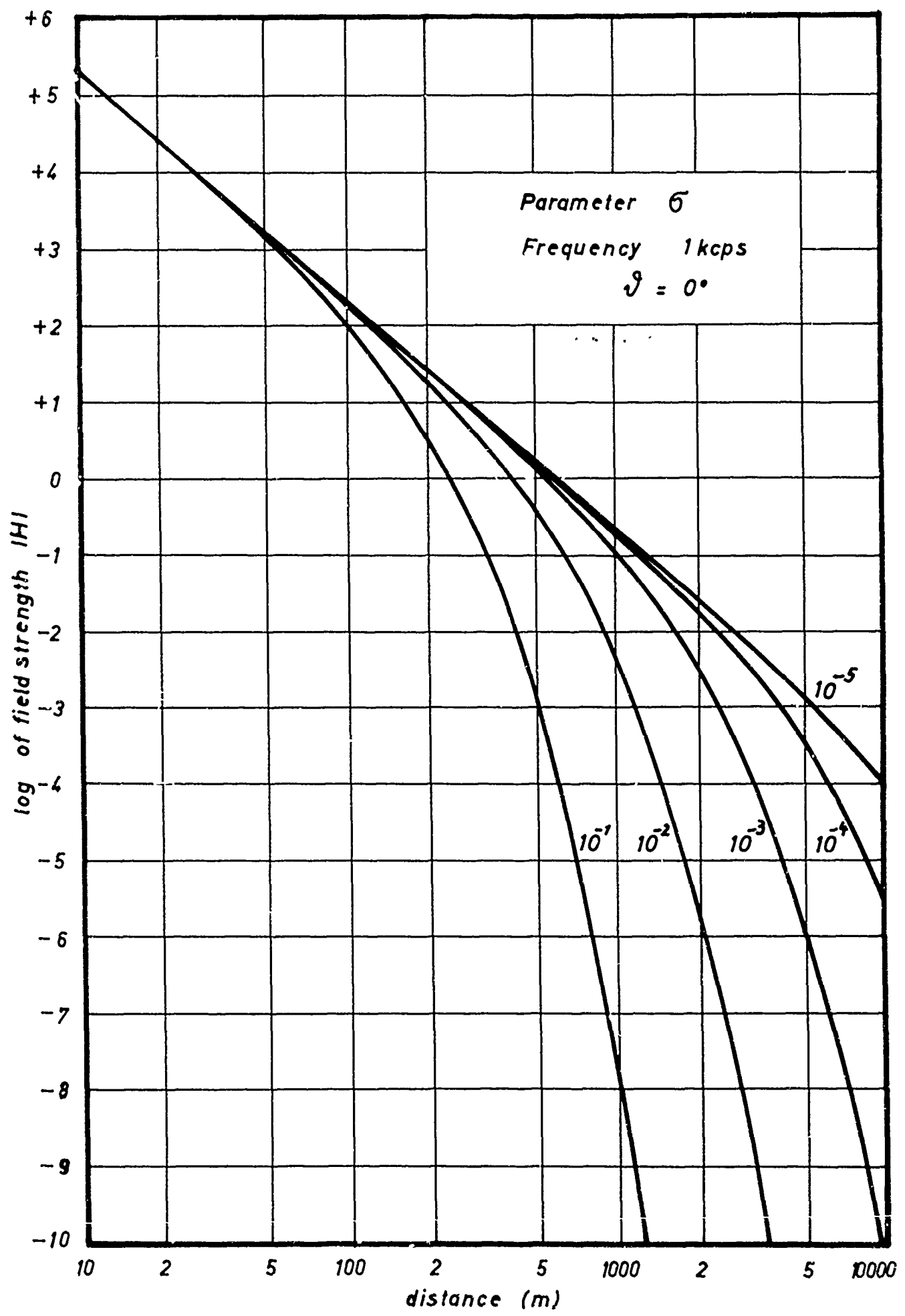


FIG. 2.3

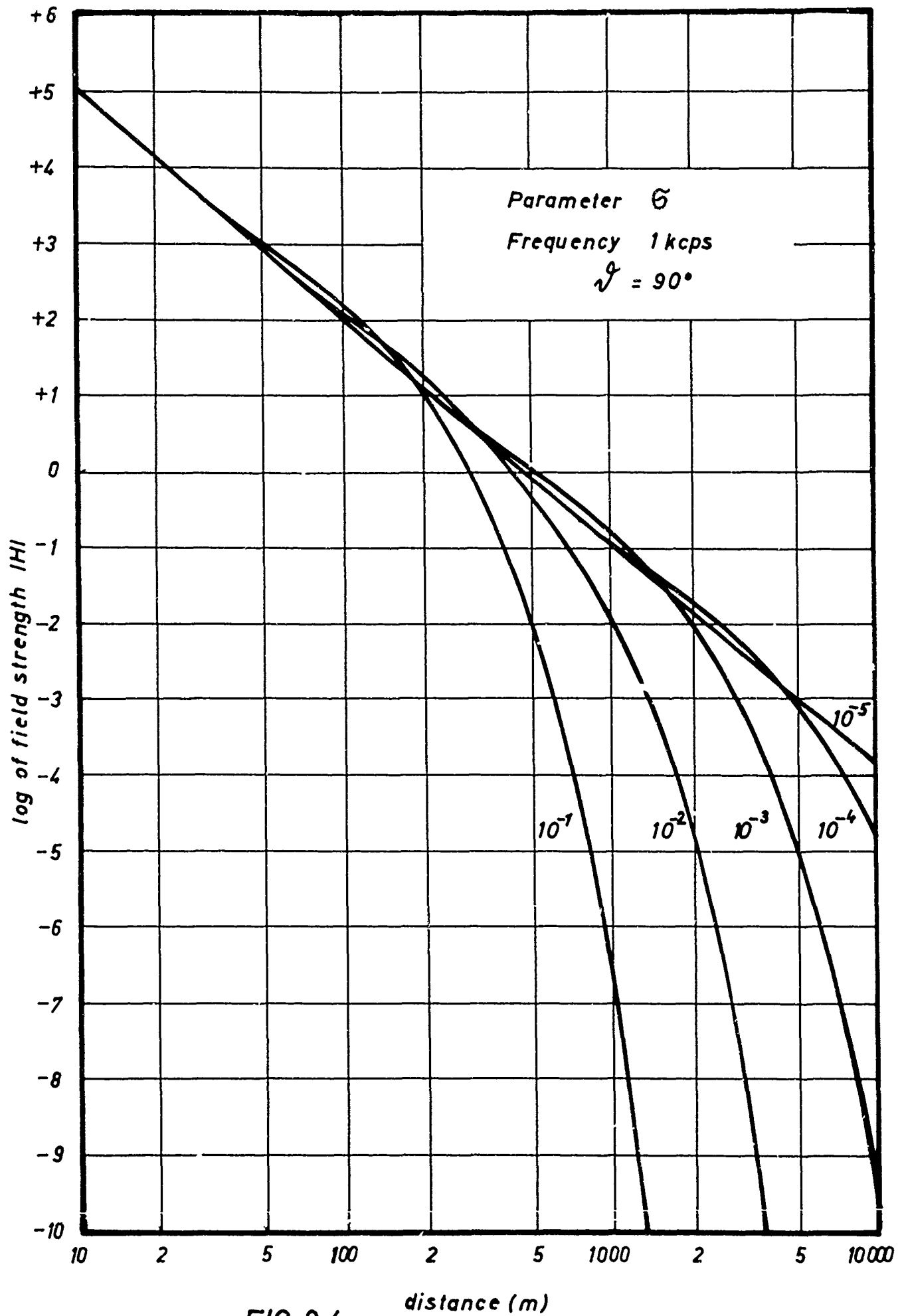


FIG. 2.4

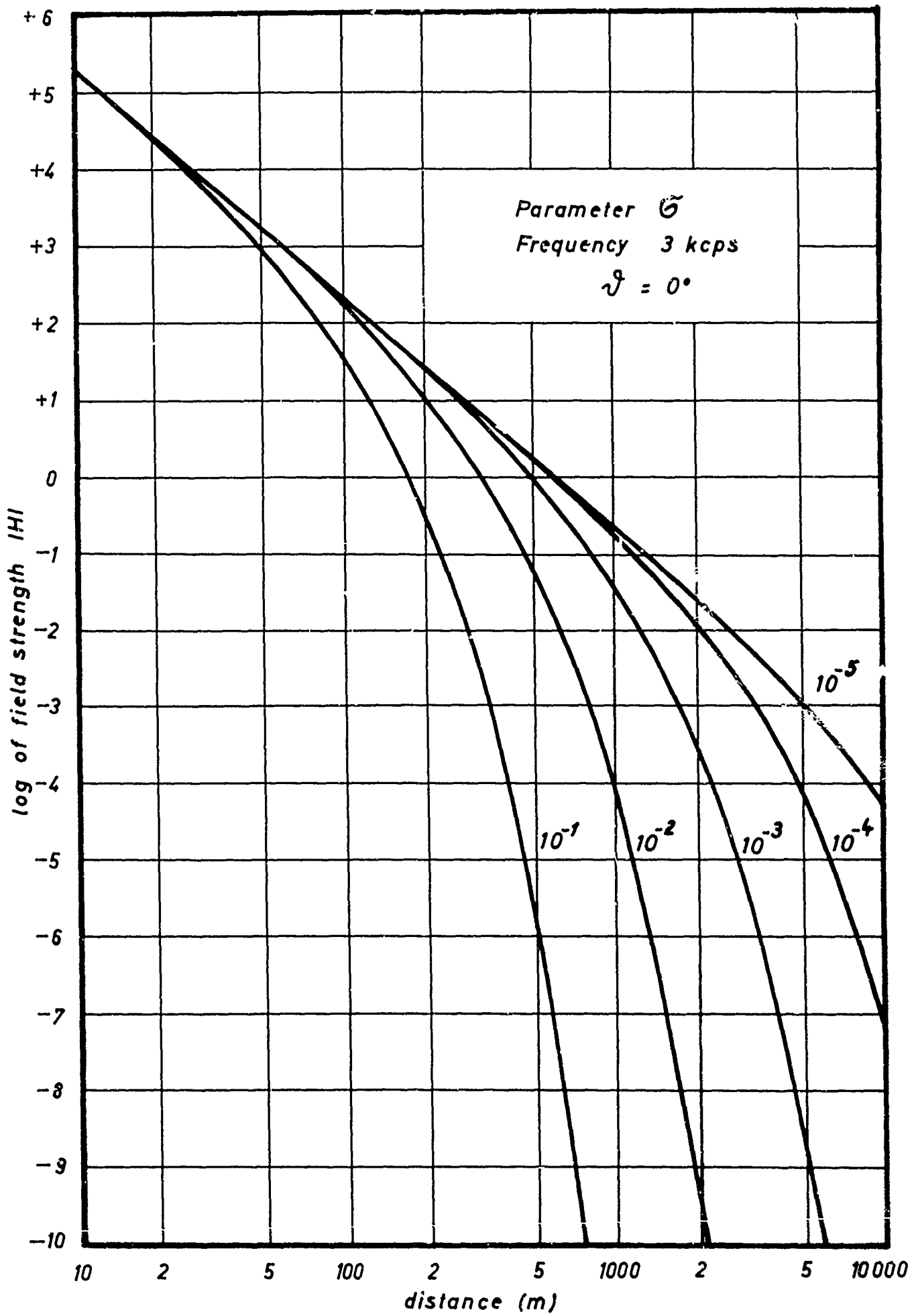


FIG. 2.5

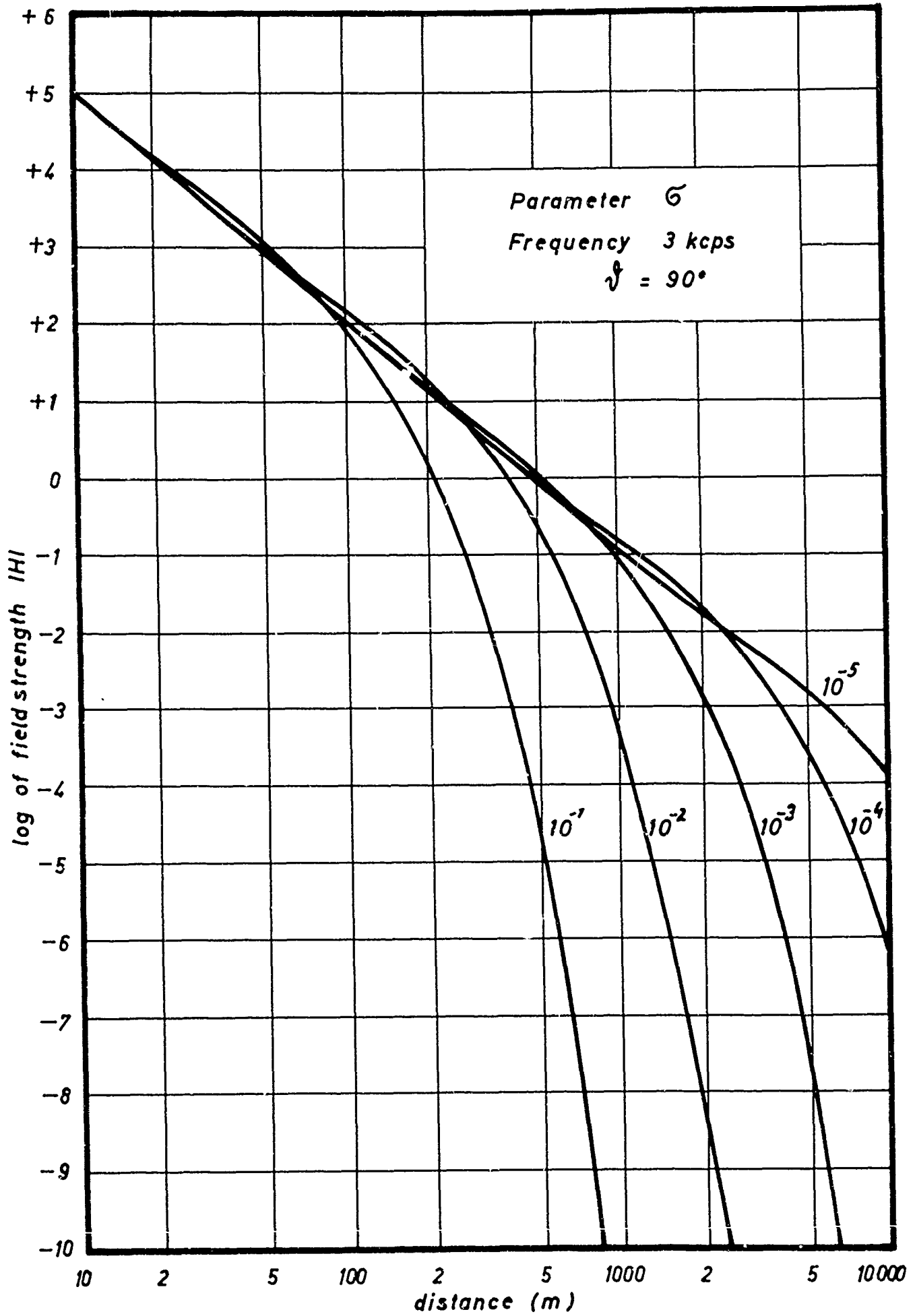


FIG. 2.6

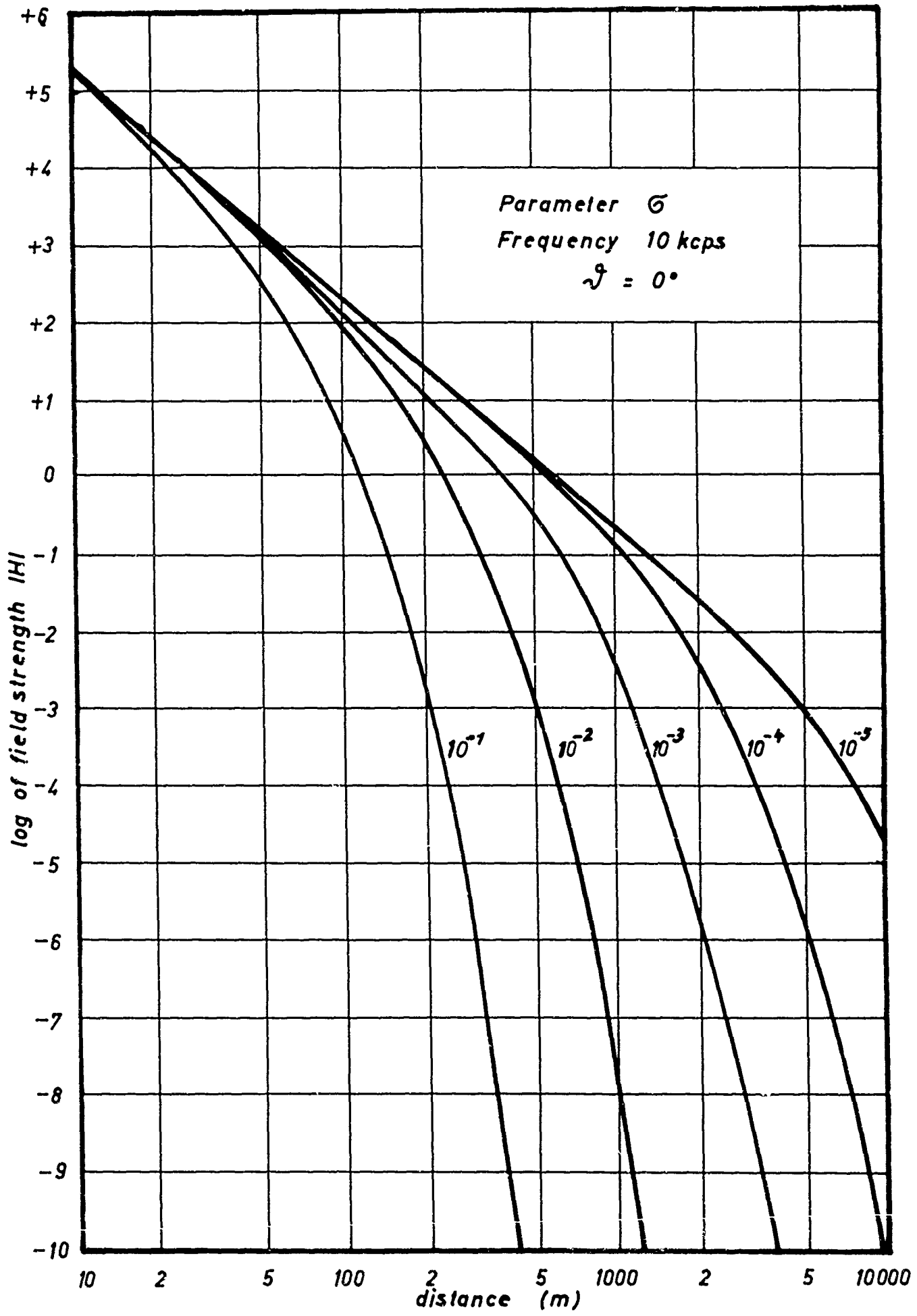


FIG. 2.7

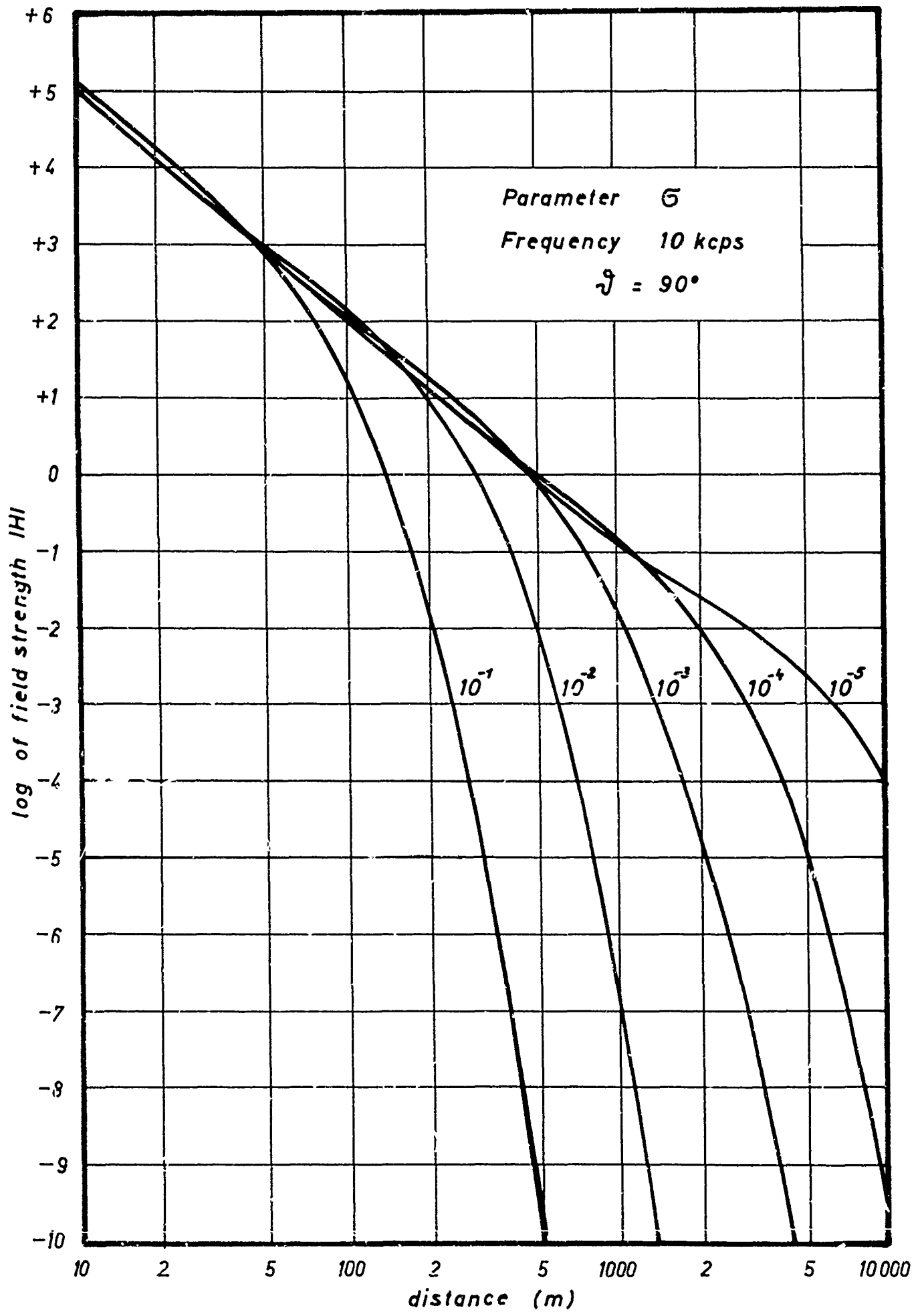


FIG. 2.8

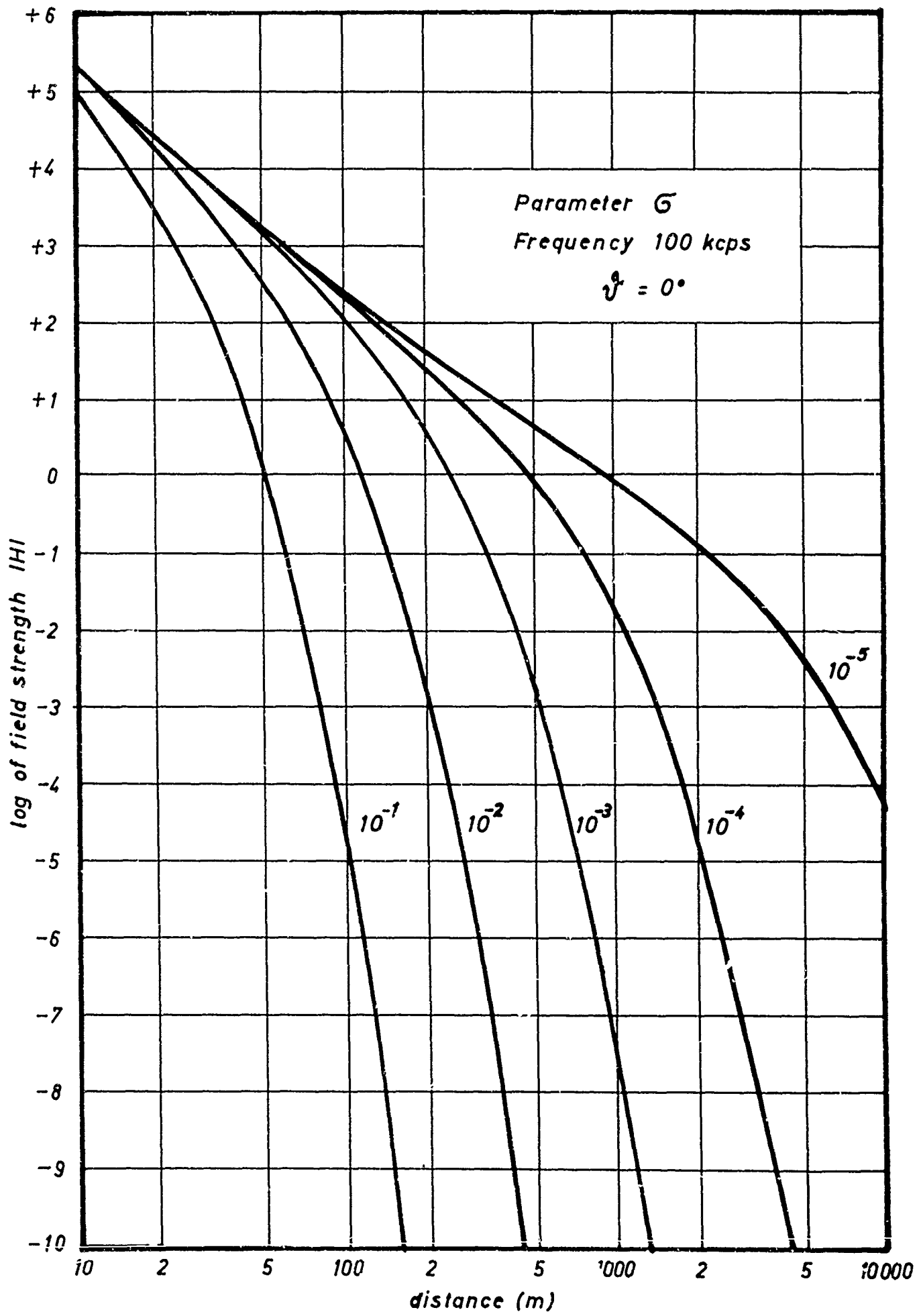


FIG. 2.9

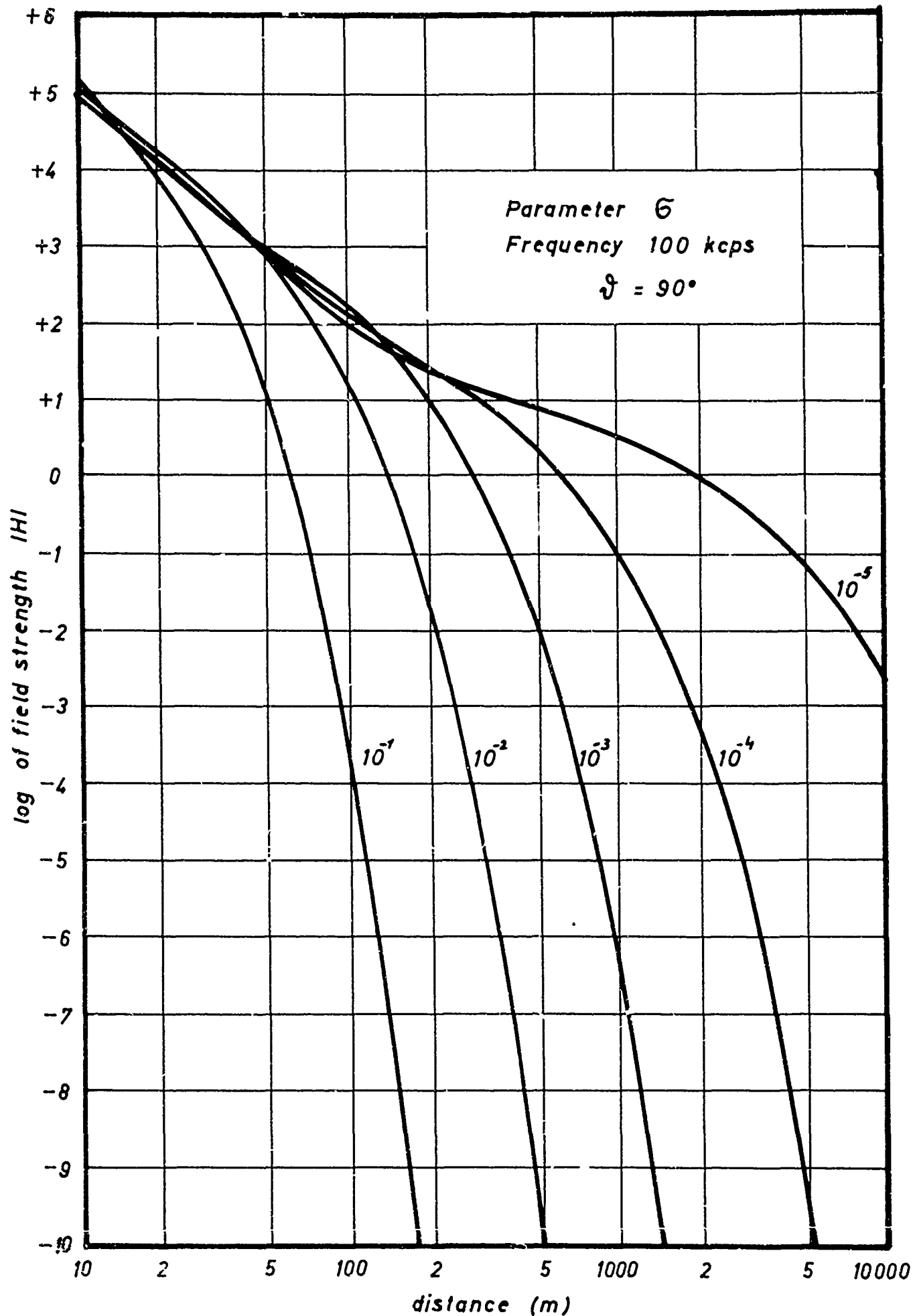


FIG. 2.10

A comprehensive investigation of the propagation of electromagnetic waves in the rock, however, has to include the field direction and its change as dependent on the properties of the medium. The results obtained so far suggest that the direction of the field is well suited to give an explanation of the structure of the medium much more accurately than the absolute value of the field strength. Whereas the latter depends on the sum of the electric properties of the medium between transmitter and receiver, a change in the field direction that can be well observed, may be caused by an inhomogeneity that is small as compared to the entire distance of measurement. The conductivity integrated over the entire region of transmission, and thus also the absolute value of the field strength, do not change noticeably owing to such a small inhomogeneity.

On the basis of the equations

$$|H| = \sqrt{H_r^2 + H_{\lambda}^2} = m \cdot h(r, \lambda, k)$$

and

$$h(r, \lambda, k) = \frac{e^{-kr}}{r} \left[4 \cos^2 \lambda \left(\frac{1}{r^2} + \frac{2k}{r} + 2k^2 \right) + \sin^2 \lambda \left(\frac{1}{r^4} + \frac{2k}{r^3} + \frac{2k^2}{r^2} + \frac{4k^3}{r} + 4k^4 \right) \right]^{1/2}, \quad (2.1)$$

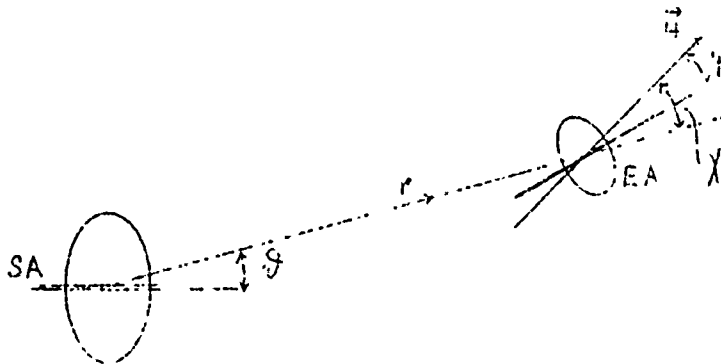
describing the magnetic field strength vector under the assumption of an unbounded and weakly conducting medium [1], the direction (χ) of the field vector can be calculated from the two components H_r and H_{λ} . In general, the following relation holds for the angle χ (see Fig. 2.11):

$$\tan \chi = \frac{H_{\lambda}}{H_r}$$

or with allowance for the dependence of the components H_r and H_{λ} on the alignment of the transmitting antenna, i.e. on the angle λ , the relation

$$\tan \chi = \frac{h(\lambda=90^\circ)}{h(\lambda=0^\circ)} \cdot \tan \lambda \quad (2.2)$$

is valid.



Substituting the function $\varphi(r,k)$ [7] and solving the equation (2.2) for χ , we obtain the desired expression for the direction of the field:

$$\pm\chi = \arctan \frac{\tan \pm \vartheta}{\varphi(r,k)} . \quad (2.3)$$

This expression shows that the direction of the field at a certain point having the distance r from the transmitting dipole, depends on ϑ as well as on the conductivity of the medium in between. At a small conductivity, i.e. if the value of $\varphi(r,k)$ lies between 0.5 and 2, the field direction χ changes almost proportionally to the direction of the antenna axis. It is only at increasing conductivity that χ is approximately 90° in a wide ϑ range. This case corresponds to the conditions of propagation characteristic of the far field of a transmitting dipole. For the parameter $\varphi(r,k)$ ranging from 2 to 0.1, the expression (2.3) has been calculated and represented in Fig. 2.12. The field direction measured in an almost homogeneous rock at St. Gertraudi is well consistent with the curves plotted in Fig. 2.12. The direction-finder antenna described in chapter 1.4, which allows angular measurements to be conducted with an accuracy of up to a few degrees, was used as a receiver.

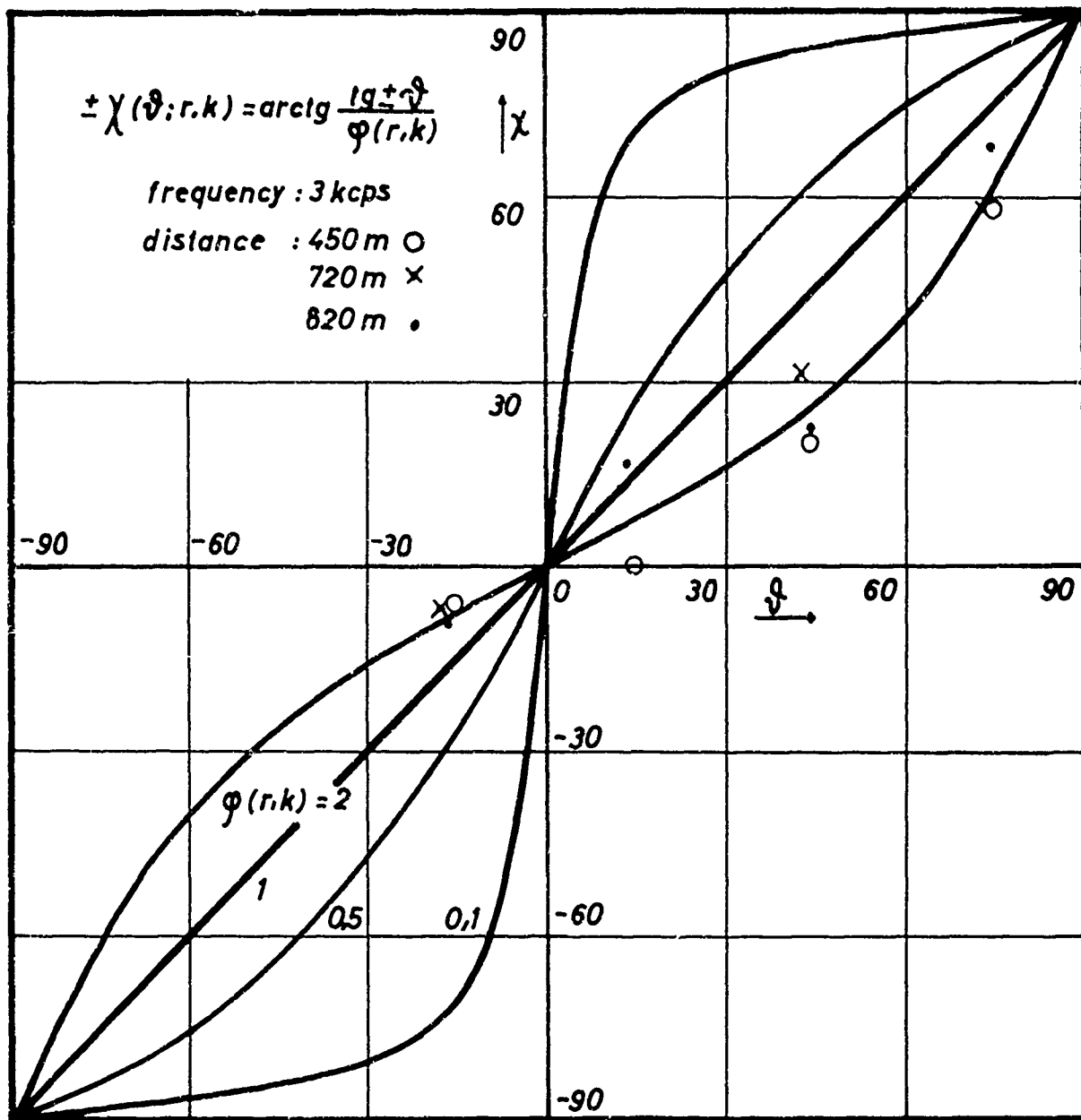


FIG. 2.12

Table 2.5

	450 m			720 m			820 m		
	11 3 kcps			11 3 kcps			11 3 kcps		
\mathcal{I}	χ	χ	\mathcal{I}	χ	χ	\mathcal{I}	χ	χ	
-15	-12	-6	-17	-6	-7	-16	-9	-9	
15	11	0	13	12	12	14	21	17	
45	39	20	43	67	31	44	40	23	
75	76	58	73	87	59	74	79	56	

2.4 Propagation measurements at St. Gertraudi

The newly developed direction-finder antenna was used for measurements in the St. Gertraudi mine in connection with the problem of the direction determination of the electromagnetic field vector H in a homogeneous or inhomogeneous rock, dealt with in chapter 2.3. It is the aim of these examinations to make statements on the dependence of the field direction on the alignment of the transmitting antenna and at the same time to get a further possibility of determining the near field and the far field.

On the whole, such a statement is always based on the prevailing component of the dipole field. This corresponds to the determination of the function $\varphi(r,k)$ introduced in [7] and represented in Fig. 2.2. If the determined function value is smaller than 0.1, i.e. if the \mathcal{I} component is 10 times as large as the r component, we may consider the measurement in the far field to be of good approximation.

This method has been expanded by allowing for the size of the field as well as for the change in field direction at the point of reception as dependent on the direction of the transmitting antenna axis. The derivation in chapter 2.3 shows that the field direction is in close relation to the electric properties of the medium through which the electromagnetic wave propagates.

Figures 2.13 and 2.14 show the results of measurement obtained at 3 kc/sec and 11 kc/sec at several distances from the transmitting antenna. Three curves are plotted in each polar diagram, for the distances 450 m, 720 m and 820 m. The scale along the periphery gives the angle of measurement ϑ . In radial direction, the receiving voltage was plotted in a logarithmic scale. The two components H_r and H_ϑ of interest (see Table 2.6) were obtained from the four points of measurement that correspond to four different ϑ values. Fig. 2.14 shows the predominance of the H_r component over the H_ϑ component even at a measuring frequency of 11 kc/sec and at a distance of 800 m. This means that the near field reaches far beyond this range. Taking into account that the wavelength in the St. Gertraudi dolomite at that frequency is at least 1 to 2 km, the above result is by no means surprising. As long as the distance of measurement is small as compared to the wavelength in rock, we cannot speak of a far zone.

Table 2.6

Voltage of reception in mv

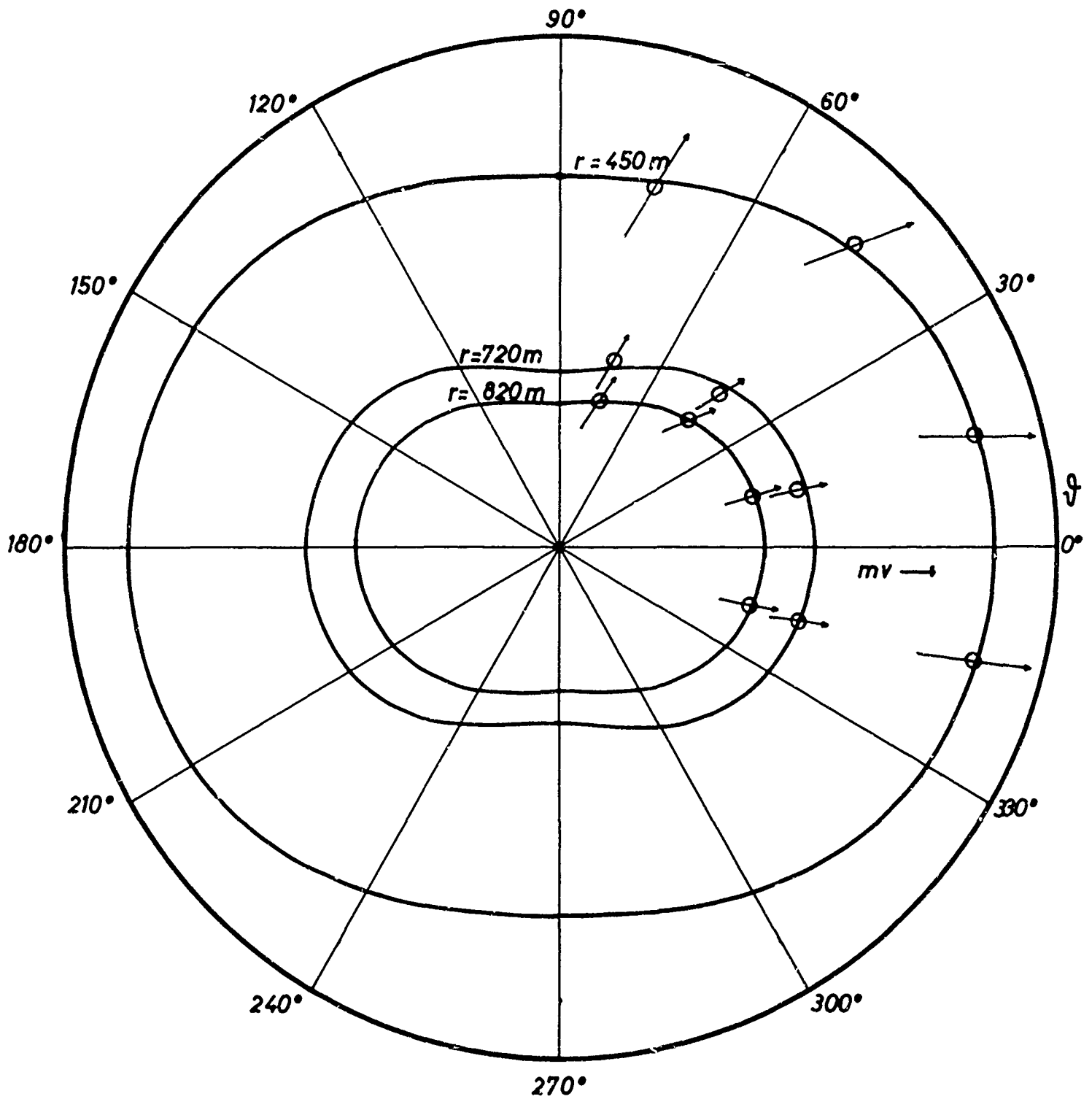
Frequency 3 kc/sec

$\vartheta/r =$	450 m	720 m	820 m
0°	30.37	7.54	4.90
30°	28.60	6.80	4.51
60°	21.50	4.99	3.60
90°	16.91	3.77	3.03

Frequency 11 kc/sec

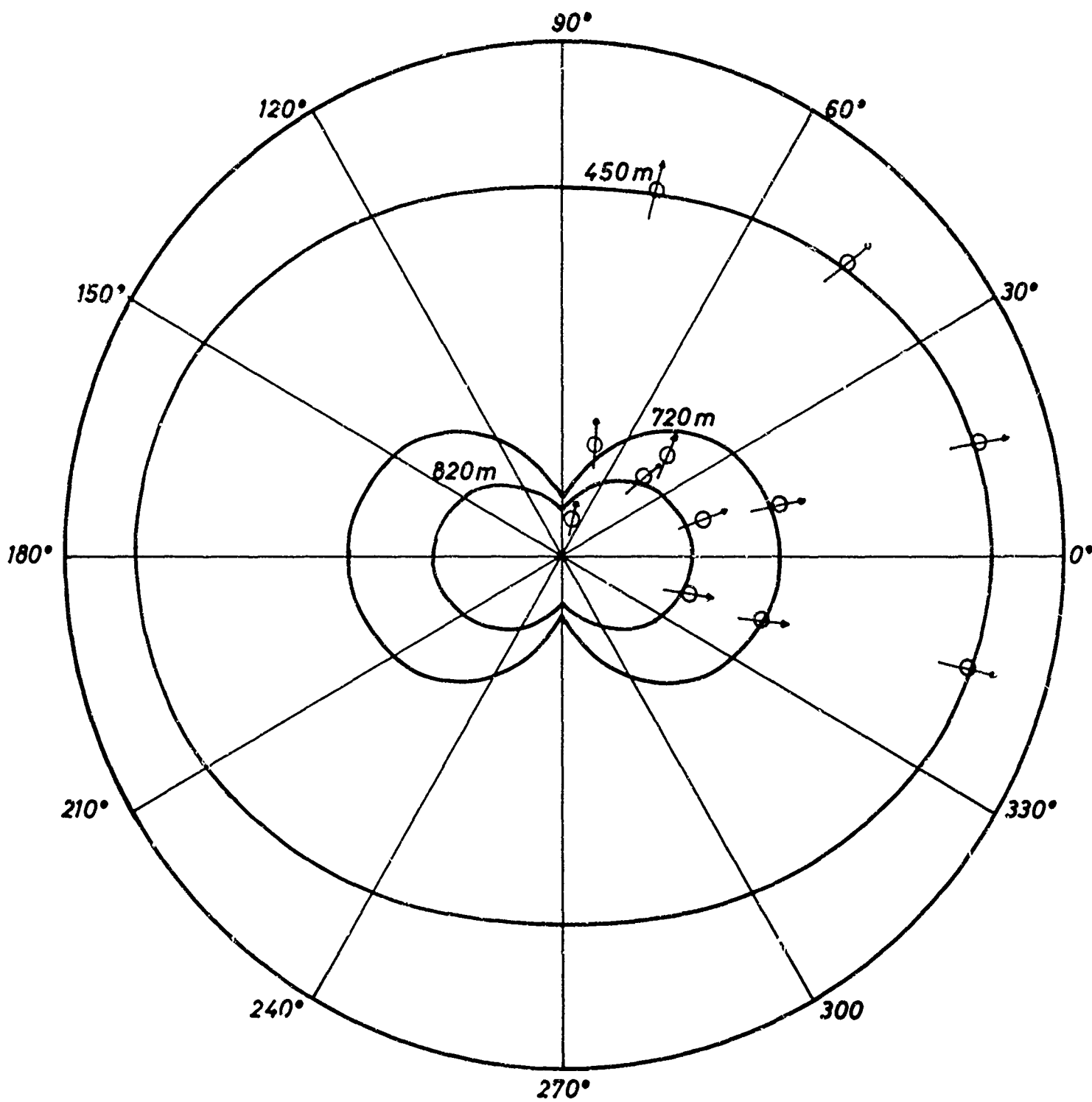
$\vartheta/r =$	450 m	720 m	820 m
0°	14.35	4.05	2.25
30°	13.30	3.55	2.07
60°	10.90	2.26	1.61
90°	9.45	1.15	1.33

The field directions which belong to every point of measurement and which fit well into the field line picture of a dipole, have been plotted in the two figures. The table 2.5 in chapter 2.3 gives a comparison of the direction of the transmitting antenna axis with the corresponding field directions. As this



scale:
 1 2 5 10
 frequency: 3 kcps

FIG. 2.13



scale :
 1 ——— 2 ——— 5 ——— 10
 frequency: 11 kcps

FIG. 2.14

measurement was conducted in the near field, a small angle of rotation χ of the field corresponds to the angle of rotation α of the transmitting antenna axis (see also Fig. 1.12 where the values measured at St. Gertraudi are plotted besides the curves derived theoretically).

In the foregoing sections it has been pointed out that a statement on the homogeneity of rock is possible by measuring the field direction. Whereas in former measurements only the quantity of the field strength vector determined by a conductivity that was averaged over the entire space, had been measured, the field may be distorted already by small spatial inhomogeneities. The measurements of St. Gertraudi, conducted in an almost homogeneous rock, are used as preliminary studies for a detailed investigation of the above problem. The next step will be similar measurements with the new and improved device in inhomogeneous or mineralized rock. In this connection, a study of the refraction of field lines along the rock - air interface might be of special interest. Such a study might make it possible that the propagation path of VLF waves can be followed when leaving the conducting earth's surface and entering the atmosphere. It has already been shown that a refraction occurs along this interface and that the field direction there is not consistent with the purely geometrical field direction that is expected. Because of the unsuited device, detailed measurements so far have not been possible. The sites of measurement at St. Gertraudi are well suited for such a program of measurement, as it is possible to conduct measurements in field direction below ground as well as along the rock -air interface. A change in measuring frequency of up to 100 kc/sec would also offer the possibility of studying the behavior at this conductivity discontinuity in the pure near field as well as in the far field. It is assumed that different effects will occur which are expected to be of great interest.

3. Conductivity measurements

3.1 Direct current measurements

In continuation of the studies discussed in the 1963 report, conductivity measurements with direct current were conducted also in 1964. The problem from what distance a on-ward the effect of the gallery space is negligibly small when applying the Wenner method, was solved. For this purpose, first a quantitative estimation regarding the required distance between the electrodes was made by means of an analytical representation of the flow pattern (section 3.1.1), secondly, the effect of the rock inhomogeneity on the result of measurement was studied by averaging over a large number of measurements conducted at different sites, and thus the result of estimation was checked by experiment (section 3.1.2). A strictly mathematical solution of the problem was found, but it has not been numerically evaluated up to date (section 3.1.3).

3.1.1 In Scientific Report Nr. 9 [8], an expression was derived giving the current distribution between two punctiform electrodes in a homogeneous full space. In the spherical coordinates r , φ and ϑ it reads:

$$j_r = \frac{I}{4\pi} \left(\frac{r - h \cos \vartheta}{\sqrt{r^2 + h^2 - 2rh \cos \vartheta}^3} - \frac{r + h \cos \vartheta}{\sqrt{r^2 + h^2 + 2rh \cos \vartheta}^3} \right)$$

$$j = 0 \quad (3.1.1)$$

$$j = \frac{I}{4\pi} \left(\frac{h \cdot \sin \vartheta}{\sqrt{r^2 + h^2 - 2rh \cos \vartheta}^3} + \frac{h \cdot \sin \vartheta}{\sqrt{r^2 + h^2 + 2rh \cos \vartheta}^3} \right)$$

From it we calculate the portion I_1 of the total current I which flows through a circle having the radius R and the center M , whose plane is perpendicular to the line connecting the two electrodes, i.e. $\vartheta = \frac{\pi}{2}$. For this case the following expression is valid:

$$i_r(r, \frac{\pi}{2}) = 0$$

$$j_r(r, \frac{\pi}{2}) = \frac{I \cdot h}{2\pi \sqrt{(r^2 + h^2)^3}}$$

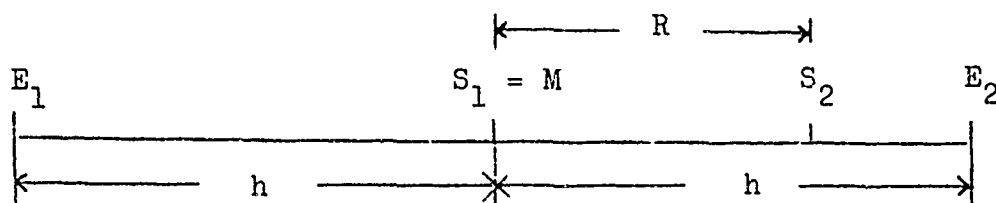
For I_1 we obtain:

$$I_1 = \int_0^{2\pi} \int_0^R \frac{I \cdot h}{2\pi \sqrt{(r^2 + h^2)^3}} r dr d\varphi = I \left(1 - \frac{h}{R^2 + h^2} \right) \quad (3.1.2)$$

Fig. 3.1.1 shows the quantity $b = \frac{I_1 \cdot 100}{I}$ which is the portion of the current I_1 (in percents) of the total current versus the quantity $R/2h$ which is the ratio between the radius of the circle on the one hand and the distance between the electrodes on the other. For $b = 10\%$ we have $R/2h = 0.25$. If the diameter of the gallery (1.5 m) is substituted for R , we obtain $2h = 6$ m. At that distance between the electrodes, in an undisturbed space, 90% of the current flows in the plane given by $\varphi = \pi/2$ and the point M outside a circle whose radius is equal to the diameter of the gallery. For a justified application of the full-space expression for the Wenner method, this distance of electrodes, however, is not sufficient, as the probes are too close to the electrodes where the disturbing effect of the gallery is larger than in the mentioned plane. In section 3.1.2 it is shown that the distance of electrodes for the Wenner method has to be at least 20 m. This would mean that in an undisturbed region (according to $R/2h = 1.5/20 \approx 0.075$) only 1% of the current would flow through the circle given by the diameter of the gallery. The study that follows below shows the suitability of the Wenner method which is favorable, because the relative error of voltage measurement becomes small owing to the great distance of the probes.

3.1.2 The voltage profile along the line connecting the electrodes and along a line at the opposite side of the gallery was measured and compared with the theoretical voltage profile for the corresponding conductivity. The measurement was made such that one voltage probe was fixed at M during the period of measurement,

the second one was fixed to the measuring points in between.



Using the denotations of the above Figure (see [2] , 1.10) the following relation is obtained for the conductivity:

$$\sigma = \frac{I}{2\pi U} \frac{R}{h^2 - R^2} \quad (3.1.3)$$

All σ values were calculated from the measured voltage values on the electrode side, and from them the arithmetic mean $\bar{\sigma}$ was calculated. For the mean value $\bar{\sigma}$, the theoretical curve of the voltage trend was plotted in a diagram.

Results of this measurement in the Morgenschlag (diameter 1.5 m) are represented in figs. 3.1.3, 3.1.5 and 3.1.6, where A is the calculated voltage trend for $\bar{\sigma}$, B is the voltage trend on the line connecting the electrodes, and C is the voltage trend on the opposite side.

The theoretical curve is in good agreement with the voltage trend on the connection line. The correct absolute value of conductivity will be obtained only if the voltage on the opposite side of the gallery is also equal to the calculated voltage. It is only then that the current distribution may be assumed to correspond to that of the homogeneous full space over the maximum portion of the space considered. For $2h = 18$ or 24 m, sufficient agreement is reached, whereas for $2h = 10$ m, the voltage between the probes at the electrode side is still twice the value of the voltage on the opposite side, when applying the Wenner method (locations of the probes in the dia-

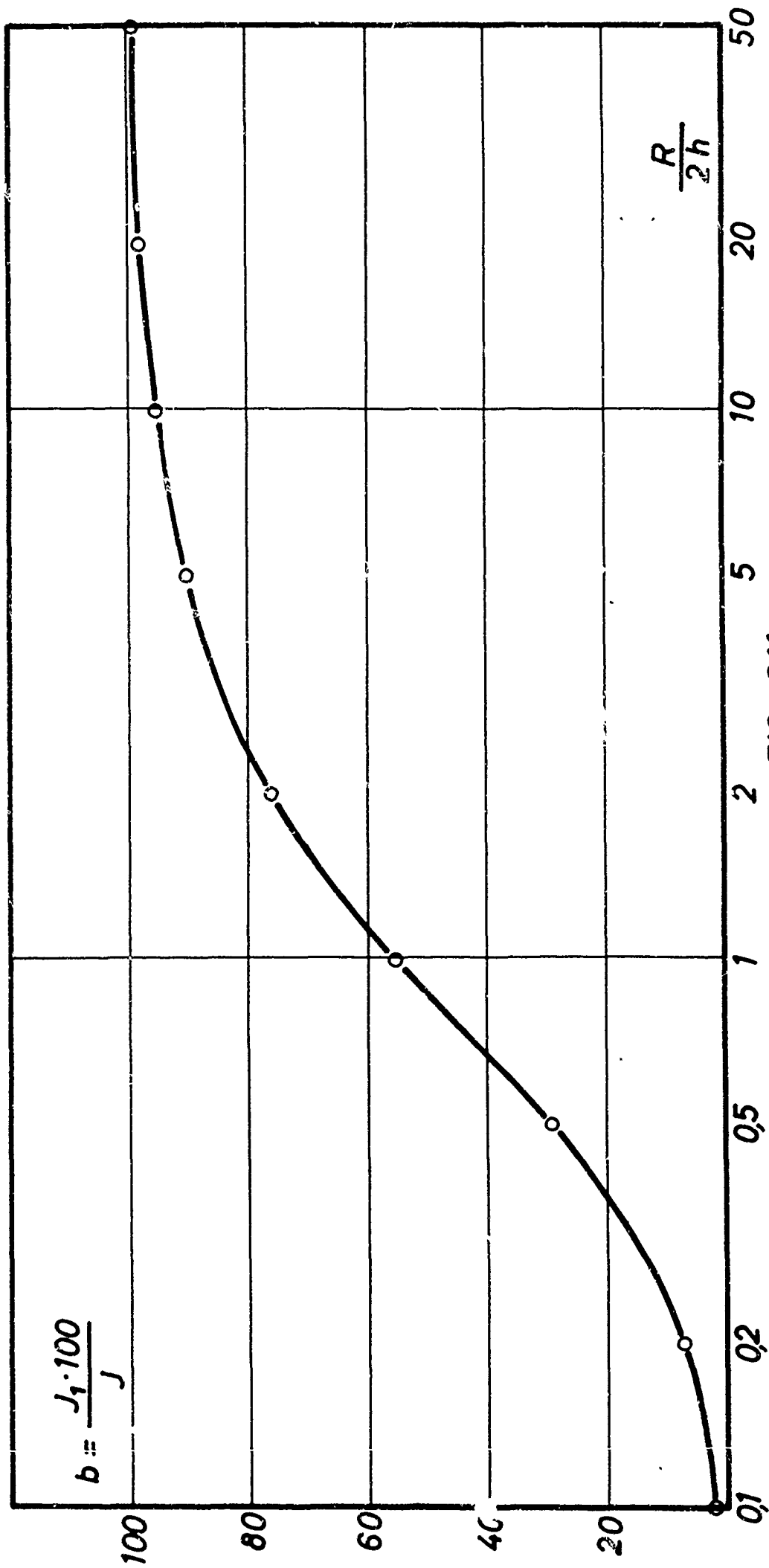


FIG. 311

MORGENSCHLAG

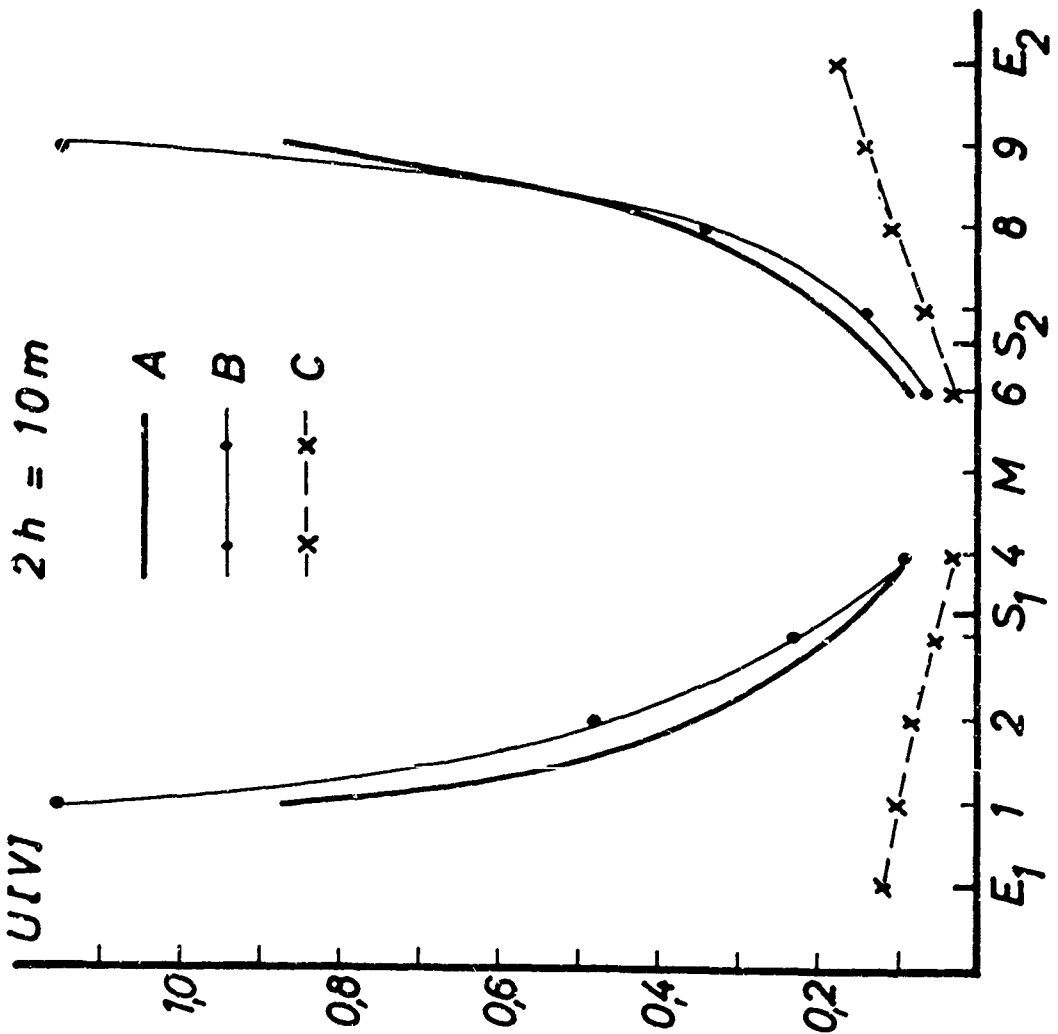


FIG. 313

GERTRAUDISTOLLEN

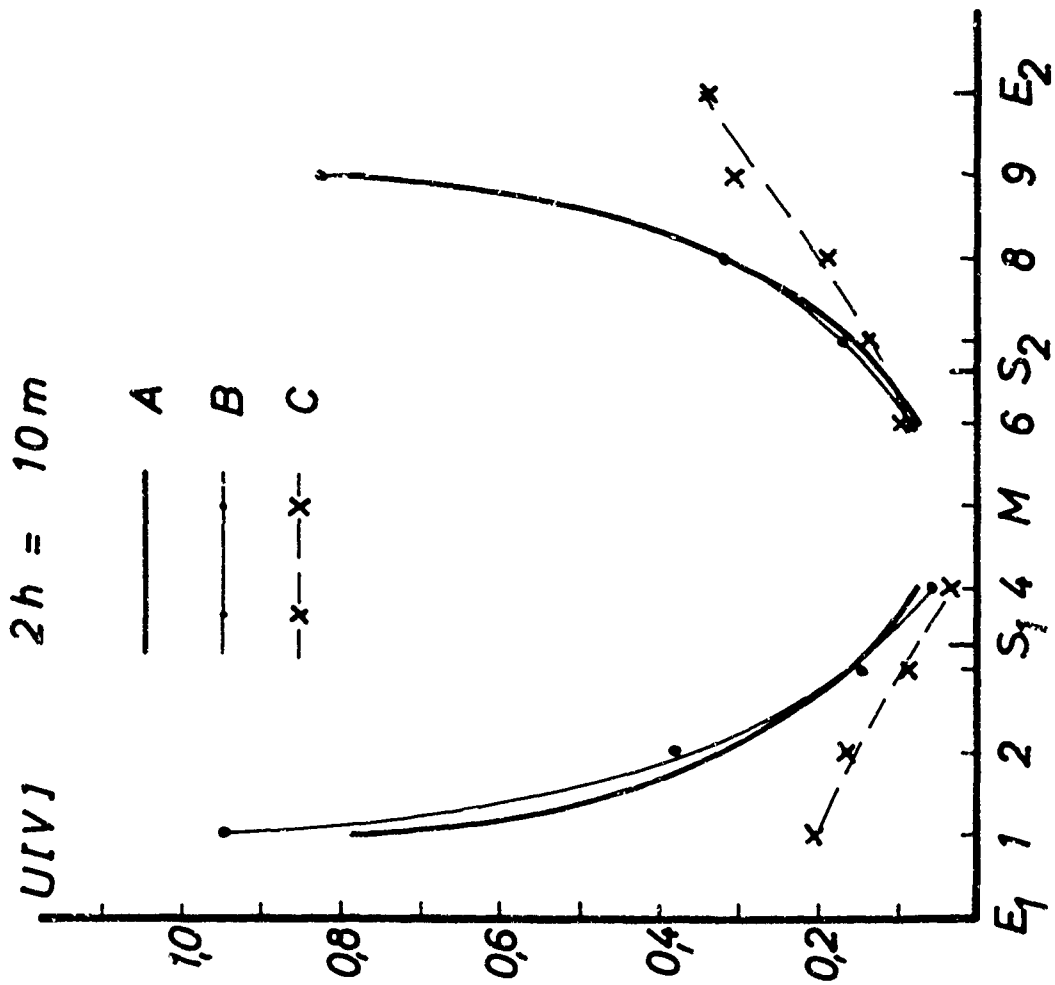


FIG. 314

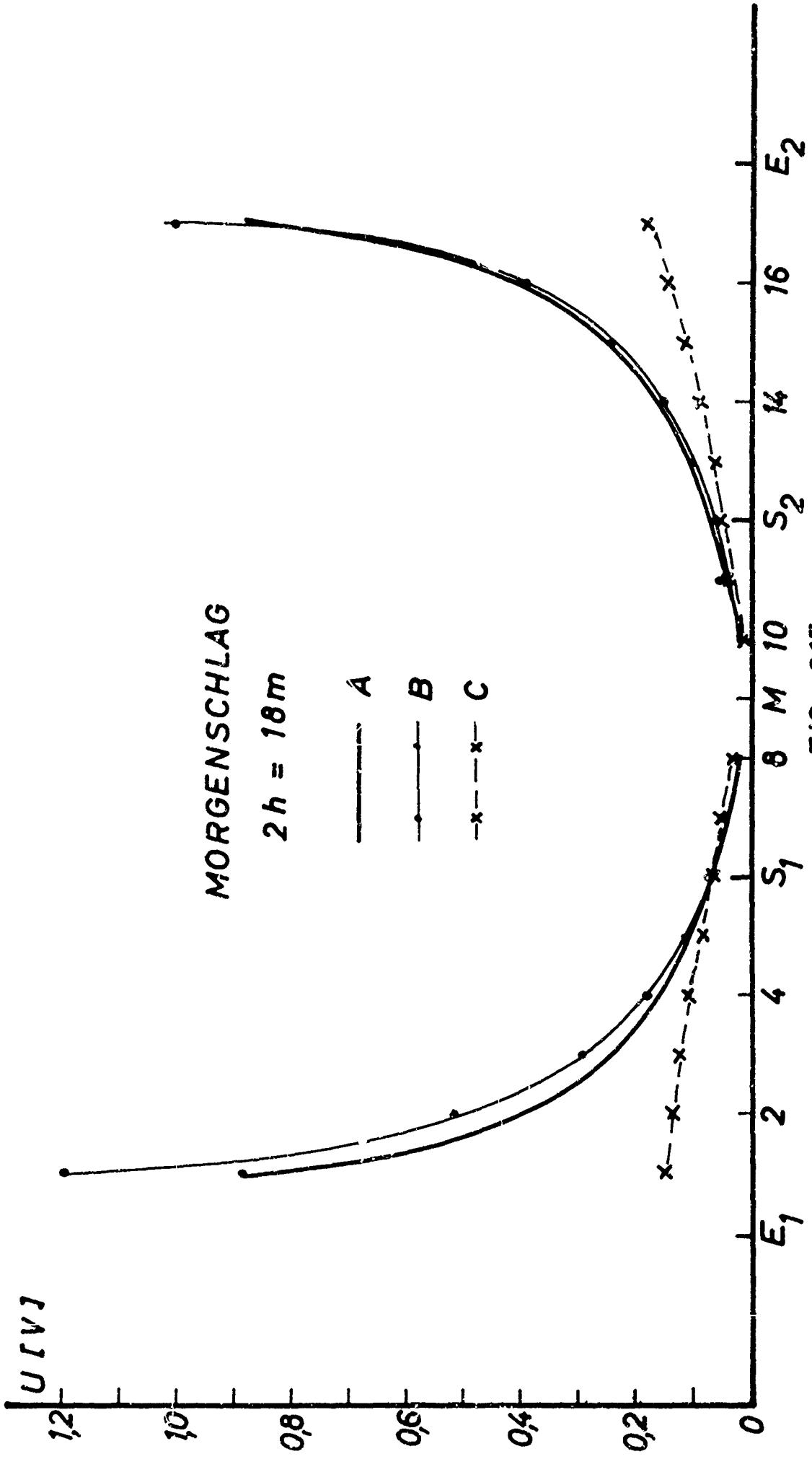


FIG. 3,15

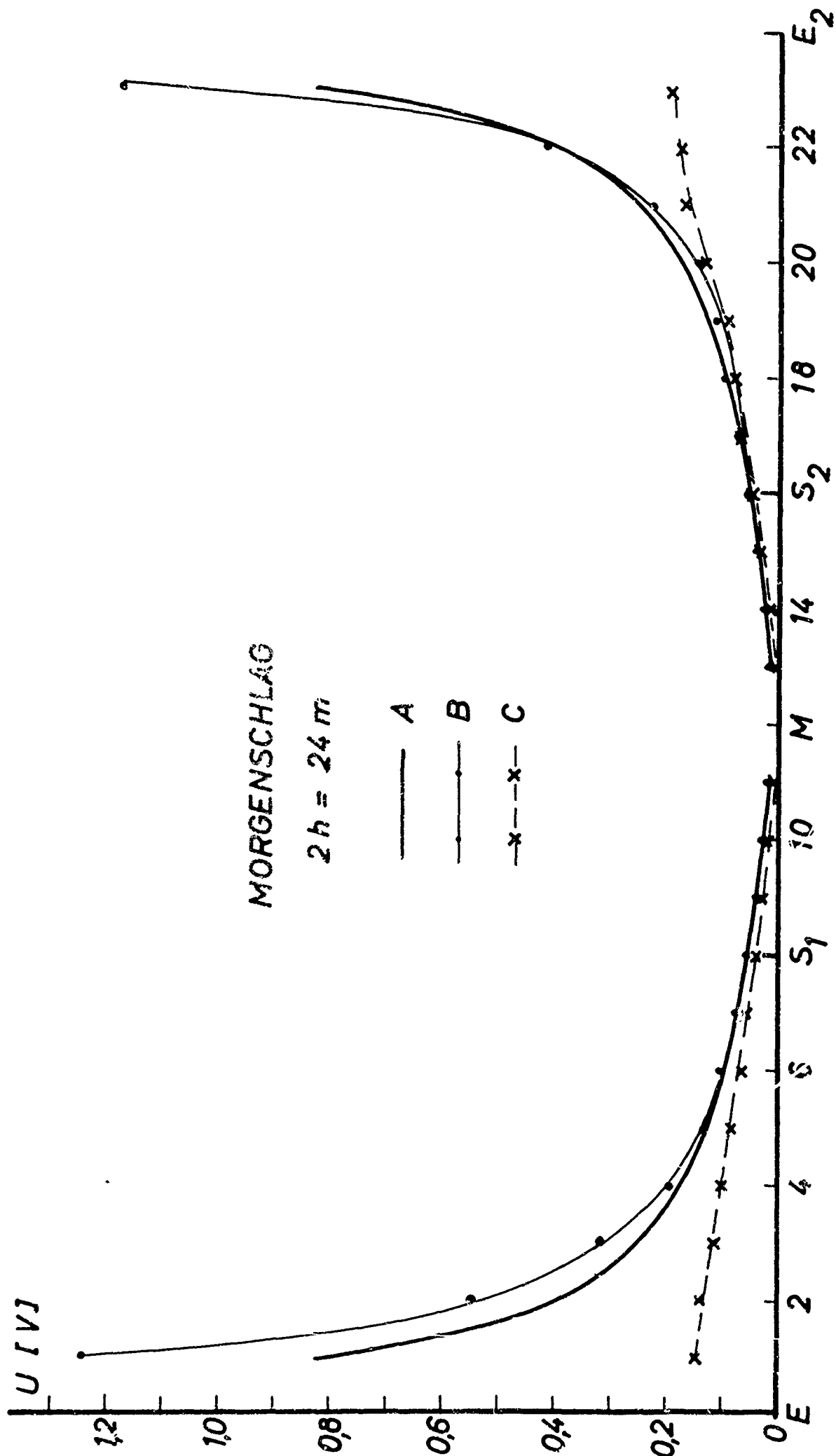


FIG. 316

gram are marked with arrows).

In the gallery at St. Gertraudi, whose cross section is much smaller, sufficient agreement is given already at $2h = 10$ m (Fig. 3.1.4).

The following measurement completes the obtained picture. For the Wenner method, the ratio U_E/U_G of the voltage between the probes on the electrode side, and the voltage on the opposite side was formed for different distances a (electrode current $I = 1$ ma). Fig. 3.1.7 gives all measured ratios U_E/U_G versus the distance a (Table 3.1.1). Furthermore, the mean value calculated from the measured values are plotted. The values measured for small a show considerable deviations due to the rock inhomogeneity. The values for $a = 5$ or 10 m were measured in the Westschlag whose dimensions correspond to those of the Morgenschlag. Here, the inhomogeneity apparently is stronger in the direction perpendicular to the gallery axis; this would explain the difference in the ratios U_E/U_G in Table 3.1.1, which occurs with the electrodes once being on one side of the gallery and then on the other side. This might also be the reason for the comparatively great deviation from unity.

The difference between the large and the small gallery which had been expected, becomes evident by the measurement. The deviation of the measured values, however, is equal for both galleries.

The conductivity measurements with direct current in the mines thus yield the following results: All sites of measurement show an inhomogeneity of rock that exists already in small regions. Therefore only a mean value of conductivity can be measured. For determining this mean value, the Wenner method proved to be well suited if the distance a is sufficiently large, under the present conditions $> 7-8$ m (diameter of the gallery 1.5 m). At that distance, the Wenner method is of sufficient accuracy also when small electrodes are used which are easy to fix.

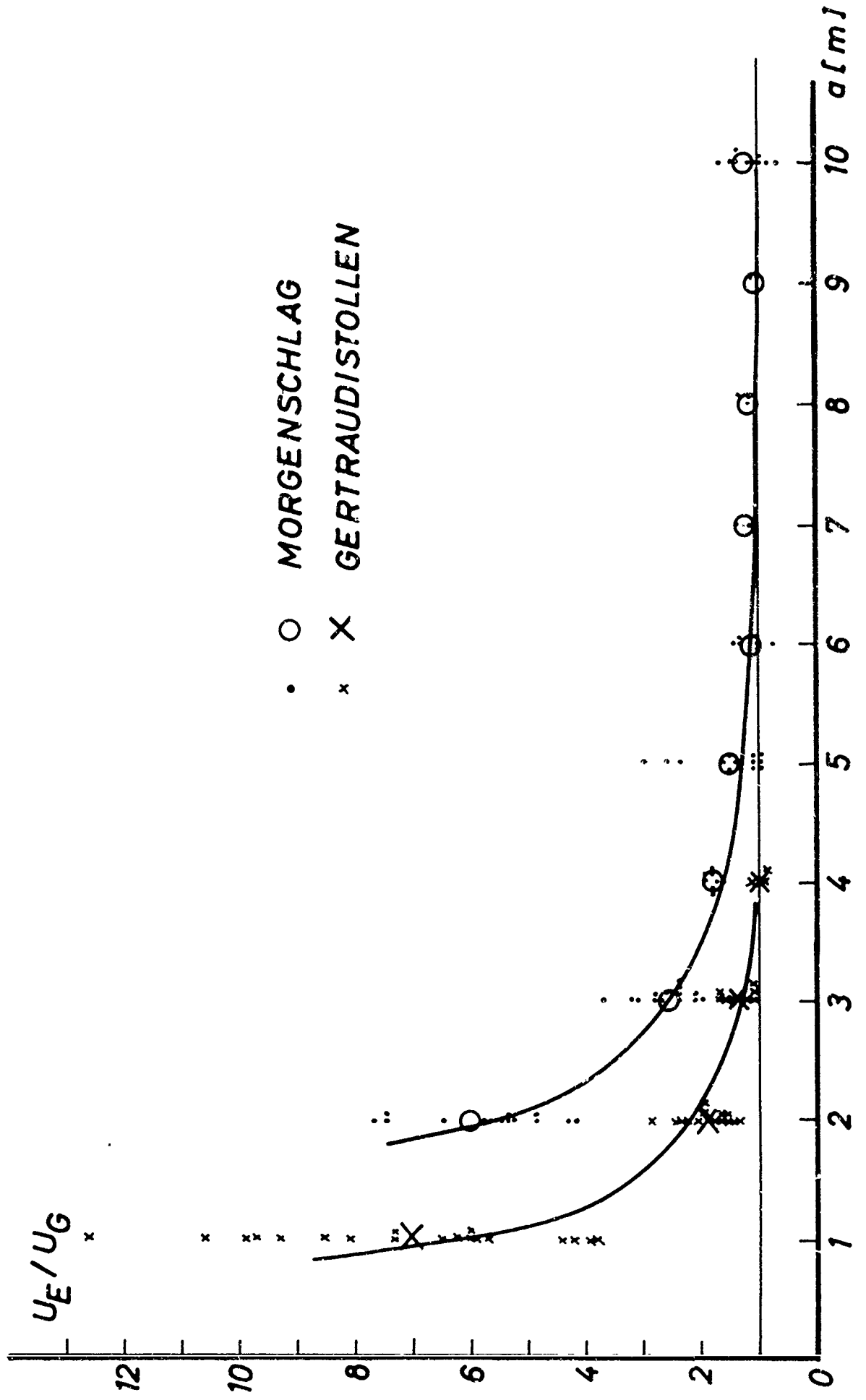


FIG. 317

Table 3.1 a

Morgenschlag, Westschlag

continued

M at	a	U_{E1}	U_{G1}	$\frac{U_E}{U_G}$	U_{E2}	U_{G2}	$\frac{U_E}{U_G}$
10.5	7	0.120	0.091	1.3	0.108	0.096	1.1
12	8	0.094	0.081	1.2	0.095	0.076	1.25
13.5	9	0.080	0.078	1.0	0.078	0.070	1.1
15	10	0.117	0.090	1.3	0.110	0.17	0.9
20	10	0.073	0.055	1.3	0.077	0.092	0.8
25	10	0.053	0.042	1.3	0.052	0.052	1.0
30	10	0.070	0.063	1.1	0.071	0.049	1.4
35	10	0.133	0.056	2.4	0.095	0.105	0.9
40	10	0.185	0.115	1.6	0.104	0.167	0.6

$$\frac{U_E}{U_G} = 1.22$$

Table 3.1 b

Gertraudistollen

M at	a	U_{E1}	U_{G1}	$\frac{U_E}{U_G}$	U_{E2}	U_{G2}	$\frac{U_E}{U_G}$
1.5	1	1.46	0.18	8.1	1.59	0.16	9.9
2.5	1	1.40	0.15	9.3	1.75	0.18	9.7
3.5	1	1.75	0.31	5.7	2.14	0.20	10.6
4.5	1	1.90	0.26	7.3	1.67	0.23	7.3
5.5	1	1.87	0.31	6.0	1.87	0.31	6.0
6.5	1	1.76	0.14	12.6	1.36	0.22	6.2
7.5	1	1.79	0.21	8.5	1.24	0.21	5.9
8.5	1	1.17	0.31	3.8	1.48		
9.5	1	1.51	0.39	3.9	1.30	0.20	6.5
10.5	1	1.01	0.244	4.2	1.06	0.24	4.4
3	2	0.85	0.40	2.1	0.72	0.31	2.3
4	2	0.67	0.42	1.6	0.96	0.40	2.4
5	2	0.66	0.37	1.8	0.82	0.42	2.0
6	2	0.91	0.36	2.5	0.60	0.35	1.7
7	2	0.65	0.22	2.9	0.60	0.39	1.5
8	2	0.84	0.53	1.6	0.66	0.38	1.7
9	2	0.52	0.36	1.4	0.62	0.31	2.0

$$\frac{U_E}{U_G} = 7.1$$

$$\frac{U_E}{U_G} = 1.96$$

Table 3.1 b

continued

Gertraudistollen

M at	a	U_{E_1}	U_{G_1}	$\frac{U_E}{U_G}$	U_{E_2}	U_{G_2}	$\frac{U_E}{U_G}$	
4.5	3	0.62	0.58	1.1	0.58	0.36	1.6	$\frac{\overline{U_E}}{\overline{U_G}} = 1.38$
5.5	3	0.43	0.28	1.5	0.46	0.38	1.2	
6.5	3	0.61	0.36	1.7	0.40	0.36	1.1	
7.5	3	0.47	0.27	1.7	0.40	0.35	1.1	
6	4	0.37	0.35	1.06	0.30	0.31	0.97	$\frac{\overline{U_E}}{\overline{U_G}} = 1.01$

3.1.3 Conductivity measurements by the potential distribution of steady currents

The current distribution of spherical electrodes (homogeneous full space) or semispherical electrodes (semispace) has been described in [8]. The current density \vec{j} was obtained as a gradient of the potential $\bar{\Phi}$

$$\vec{j} = -\text{grad } \bar{\Phi},$$

which can be found by elementary considerations and which must be a solution to the equation $\Delta \bar{\Phi} = 0$ with the corresponding boundary conditions. In [8] the possibility of determining the contact resistance between the electrodes and the medium has been discussed and the definition and determination of the penetration depth of the excitation was taken into account. The conditions that must be fulfilled for applying the expressions to the homogeneous semispace have also been discussed. The expressions considered in [8] thus hold for a plane interface in a homogeneous semispace. Measurements below ground,

however, were conducted in the gallery of a mine and it has been shown by experiment that a measurable excitation occurs on the opposite wall at least at large electrode distances. How far the potential lines and the depth of penetration are affected by the curvature of the gallery wall is to be shown in further studies. The gallery of the mine may approximately be looked upon as a cylinder of infinite length and the radius $\varrho = a$. The electrodes are to have a distance of $\varrho = \varrho_0$ from the cylinder axis and $z = z_0$ from the $z = 0$ plane (Fig. 3.1.8).

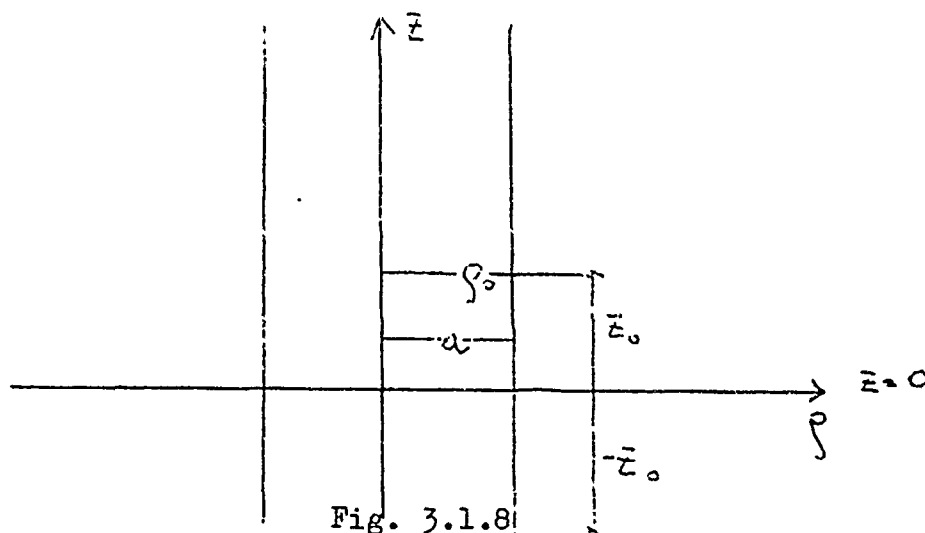


Fig. 3.1.8

Without the cylinder being present, their potential would be given by:

$$\Phi^{(1)} = I/4\pi \left[\frac{1}{(\varrho_1^2 + (z - z_0)^2)^{1/2}} - \frac{1}{(\varrho_1^2 + (z + z_0)^2)^{1/2}} \right] \quad (3.1.4)$$

If this is changed so that

$$\Phi = \Phi^{(1)} + \Phi^s, \quad (3.1.5)$$

where Φ^s is the stray field conditioned by the hollow cylinder, then Φ is a solution to the following boundary problem:

$$\Delta \Phi = 0 \quad (3.1.5a)$$

$$-\frac{\partial \Phi}{\partial \varrho} \Big|_{\varrho=a} = -\left(\frac{\partial \Phi^{(1)}}{\partial \varrho} + \frac{\partial \Phi^s}{\partial \varrho} \right) \Big|_{\varrho=a} = 0, \quad (3.1.5b)$$

thus,

$$\left. \frac{\partial \Phi(1)}{\partial \varrho} \right|_{\varrho=a} = - \left. \frac{\partial \Phi^S}{\partial \varrho} \right|_{\varrho=a} . \quad (3.1.5c)$$

(3.1.5c) follows from the fact that for $\varrho = a$ there cannot exist a component of the current density \vec{j} that is vertical to the cylinder mantle.

(3.1.5a) expressed in cylinder coordinates reads

$$\frac{\partial^2 \Phi}{\partial \varrho^2} + \frac{1}{\varrho} \frac{\partial \Phi}{\partial \varrho} + \frac{1}{\varrho^2} \frac{\partial^2 \Phi}{\partial \varphi^2} + \frac{\partial^2 \Phi}{\partial z^2} = 0 .$$

A particular integral of this relation is the following expression:

$$K_0(m\varrho_1)g(z) \quad (3.1.6a)$$

$$\varrho_1 = \sqrt{\varrho^2 + \varrho_0^2 - 2\varrho\varrho_0 \cos \varphi} \quad m \dots \text{separation parameter}$$

$$g(z) = \cos m(z - z_0) - \cos m(z + z_0)$$

$K_0(x)$... modified Neumann function.

It will be seen that the boundary condition $\varrho = a$ can be fulfilled with the formulation for Φ^S

$$\Phi^S = \int_0^\infty f_n(m) K_0(m\varrho_1) g(z) dm = \quad (3.1.6b)$$

$$= \sum_{n=0}^{\infty} \varepsilon_n (-1)^n \int_0^\infty f_n(m) K_n(m\varrho) I_n(ma) g(z) dm \cos n \varphi \quad (3.1.6c)$$

$I_n(x)$... modified Bessel function $\varepsilon_0 = 1, \varepsilon_n = 2$
 ε_n ... Neumann number $n = 1, 2, \dots$

and that the integrals of (3.1.6c) are convergent. (3.1.6c) follows from (3.1.6b) by applying the addition theorem

$$K_0(m\varrho_1) = \sum_{n=0}^{\infty} \varepsilon_n (-1)^n \cos n \varphi K_n(m\varrho) I_n(ma) , \quad (3.1.6d)$$

$$\varrho > a$$

For $\varrho = a$ the following expression is valid:

$$\begin{aligned}
 -\frac{\partial \Phi^s}{\partial \varrho} &= - \sum_{n=0}^{\infty} \varepsilon_n (-1)^n \int_0^{\infty} f_n(m) K_n'(ma) I_n(ma) mg(z) dm \cdot \cos n \varphi \\
 &= \frac{\partial}{\partial \varrho} \left[\frac{1}{\sqrt{\varrho_1^2 + (z - z_0)^2}} - \frac{1}{\sqrt{\varrho_1^2 + (z + z_0)^2}} \right]_{\varrho=a} \\
 &\quad \text{(except for the constant } 1/4\pi \text{ which is omitted here)} \\
 &= \frac{\partial}{\partial \varrho} \sum_{n=0}^{\infty} \varepsilon_n \cos n \varphi \int_0^{\infty} I_n(m\varrho) K_n(m\varrho_0) g(z) dm \Big|_{\varrho=a} \quad (3.1.7)
 \end{aligned}$$

For $mf_n(m)$ we thus obtain

$$mf_n(m) = (-1)^n \frac{K_n(m\varrho_0) I_n'(ma)}{K_n'(ma) I_n(ma)} \quad (3.1.7b)$$

Hence we have

$$\Phi^s = -\frac{1}{4\pi} \sum_{n=0}^{\infty} \varepsilon_n \cos n \varphi \int_0^{\infty} \frac{K_n(m\varrho_0) I_n'(ma)}{K_n'(ma)} K_n(m\varrho) g(z) dm \quad (3.1.8a)$$

This means that the total field $\bar{\Phi}$ is given by the expression

$$\begin{aligned}
 \bar{\Phi} &= \Phi^{(1)} + \Phi^s = \\
 &= \frac{1}{4\pi} \left[\frac{1}{\sqrt{\varrho_1^2 + (z - z_0)^2}} - \frac{1}{\sqrt{\varrho_1^2 + (z + z_0)^2}} \right] \\
 &\quad - \frac{1}{4\pi} \sum_n \varepsilon_n \cos n \varphi \int_0^{\infty} \frac{K_n(m\varrho_0) I_n'(ma)}{K_n'(ma)} K_n(m\varrho) g(z) dm \quad (3.1.8b)
 \end{aligned}$$

Choosing the integral representation for the first part of (3.1.8b) like that of (3.1.7), we may also write

$$\bar{\Phi} = \frac{1}{4\pi} \left\{ \sum_n \varepsilon_n \cos n \varphi \int_0^{\infty} K_n(m\varrho_0) I_n(m\varrho) g(z) dm - \right.$$

$$\begin{aligned}
& \left. - \sum_n \varepsilon_n \cos n \varphi \int_0^\infty \frac{K_n(m \varrho_0) I_n'(ma) K_n(m \varrho)}{K_n'(ma)} g(z) dm \right\} = \\
& = \frac{1}{4\pi} \sum_n \varepsilon_n \cos n \varphi \int_0^\infty \frac{K_n(m \varrho_0)}{K_n'(ma)} \left[I_n(m \varrho) K_n'(ma) - I_n'(ma) K_n(m \varrho) \right] g(z) dm .
\end{aligned} \tag{3.1.8c}$$

For $\bar{\Phi}$ we thus obtain an expansion into Fourier series in \cos

$$\bar{\Phi} = \frac{1}{4\pi} \sum_n \varepsilon_n \cos n \varphi A_n \tag{3.1.9}$$

whose coefficients $A_n(\varrho, z)$ are given by the integrals

$$A_n(\varrho, z) = \int_0^\infty \frac{K_n(m \varrho_0)}{K_n'(ma)} \left[I_n(n \varrho) K_n'(ma) - I_n'(ma) K_n(m \varrho) \right] g(z) dm . \tag{3.1.9a}$$

For $\varrho = a$, the parenthetical expression under the integral of (3.1.9a) becomes equal to the Wronski determinant $\Delta(I_n(ma), K_n(ma))$; its value is thus:

$$\Delta(I_n(ma), K_n(ma)) = - 1/ma . \tag{3.1.9b}$$

This is the problem which is of greatest interest. On the cylinder surface, the potential is given by the following expression:

$$\bar{\Phi}(a, z, \varphi) = - \frac{1}{4\pi a} \sum_n \varepsilon_n \cos n \varphi \int_0^\infty \frac{K_n(m \varrho_0) g(z)}{m K_n'(ma)} dm . \tag{3.1.9c}$$

The convergence of the integrals in (3.1.9c) is easy to prove.

Writing

$$\begin{aligned}
A_n(a, z) & \sim \int_0^\infty \frac{K_n(m \varrho_0) g(z)}{m K_n'(ma)} dm = \\
& = \int_0^M \cdot / \cdot dm + \int_M^\infty \cdot / \cdot dm = J_1 + J_2, \tag{3.1.10}
\end{aligned}$$

the estimation

$$\begin{aligned}
 |J_2| &= \left| \int_M^\infty \frac{K_n(m\rho_0)g(z)}{mK'_n(ma)} dm \right| \leq \\
 &\leq \int_M^\infty \left| \frac{K_n(m\rho_0)}{mK'_n(ma)} \right| |g(z)| dm \leq \int_M^\infty \left| \frac{K_n(m\rho_0)}{mK'_n(ma)} \right| dm \quad (3.1.10a)
 \end{aligned}$$

is obtained for J_2 ; if M is sufficiently large, we may use the asymptotic expression for K_n and K'_n .

$$\begin{aligned}
 K_n(m\rho_0) &\longrightarrow \sqrt{\frac{2}{\pi m\rho_0}} e^{-m\rho_0} \\
 K'_n(ma) &\longrightarrow \sqrt{\frac{2}{\pi ma}} e^{-ma}.
 \end{aligned}$$

Thus,

$$J_2 \leq \int_M^\infty \frac{e^{-m(\rho_0 - a)}}{m} dm \sqrt{\frac{a}{\rho_0}} \quad (3.1.10b)$$

this integral being convergent für $\rho_0 \neq a$. As the integrand in J_1 stays finite, i.e. Cauchy's principal value exists for $n = 0$, convergence is guaranteed. The current passing through a circular plane having the radius R in the plane $z = 0$, is a measure for the depth of penetration. This current is given by

$$\begin{aligned}
 J(R) &= -\frac{I}{4\pi} \int_0^{2\pi} \int_a^R \frac{\partial \Phi}{\partial z} \rho d\rho d\varphi \quad (3.1.11) \\
 &= -\frac{I}{4\pi} \int_0^{2\pi} \sum_n \varepsilon_n \cos n\varphi \int_a^R \frac{\partial A_n}{\partial z} \Big|_{z=0} \rho d\rho d\varphi = \\
 &= -\frac{I}{2} \int_a^R \frac{\partial A_0}{\partial z} \rho d\rho
 \end{aligned}$$

$$J(R) = \frac{I}{2} \int_a^R \int_0^\infty \frac{K_0(m\rho_0)}{K'_0(ma)} \left[I_0(m\rho)K'_0(ma) - I'_0(ma)K_0(m\rho) \right] m \sin mz_0 \cdot dm \rho d\rho. \quad (3.1.11a)$$

The latter expression (3.1.11b) is valid only for $\rho < \rho_0$. For $\rho > \rho_0$ the incident field $\Phi^{(1)}$ reads:

$$\Phi^{(1)} = \sum \epsilon_n \cos n\varphi \int_0^\infty I_n(m\rho_0) K_n(m\rho) g(z) dm$$

yielding

$$\begin{aligned} J(R) &= - \int_a^{\rho_0} \int_0^{2\pi} \frac{\partial \Phi}{\partial z} \rho d\varphi d\rho - \int_{\rho_0}^R \int_0^{2\pi} \frac{\partial \Phi}{\partial z} \rho d\varphi d\rho \\ &= \frac{I}{2\pi} \int_0^\infty \frac{K_0(m\rho_0)}{K'_0(ma)} \left[K'_0(ma) (\rho_0 I_1(m\rho_0) - a I_1(ma)) - \right. \\ &\quad \left. - I'_0(ma) (a K_1(ma) - \rho_0 K_1(m\rho_0)) \right] \sin mz_0 dm + \\ &\quad + \frac{I}{2\pi} \int_0^\infty \frac{I_0(m\rho_0) K'_0(ma) - K_0(m\rho_0) I'_0(ma)}{K'_0(ma)} \cdot \left[\rho_0 K_1(m\rho_0) - \right. \\ &\quad \left. - RK_1(mR) \right] \sin mz_0 dm. \quad (3.1.12) \end{aligned}$$

The expressions (3.1.12) and (3.1.9c) can now be evaluated numerically which is planned to be done in the near future.

3.2 Measurements with samples

3.2.1 The frequency dependence of ϵ and ϵ' was measured by means of rock samples. The measuring arrangement used is described in [2]. It was studied whether the samples have a high surface conductivity. For this purpose, a guard ring capacitor was used. Since, however, the results with and without guard ring are consistent,

the rest of the measurements were conducted without a guard ring as balancing the guard ring circuit is very time consuming.

The results of the measurement were evaluated by K.W. Wagner's [9] dispersion theory. In this theory it is assumed that the frequency dependence of ϵ and δ is determined not by a single relaxation time τ , but by a relaxation function $\varphi(\tau)$. τ changes continuously from 0 to ∞ , whereas $\varphi(\tau)$ is determined by the distribution function $k(\tau)$ of the relaxation times. Wagner assumes that the distribution of τ is governed by a probability function. He assumes a distribution of the relaxation times round about a predominant relaxation time τ_0 , the density of the distribution being given by the distribution constant b . Wagner's distribution function has the following form:

$$k(\tau)d\tau = \frac{k \cdot b}{\sqrt{\pi}} e^{-b^2 z^2} dz \quad (3.2.1)$$

This leads to a relaxation function $\varphi(\tau)$

$$\varphi(\tau) = \frac{k \cdot b}{\sqrt{\pi} \tau_0} \int_{-\infty}^{\infty} e^{-b^2 z^2 - z - (\tau/\tau_0)e^{-z}} dz \quad (3.2.2)$$

with the quantities

$$\begin{aligned} z_0 &= \ln \omega \tau_0 \\ z &= \ln \tau / \tau_0 \end{aligned}$$

By means of this relaxation function we obtain the following expression for the real part and for the imaginary part of the complex dielectric constant ϵ^x :

$$\begin{aligned} \epsilon' &= \epsilon_{\infty} \left[1 + \frac{k \cdot b}{\sqrt{\pi}} e^{-b^2 z_0^2} \int_0^{\infty} e^{-b^2 n^2} \cdot \frac{\cosh(2b^2 z_0 - 1)n}{\cosh n} dn \right] \\ \epsilon'' &= \frac{\epsilon_{\infty} \cdot k \cdot b}{\sqrt{\pi}} e^{-b^2 z_0^2} \int_0^{\infty} e^{-b^2 n^2} \frac{\cosh 2b^2 z_0 n}{\cosh n} dn \end{aligned} \quad (3.2.3)$$

with $n = z + z_0 = \ln \omega \tau$.

These expressions contain four constants, each having a physical meaning: ϵ_{∞} , b , τ_0 and k . ϵ_{∞} is the dielectric constant at optical frequencies, b gives, as has already been said, the density of distribution of relaxation times about the predominating value τ_0 . For τ_0 the following expression is valid:

$$\tau_0 = \frac{1}{2\pi f_m} \quad (3.2.4)$$

with f_m being the frequency at which ϵ'' has a maximum. k is a measure for the total dispersion, since

$$\epsilon_c = \epsilon_{\infty}(1 + k) \quad \text{or} \quad k = \frac{\epsilon_0 - \epsilon_{\infty}}{\epsilon_{\infty} \cdot k} \quad (3.2.5)$$

for all values of b at $\omega = 0$.

A good reproduction of the experimental data by this theory would prove that the measurement was not affected by any disturbing factors such as for example those that may occur by electrode polarization.

For examining experimental data on the basis of Wagner's theory, W.A. Yager presented a graphic method that has been applied in the present study [10].

3.2.2 Graphical method by W.A. Yager:

A new variable δ defined by $\delta = \epsilon''_a / \epsilon''_x$ is introduced, with $\epsilon''_a = \epsilon''$ at $f(a)$ and $\epsilon''_x = \epsilon''$ at $f(x)$.

For $f_x > f_m$ we choose $f(a) = 10 f(x)$, then we have $\delta < 1$. For z_x we obtain

$$z_x = \ln f_x / f_m .$$

For a given frequency ratio, δ is independent of ϵ_{∞} and k , but is a function of b and z_x . Yager calculated δ as dependent on b for various values of z_x . From two experimental δ values we may thus plot two curves z_{x_1} versus b yielding a point of intersection, b and z_{x_1} and f_m , respectively, are determined by this point of intersection. Furthermore, Yager calculated the

curves $\epsilon''/\epsilon_{\infty}k$ and $(\epsilon' - \epsilon_{\infty})/\epsilon_{\infty}k$ for values of $b \leq 2$ and for different values of z_0 . For the value of b , which has already been determined, the curves calculated by Yager yield $\epsilon''/\epsilon_{\infty}k$ and $(\epsilon' - \epsilon_{\infty})/\epsilon_{\infty}k$ for different z_0 values. For equal frequency values f we then plot $\epsilon''/\epsilon_{\infty}k$ versus ϵ''_{exp} and $(\epsilon' - \epsilon_{\infty})/\epsilon_{\infty}k$ versus ϵ'_{exp} . If the experimental data can be represented by Wagner's theory, two parallel lines must be obtained whose slope is given by $\epsilon_{\infty}k$. The point of intersection of the ordinate with the straight line for ϵ' yields the value of ϵ_{∞} . Thus, all constants of Wagner's theory are determined.

3.2.3 Experimental measurements:

The 716-C General Radio capacitance bridge was used for the measurements applying a substitution method. The first balancing was made with the grounded plate of the capacitor altogether removed, i.e. only the intrinsic capacitance C_s of the measuring capacitor being connected. According to the expression given in the General Radio 716-C Capacitance Bridge Manual we obtain:

$$C' = C_P - C_s$$

C_P ... constant capacitance in the second bridge branch. For the second balancing, the capacitor contained the sample:

$$C = C_P - (C_m + C_s).$$

According to expression (5) of the Manual we obtain

$$C_x = \Delta C = C' - C = C_m,$$

and for the real part ϵ' of the complex dielectric constant:

$$\epsilon' = \frac{C_m}{C_0} = \frac{\Delta C}{C_0}.$$

C_0 was calculated from the geometrical dimensions of the sample. For the loss factor D_x the following expression is valid:

$$D_x = \frac{C'}{\Delta C} \cdot (D - D') = \frac{C'}{\Delta C} \cdot D, \quad (3.2.7)$$

as D' was zero in all measurements.

The complex dielectric constant has the form

$$\epsilon^* = \epsilon' - i\epsilon'',$$

the loss factor

$$\tan \delta = D_x = \frac{\epsilon''}{\epsilon'}.$$

If (3.2.6) is substituted,

$$\epsilon'' = \epsilon' \cdot D_x = \frac{\Delta C}{C_0} \cdot \frac{C'}{\Delta C} \cdot D = \frac{C'}{C_0} \cdot D \quad (3.2.8)$$

is obtained for the imaginary part of the complex dielectric constant. As the curves calculated by Yager comprise only a certain range of frequencies, which depends on f_m , not all curves could be evaluated. Especially the humid samples that are most similar to the natural state of the rock are unsuited for an evaluation; their D values are very high at low frequencies, therefore they cannot be measured with the available bridge. Very dry samples for which f_m is much smaller than 1 cps are also unsuited for evaluation, as the measuring bridge cannot be used for $f < 30$ cps. For medium values of humidity, however, all four constants of Wagner's theory could be determined.

In the present report the result of measurement obtained with a dolomite sample that was studied at seven different values of humidity, shall be discussed. Humidity was changed in the same way as described in [11]. In [11] it was stated that especially the humid samples showed certain difficulties in reproducing the measured values as well as a considerable change of the measured value during the measurement. This could be avoided by storing the samples for several days in a room of constant absolute atmospheric moisture. In order to increase the moisture content of the samples, the absolute atmospheric moisture was increased by raising the temperature, the relative

atmospheric moisture being kept at 100%. Attention must be paid to the fact that the samples had to be stored under constant conditions for a sufficient period of time in order to keep them uniform as to their moisture content.

The sample discussed here is a dolomite sample of low porosity. It was first dried (measurement 1) and then stored in a humid atmosphere (measurements 2 - 6). Then the sample was kept under water for one week (measurement 7). Keeping the sample under water for a longer period did not increase its water content. The amount of contained water was determined by weighing, it is expressed by the value $p = \frac{\Delta G \cdot 100}{G}$

$$G = G_1 = \text{weight of the dry sample}$$

$$\Delta G = G_N - G.$$

3.2.4 Results of measurement

The results of the seven measurements of the sample D₃ (dolomite) at different values of water content are shown in Figs. 3.2.1, 3.2.2 and 3.2.3, respectively, ϵ' , ϵ'' and σ being plotted versus the frequency f . The values for σ are obtained from those for ϵ'' calculated from the complex dielectric constant.

$$\epsilon^* = \epsilon_0 (\epsilon' - j\epsilon'') = \epsilon_0 \left(\epsilon' - j \frac{\sigma}{\omega \epsilon_0} \right).$$

This yields:

$$\sigma = \epsilon'' \cdot \epsilon_0 \cdot \omega \quad (3.2.9)$$

The σ values were plotted to make possible a comparison with the measured values of [2]. At all humidity values, σ was found to increase with frequency, but the increase becomes smaller as the water content increases. This fact might be an explanation of the observation that the conductivity measurements made in solid rock (section 3.3) and the measurements reported in [12] and [13] do not remarkably depend on the frequency, since it is not known whether the water content of the sample after the treatment required for its production can be restored to its

original value. At a further increase in humidity, an even smaller increase of δ with frequency is possible.

All four constants of Wagner's theory could be determined only for the measurements Nr. 3, 4, 5 and 6. For measurement Nr. 1 (dry sample), only the value of b could be estimated, whereas for Nr. 2 an estimation was possible also for f_m . The estimation given for measurement Nr. 7 (after saturation in water) is very unexact, since the diagram b versus z_x gives a grazing intersection.

In 3.2.2 it has already been mentioned that the straightness of the curves $\epsilon''/\epsilon_\infty k$ versus ϵ''_{exp} and $(\epsilon' - \epsilon_\infty)/\epsilon_\infty k$ versus ϵ'_{exp} is a measure of the accuracy with which Wagner's equations explain the experimental data. For measurements Nr. 3, 4, 5 and 6 the respective diagrams are shown in Fig. 3.2.4. The points of measurement all lie on a straight line with sufficient accuracy to make possible the determination of ϵ_∞ and k . The results are summarized in Table 3.2.1. The first column gives the number N of the measurement, the second one the weight G of the sample, the third one the increase in weight P in percents as compared to the weight G_1 of the dry sample.

Table 3.2.1

N	G [g]	P [%]	b	f_m (cps)	ϵ_∞	k
1	34.9518	0	≈ 0.10	.		
2	34.9523	0.00143	0.12	0.017		
3	34.9531	0.00372	0.19	0.36	9.2	27.8
4	34.9560	0.0120	0.24	11	11	24.4
5	34.9563	0.0129	0.26	41	16	14.7
6	34.9569	0.0146	0.29	81	17	11.8
7	35.0157	0.183	> 1.0	≈ 800 cps		

The table shows that the four constants of Wagner's theory depend on the water content of the rock. The value b giving the density

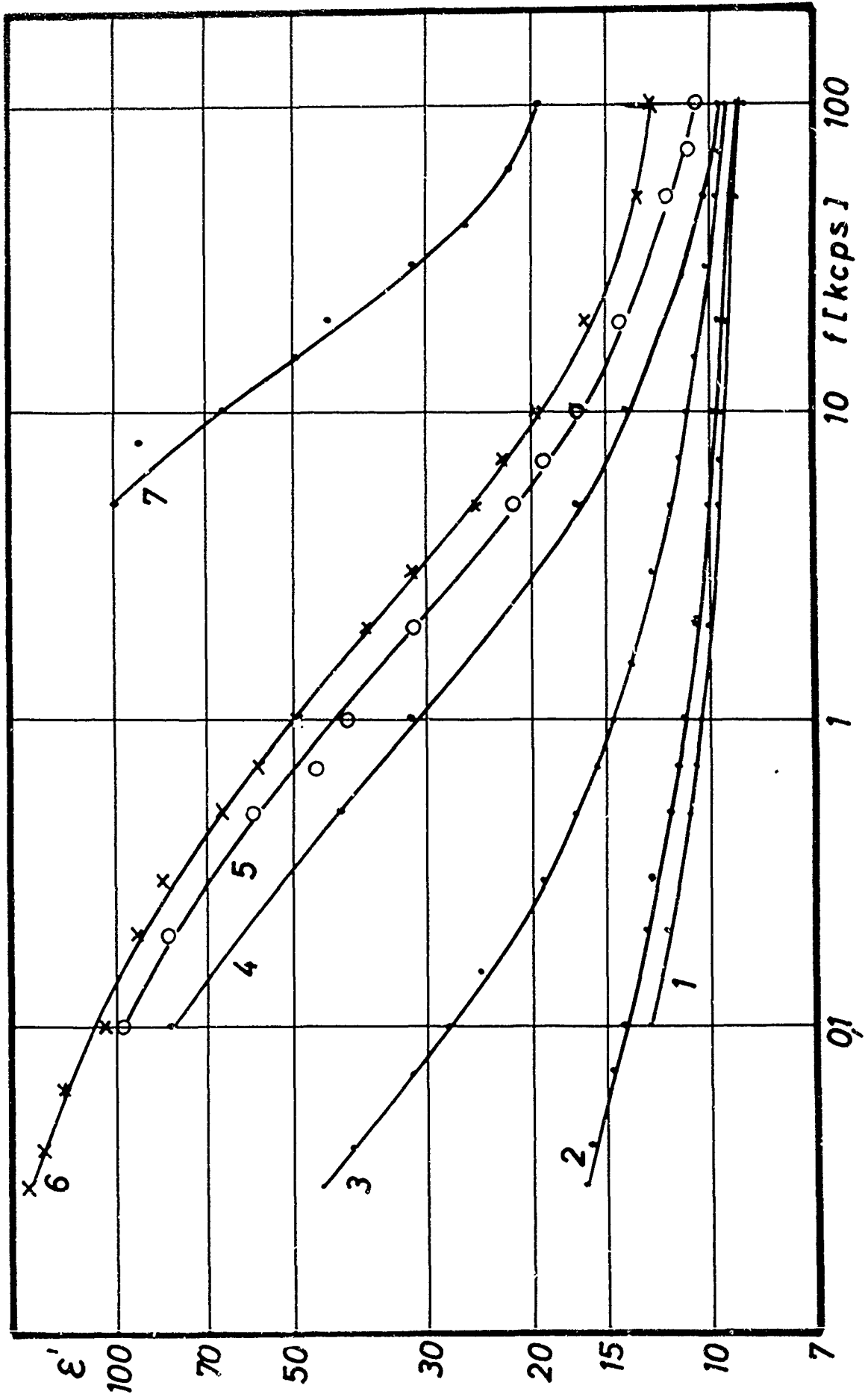


FIG. 3,21

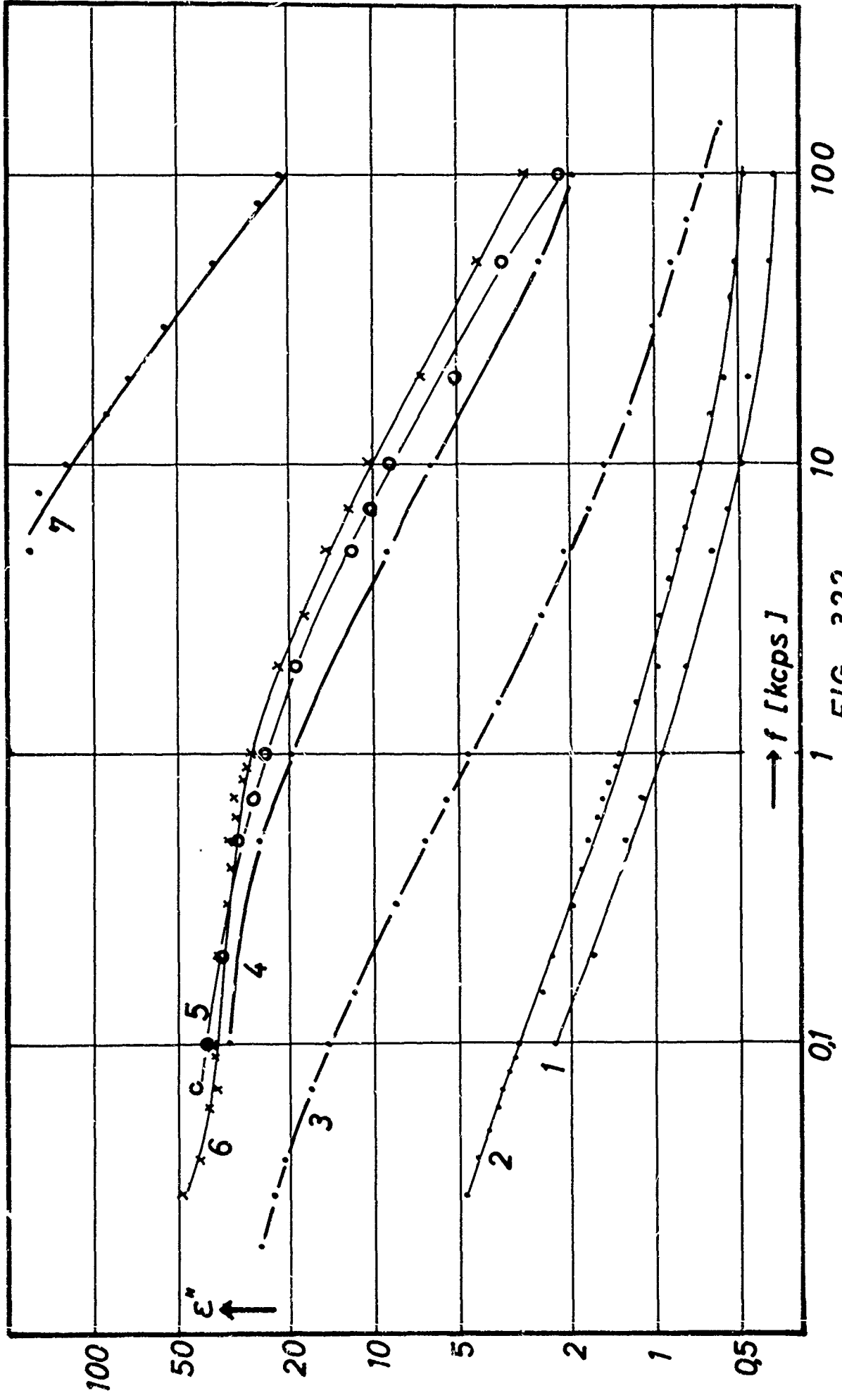


FIG. 3,22

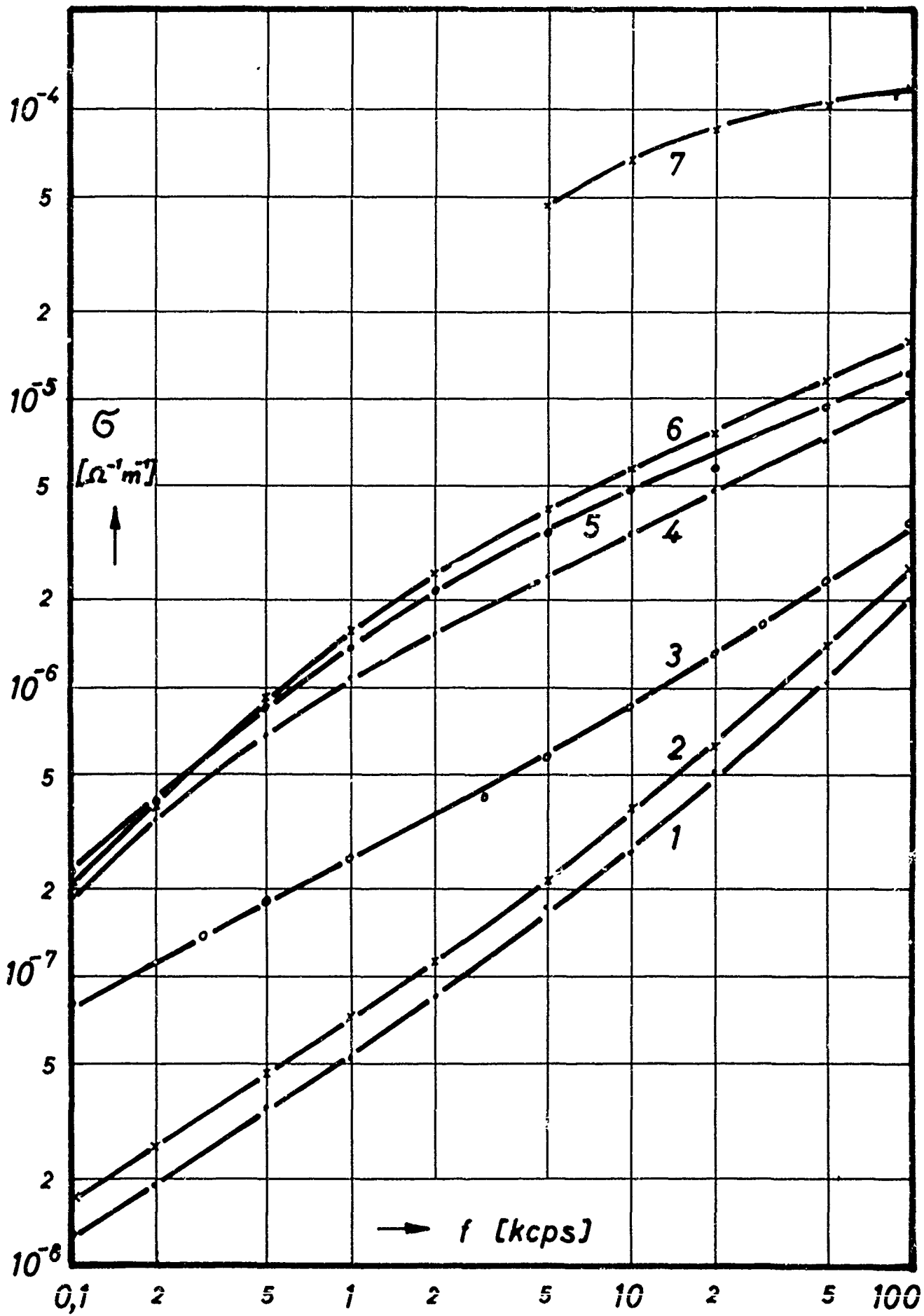


FIG. 3,23

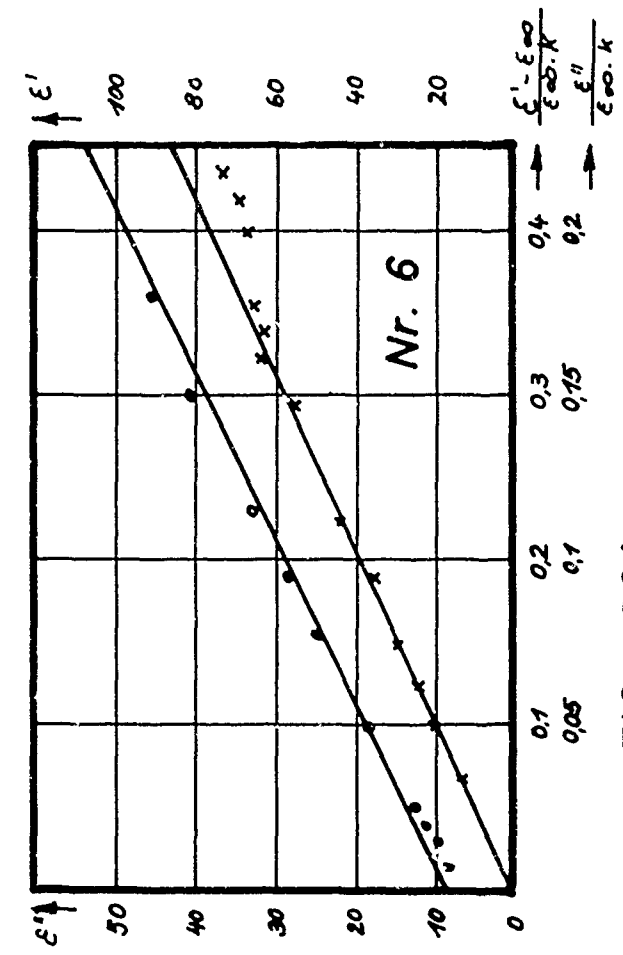
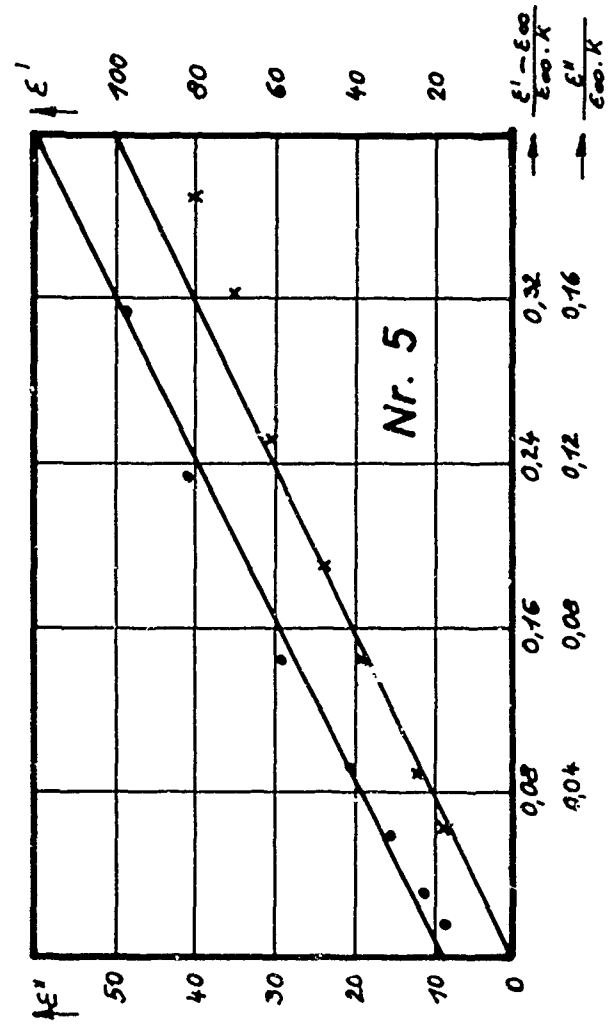
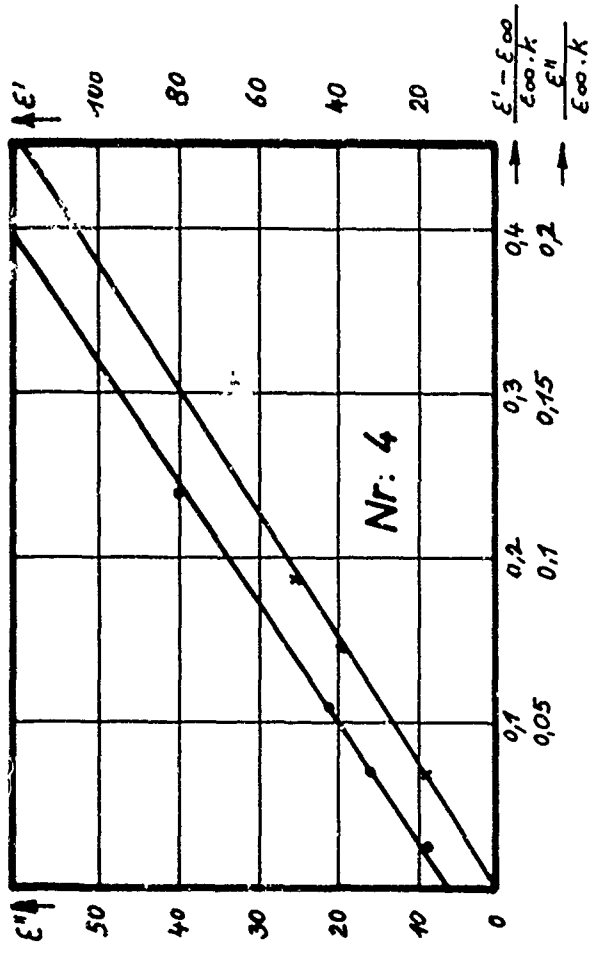
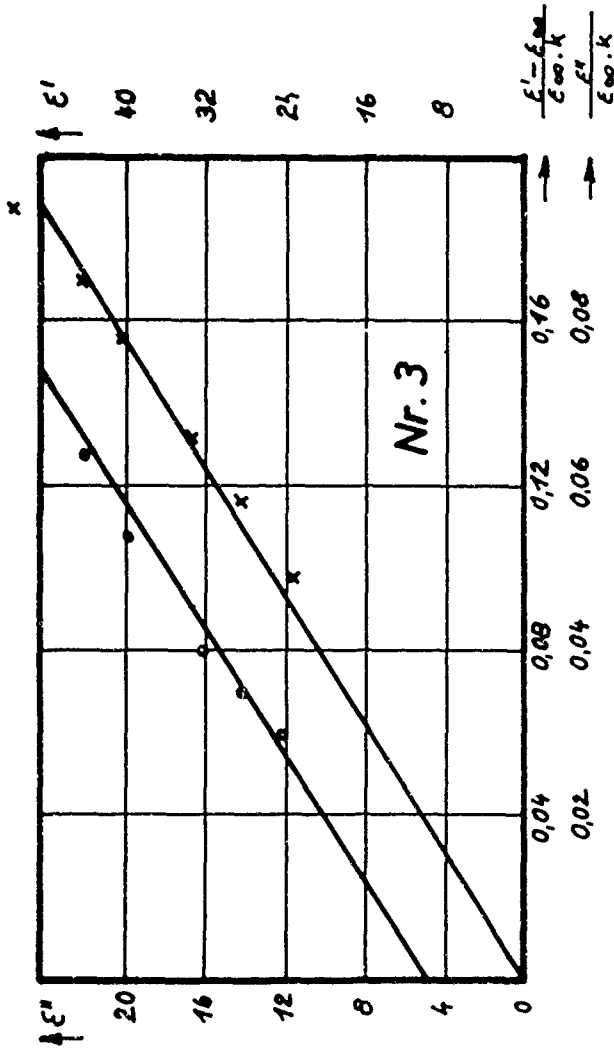


FIG. 3,24

of the distribution of relaxation times about the predominating value τ_0 increases with the moisture content. This corresponds to a decrease of the frequency range of anomalous dispersion. The value f_m , i.e. the frequency at which ϵ'' has a maximum, also increases with the moisture content. Only the value k which is a measure of the total dispersion between $f = 0$ and $f = \infty$, decreases. The increase in ϵ_∞ with p can be explained by the mixed body theories, since the value of the dielectric constant increases with the portion by volume of the constituent that has the highest dielectric constant, in this case it is water having $\epsilon = 81$.

Fig. 3.2.5 shows the frequency dependence of the experimental values ϵ'_{exp} and ϵ''_{exp} as well as the values ϵ'_W and ϵ''_W of measurement 6, calculated by Wagner's theory, since the curves calculated by Yager comprise best the used frequency range for this measurement, whereas for the other measurements they comprise only smaller parts of the frequency range. In order to illustrate the effect of the constant b on the result, the data for the correct value of $b = 0.29$ (solid line) and for the arbitrarily increased value $b = 0.31$ (dashed line) were plotted. The measured points of the two quantities ϵ' and ϵ'' are well reproduced by the curves calculated with $b = 0.29$. Too high a value of b yields a steeper slope of the curves and thus also a frequency dispersion of σ which decreases with the moisture content, since σ is calculated by multiplying ϵ'' with $\omega \epsilon_0$.

This examination was also made with other samples of rock, but only for 2 values of humidity. A measurement conducted with a second dolomite sample yielded the same results as above. Also for new red sandstone used for studying the reproducibility [11], the constants b , f_m , ϵ_∞ and k assume similar values as for dolomite, as well as the samples described in [2] from the mine at Willroth, which consist of ore embedded in dead rock. All these different sorts of rock have approximately the same po-

rosity. The results obtained for a sample from the ore mine of Salzgitter (oolitic ore) cannot be explained by Wagner's theory. In Fig. 3.2.6 they are shown for two different values of water content.

In contrast to the other samples, the curves for ϵ'' show a minimum that cannot be explained by Wagner's theory. The dispersion cannot be represented by a relaxation function for which a distribution of relaxation times about a prevailing value of τ_0 is assumed. The shape of the curves, however, would rather suggest two different prevailing relaxation times. An evaluation in this sense has not been attempted so far.

On the whole it may be said that the frequency dispersion of conductivity and dielectric constant of minerals observed in rock samples can be well described by Wagner's dispersion theory. As this theory only contains four constants which all have a physical meaning, and as it is based on the Curie law saying that the reversible absorption current is proportional to the applied voltage and to the geometric capacitance, this agreement may be taken as a proof of the fact that the sample measurement yields correct values for ϵ' and ϵ'' and thus also for σ , and that the results of measurement are not affected by other effects.

3.3 Measurements with alternating current in solid rock

3.3.1 The 716-C General Radio Capacitance Bridge was also used for measuring the propagation resistance between two electrodes fixed to the rock, namely steel pins described in [2] which have also been used for the d-c measurements described in section 3.1. They have a diameter of $2a = 0.7$ cm and a length of $h = 5$ cm. The propagation resistance of such an electrode can be calculated easily (see e.g. [18]). We obtain

$$R = \frac{1}{2\pi h \sigma} \ln \frac{2h}{a} . \quad (33.1)$$

From a certain electrode spacing onward, the total resistance of

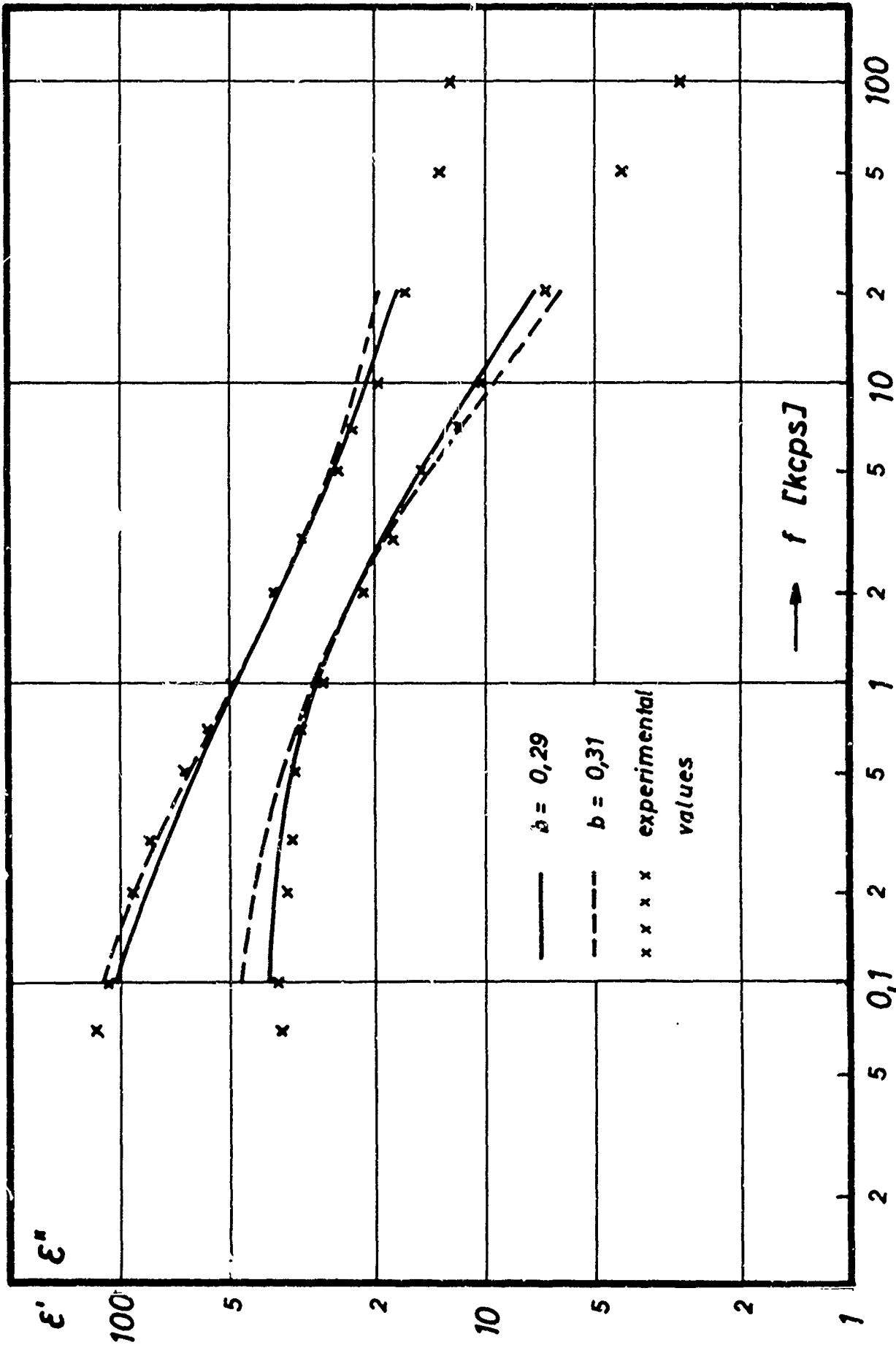


FIG. 325

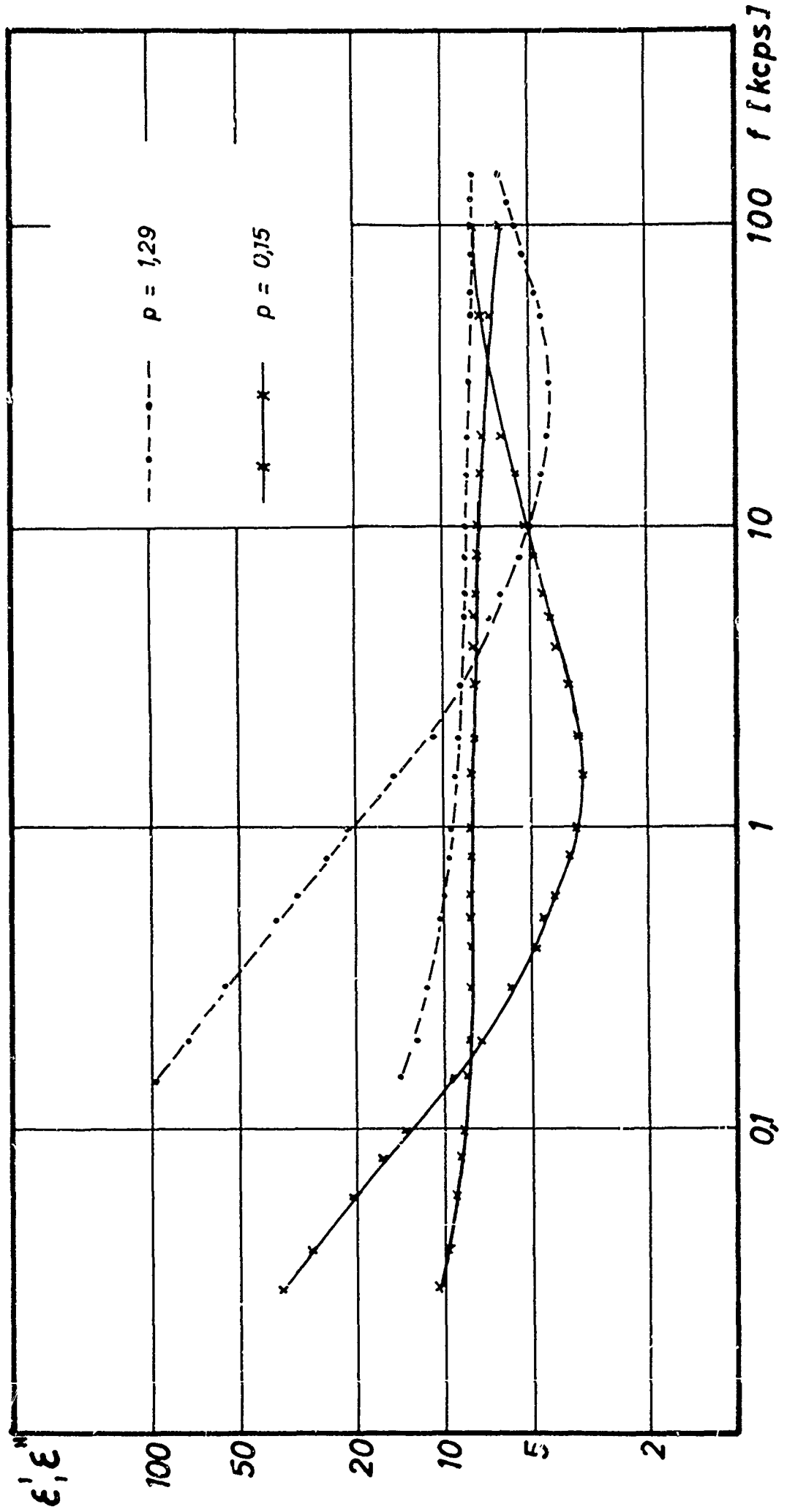


FIG. 3,26

the arrangement is practically independent of that distance. This is the case when the electrical flow pattern near one electrode does not change when the electrode spacing is varied. The total resistance then is twice that of one electrode

$$R = \frac{1}{\pi 4h} \ln \frac{2h}{a} . \quad (3.3.2)$$

The above expression is the same as that used in [13]. The constant factor which is contained therein and which causes a decrease in resistance, is due to the fact that for the used dipole arrangement the distance between the two dipole halves still has a certain effect on the resistance.

A Schering capacitance bridge, e.g. the 716-C General Radio Bridge can be used for determining the quantities C and R of an equivalent circuit diagram of a dissipative capacitor. As the capacitance between two electrodes of the above form is very low for rock with a small dielectric constant, parasitic capacitance of the feeder cables and bridge screening are usually higher than the capacitance between the electrodes. Their elimination by a substitution method, however, is difficult when measuring in solid rock, since the measuring bridge during the measurement is located opposite a wall having not a uniform potential, but a potential drop along it. This makes impossible to get an accurate measurement of the capacitance between the electrodes. The quantity of the resistance R of the equivalent circuit diagram, however, can be determined accurately, because it is not affected by the geometrical arrangement of the feeder cables in contrast to the total capacitance, i.e. the sum of the parasitic capacitance and the capacitance between the electrodes. This can also be shown by means of measurements, e.g. by conducting two measurements with the same geometrical arrangement, where one electrode first is located on the potential of the bridge screen, then it is used as a hot electrode. Whereas the value of capacitance

differs considerably in the two measurements, the value of the resistance R remains constant.

3.3.2 Results:

In contrast to the sample measurements (section 3.2), the results of conductivity measurements in solid rock do not yield a remarkable frequency dispersion. They are shown in Fig. 3.3.1. The values are calculated from

$$\sigma = \frac{1}{\pi R \cdot h} \cdot \ln \frac{2h}{a} . \quad (3.3.3)$$

Because of the limited resistance range of the capacitance bridge at low frequencies, σ could only be determined between 5 and 100 kc/sec. Fig. 3.3.1 shows five measurements made at electrode spacings of $d = 0.5, 1, 2, 3$ and 4 m. The dependence of conductivity on frequency is very small and the value of σ is of the same order of magnitude as the d-c value determined by a four-electrode arrangement. The small frequency dispersion and the resulting absolute value are in good agreement with the results of conductivity measurements in rock described in [13], which were conducted in drill holes. In the above report, R was not directly measured with a bridge because of the long connection wires, but the observed impedance was substituted by an equivalent circuit. From it, R was determined. This complicated method is superfluous in the method described in the present report, since it does not require long cables causing a considerable loss factor; for the present method bare wires were used, but the principle of measurement was equal to that of the above report.

The results, however, do not agree sufficiently with the σ values measured in samples, neither with respect to the absolute amount of σ , nor to the frequency dependence. The reason for the differences in the results of the two methods of measurement has not been explained satisfactorily. Above all it seems necessary to conduct measurements with humid samples

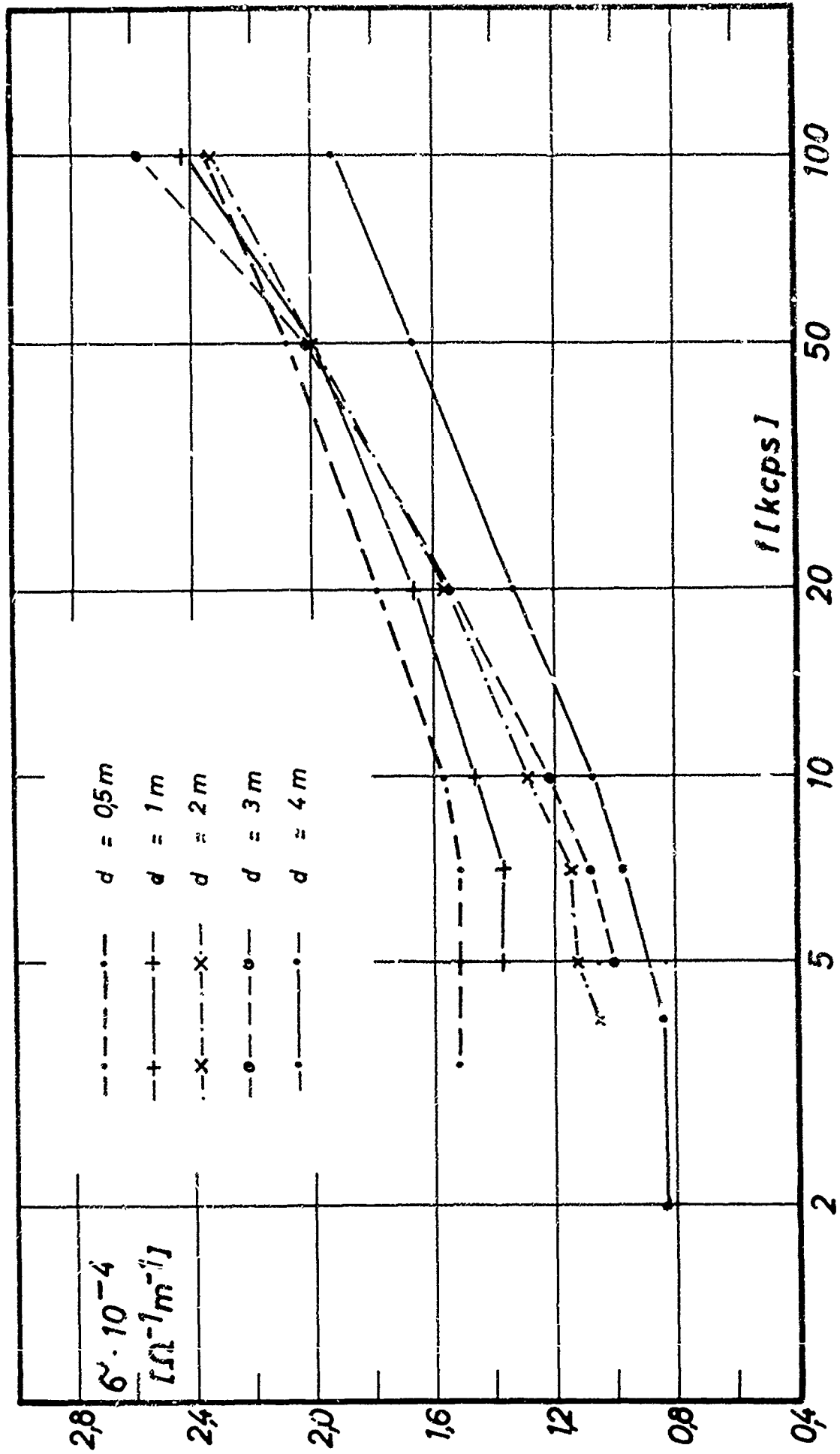


FIG. 331

and to extend the measurements in solid rock up to the frequency region of 30 cps - 200 kc/sec, by improving the measuring device, in order to conduct an accurate comparison of the results. This shall be done in continuation of the present studies. Furthermore, an attempt shall be made to apply the evaluation of measurements by Wagner's theory also to rock samples having their natural water content.

4. Theoretical part4.1 Model tests

The great interest in the propagation and excitation of electromagnetic waves of low frequencies as well as the technological and financial difficulties involved by VLF-wave studies favored the use of model tests. Such tests have already been conducted, e.g. in [14]. Some general considerations on the results of model tests in conducting material of this special type, which are intended to describe the propagation below ground, however, show that they are not of very great importance.

Discussions on such model tests have already been published in [15] and shall be repeated in a more critical form in the present paper. The wave equation for the dimensionless direction vector \vec{E}_0 yields the relations between the scale factor α , the electric parameters ϵ , μ , and σ of the simulating model and the model medium, as well as the frequency

$$\alpha = r/r_m = (\epsilon_m/\epsilon)^{1/2} \omega_m/\omega \quad (4,1a)$$

$$\sigma_m/\sigma = (\epsilon_m/\epsilon)^{1/2} \omega/\omega_m \quad (4,1b)$$

The index m indicates the model size.

On the whole, only one quantity, namely σ_m of the equations (4,1a) and (4,1b) can be chosen. It determines above all the maximum attainable model factor α , being itself determined by the maximum attainable model conductivity (in such a way that the medium is in a state in which tests below ground are still possible).

Assume that the most favorable model material representing a homogeneous full space has been found and a model factor α can be reached which makes possible measurements over a distance of up to 100 km in laboratory tests, there are still several difficulties. In this case, antennas whose dimensions are much larger than the used wave length would be required for studying the process of propagation. The model test would then yield results on a process which could never be materialized, as no antenna can be built whose length is

a multiple of the wave length. If the conditions were so favorable that the antenna dimensions are only fractions of the wave length also in the model test, the emission of such antennas would be proportional to their length and the excitation would decrease so rapidly that also in the model test only the near field could be studied. In situ such studies do not involve any additional technological and financial expenses. All what has been said above regards the homogeneous full space.

A simulation of the homogeneous full space, i.e., investigation of VLF propagation below ground and at a great distance from the earth's surface, in the optimum case would only represent a measure of estimating the underground homogeneity. Although this is of great interest, it does not justify the great expenses.

It would be much more important, however, to simulate the system air - earth, since the conditions at the earth - air interface which are of great practical importance would thus be made accessible to detailed studies. Here too, the model factor α has to be chosen in such a way that the conductivity of the model ground does not exceed the conductivity of water, acidified water or any other liquid exhibiting favorable properties. Otherwise, underground measurements would be impossible. The possibility of simulating the ground by metals and measurements in boreholes has already been mentioned in [15], at the same time, however, we have pointed out that the measurement can no longer be adapted to reality owing to secondary effects, e.g. skin effect. The use of a comparatively small maximum conductivity (of liquids) requires the choice of a low model factor α which means that only the near field can be studied if the dimensions of the model are to be kept in tolerate boundaries. The latter, however, is necessary as otherwise the model test would in no way be superior to field experiments.

When studying the near field where no ionospheric effects are to be expected and where the earth - air model is quite sufficient for simulating the field conditions, model tests are suitable. Model tests in conducting media thus are only adequate for studying underground antennas (or antennas under water) and are certainly very useful as long as the used model factors make possible the

simulation of the antenna dimensions themselves. Laboratory tests with antennas whose dimensions are approximately equal to the used wave length or even larger, might be of interest in the same way as investigations of the directional properties of antenna arrays with elements having distances of several wave lengths, but they cannot be applied in practice. Their results therefore have no practical importance at least not for studying VLF waves.

Summing up we may say that a model test under the above conditions can only yield useful results concerning the antenna properties and the near field. For reasons of better understanding let us explain the expressions near field and far field used in the present report. In order to decide whether a point of observation is situated in the near field or in the far field of an antenna, only the ratio of the wave length to the distance between the site of observation and antenna is decisive (in contrast to the definition of some authors, the antenna size is not important).

Near field $2\pi R \ll \lambda$

Far field $2\pi R \gg \lambda$

4,2 Dipole radiation in conducting media

The field of an electric or magnetic dipole embedded in a conducting uniform and unbounded medium is mathematically described in the same way as for a vacuum. The parameters characterizing the medium are to be replaced by the corresponding complex values in which the conductivity is taken into account. Under certain circumstances, with the conductivity being sufficiently high, the displacement current may be neglected and simpler expressions may be substituted for the individual parameters. Thus, for example, the complex propagation constant reads

$$\begin{aligned}
 i\beta^* &= (i\omega\mu(\sigma + i\omega\epsilon))^{1/2} \approx (i\omega\mu\sigma)^{1/2} = (\omega\mu\sigma/2)^{1/2}(1 + i) \\
 &= \beta(1 + i) = 2\pi/\lambda(1 + i) = 2\pi/\lambda i + 1/\delta \quad (4,2,1)
 \end{aligned}$$

where δ is the depth of penetration.

The wave resistance $\eta = \vec{E}/\vec{H}$, which in vacuo is $(\mu/\epsilon)^{1/2}$, also becomes complex

$$\eta = \sqrt{\frac{\mu}{\epsilon - i\frac{\sigma}{\omega}}} \approx \sqrt{\frac{i\omega\mu}{\sigma}} = \sqrt{\frac{\omega\mu}{2\sigma}} (1 + i) = S(1 + i) \quad (4,2,2)$$

Let the following relations be valid:

$$\beta = S\sigma \quad \lambda = 2(\pi/f\mu\sigma)^{1/2} \quad (4,2,3)$$

f ... frequency

μ ... permeability

σ ... conductivity

ϵ ... dielectric constant

λ ... wave length

δ ... depth of penetration

With allowance for these values, the following expressions are valid for an electric dipole in a homogeneous conducting medium:

$$E_{\vartheta} = (Il/4\pi) e^{-i\beta R}/R(i\omega\mu + \eta/R + 1/i\omega\epsilon R^2) \sin \vartheta \quad (4,2,4a)$$

$$H_{\varphi} = (Il/4\pi) e^{-i\beta R}/R(i\beta + 1/R) \sin \vartheta \quad (4,2,4b)$$

For the magnetic dipole we have:

$$H_{\vartheta} = (Kl/4\pi) e^{-i\beta R}/R(i\omega\epsilon + 1/\eta R + 1/i\omega R^2) \sin \vartheta \quad (4,2,5a)$$

$$E_{\varphi} = (Kl/4\pi) e^{-i\beta R}/R(i\beta + 1/R) \sin \vartheta \quad (4,2,5b)$$

I ... current intensity

R, ϑ, φ ... spatial polar coordinates

l ... antenna length

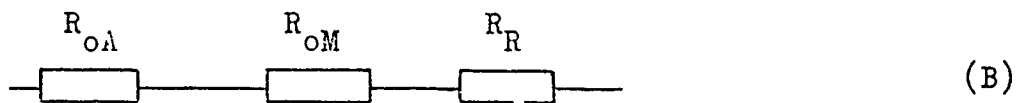
K ... magnetic flux.

Although the mathematical derivation of the expressions (4,2,4) and (4,2,5) do not differ from those for a dipole vacuum, their interpretation and further requirements resulting from them are

quite different. First of all it is very difficult to give an adequate definition of the radiation resistance. In air the antenna may be looked upon as a combination of the ohmic resistance and the radiation resistance



The radiation resistance is obtained by calculating the expression for the total energy passing through any spherical surface that envelopes the antenna, and dividing it by the square of the effective input current. In a conducting medium, the energy penetrating a spherical surface depends on the radius of the sphere; instead of (A) we now have to consider the antenna and its neighborhood:



R_{OM} is now the resistance of the surrounding medium. This means that the majority of the energy emitted by the antenna is consumed in the immediate neighborhood of the antenna by the generation of Joulean heat.

Furthermore it can be shown that the definition of the antenna gain used in vacuo has to be modified for a conducting medium. In the far field, the pattern of the antenna field lines depends on the choice of the center of the coordinate system. This does not mean that the structure of the field depends on the coordinate system. The structure itself is invariant. On the basis of the exponential attenuation, the field strength at a point of observation depends on the distance from an antenna point in a different manner than it does for a vacuum.

The three differences between dipole radiation in vacuo and in a conducting medium mentioned herein are represented in [17]. Unfortunately, the description of the first point, i.e. the calculation of the radial energy flux, shows considerable errors there. An exact derivation of the energy phenomena, a

comparison of the electric dipole with a magnetic dipole which is more comprehensive than the description in [5] as well as a discussion of the results regarding the dependence on the wave length of radiation shall be given in what follows.

From the expressions (4,2,4) we obtain the following expression for the radial energy flux:

$$\begin{aligned} \bar{P}^e &= 1/2 \operatorname{Re} E_\theta H_\phi^* \\ &= \frac{1}{2} \left(\frac{I l}{4\pi} \right)^2 \frac{e^{-2\beta R}}{R^2} \operatorname{Re} \left[i\omega\mu + \frac{\mu}{R} + \frac{1}{i\omega\epsilon R^2} \right] \left[i\beta + \frac{1}{R} \right]^* = (4,2,6a) \end{aligned}$$

$$= \frac{1}{2} \left(\frac{I l}{4\pi} \right)^2 \frac{e^{-2\beta R}}{R^2} \left(\omega\mu\beta + \frac{2\beta S}{R} + \frac{2S}{R^2} + \frac{1}{R^3} \right) \quad (4,2,6b)$$

i.e. an expression which depends on R in powers higher than R², which also contains the factor e^{-2βR}. In the case of vacuum it reads:

$$P_v^e = 1/2 \left(I l / 4\pi \right)^2 \omega\mu\beta / R^2 \sin^2 \theta. \quad (4,2,6c)$$

Integration over a spherical surface of radius R yields the total energy W^e propagating through this surface.

$$W^e = 8\pi/3 \left(I l / 4\pi \right)^2 \frac{e^{-2\beta R}}{2} \left(\omega\mu\beta + 2\beta S/R + 2S/R^2 + 1/5R^3 \right). \quad (4,2,6d)$$

In the case of vacuum, this expression is reduced to

$$W_v^e = 40\pi^2 (I l / \lambda)^2 \quad (4,2,6e)$$

In order to obtain the wave length dependence of (4,2,6d) this expression can be rewritten by means of (4,2,1) and (4,2,2):

$$\begin{aligned} W^e &= \left(\frac{I l}{3} \right)^2 e^{-4\pi/\lambda R} \left(4\pi^2/\lambda^3 + 2\pi/\lambda^2 \epsilon R + 1/\lambda \epsilon R^2 + 1/4 \pi \epsilon R^3 \right) \\ &= \left(I l / \lambda \right)^2 \frac{e^{-(4\pi/\lambda)R}}{3} \left(4\pi^2/\lambda + 2\pi/R + \lambda/R^2 + \lambda^2/4\pi R^3 \right). \quad (4,2,6f) \end{aligned}$$

where no term is independent of R . For $R \gg \lambda$ the dependence on R is reduced to the exponential factor, yielding

$$\begin{aligned} W_{R \gg \lambda}^e &= 4\pi^2 / 3 (Il/\lambda)^2 e^{-(4\pi/\lambda)R/\delta\lambda} = \\ &= W_{\text{air}}^e e^{-(4\pi/\lambda)R/\delta\lambda}. \end{aligned} \quad (4.2.6g)$$

Since the energy propagating through a spherical surface depends on the radius R , the radiation resistance cannot be defined in the usual way. It must be pointed out that in all expressions (4.2.6) and in the calculation that follows, passing to the limit $\delta \rightarrow 0$ is not allowed, since the condition for neglecting the displacement current is no longer fulfilled for very small δ . δ may increase infinitely in the same way as λ . Since, however, δ and λ are not independent of each other according to (4.2.3), we preferably write

$$\begin{aligned} \delta\lambda &= 2(\pi/f\mu\delta)^{1/2}\delta = 2(\pi\delta/f4\pi10^{-7})^{1/2} = (10^7\delta/f)^{1/2} \\ \lambda &= 1/(10^{-7}f\delta)^{1/2}. \end{aligned}$$

Thus, (4.2.6g) reads

$$W_{R \gg \lambda}^e = W_{\text{air}}^e \frac{e^{-\pi(10^{-7}f\delta)^{1/2}R}}{(10^7\delta/f)^{1/2}}. \quad (4.2.6h)$$

This expression holds for such pairs of f and δ values that yield $\delta/2\pi f \gg \epsilon$. The energy flux in the magnetic case is calculated from the expressions (4.2.5):

$$\begin{aligned} \bar{P}^m &= -1/2 \operatorname{Re}(E_{\mathcal{J}} H_{\mathcal{J}}^*) = \\ &= 1/2(Kl/4\pi)^2 e^{-2\beta R}/R^2 \operatorname{Re}(i\beta + 1/R)(i\omega\epsilon + 1/\eta R + 1/i\omega\mu R^2)^* \sin^2 \vartheta = \\ &= 1/2(Kl/4\pi)^2 e^{-2\beta R}/R^2 \delta(\beta + 1/R) \sin^2 \vartheta. \end{aligned} \quad (4.2.7a)$$

Here too, W depends on R , but not quite as strongly as in the

electric case. Integration over the spherical surface of radius R yields:

$$W^m = (Kl/\lambda)^2 \left[e^{-(4\pi/\lambda)R} \frac{\lambda}{6} (1 + \lambda/4\pi R) \right] \quad (4.2.7b)$$

In a vacuum, this expression is reduced to

$$W_v^m = \pi/3r_1 (Kl/\lambda)^2$$

Considering the limiting case $R \gg \lambda$, the situation is qualitatively the same as in the electric case, no term being independent of R; quantitatively, a change in favor of the magnetic dipole takes place as shall be shown later on.

$$W_{R \gg \lambda}^m = (Kl/\lambda)^2 \frac{\lambda}{6} e^{-(4\pi/\lambda)R} = W_{\text{air}}^m 60(10^7 \sigma/f)^{1/2} e^{-4\pi(10^{-7} \sigma f)^{1/2} R} \quad (4.2.7c)$$

In order to obtain the dependence of the energy flux of σ and f , we write the following expression for (4.2.6f) and (4.2.7b)

$$W^e = W_{\text{air}}^e e^{-4\pi(10^{-7} f \sigma)^{1/2} R} / 30(10^7 \sigma/f)^{1/2} \left[1 + (10^7/\sigma f)^{1/2} / 2\pi R + \right. \\ \left. + (10^7/\sigma f) / 4\pi^2 R^2 + \left[10^7/f \sigma (10^7/f \sigma)^{1/2} / 16\pi^3 R^3 \right] \right] \quad (4.2.8a)$$

$$W^m = W_{\text{air}}^m 60(10^7 \sigma/f)^{1/2} e^{-4\pi(10^{-7} f \sigma)^{1/2} R} (1 + (10^7/\sigma f)^{1/2} / 2\pi R) \quad (4.2.8b)$$

Let us assume that there exists a radius R_0 so that the energy radiation of both dipoles through a spherical surface having the radius R_0 is equal. Then we obtain a relation between the energies W_{air}^e and W_{air}^m and thus also for the moments Il and Kl of the two dipoles. If the parenthetical expressions of (4.2.8a) and (4.2.8b) are denoted with $h_1(R)$ and $h_2(R)$, respectively, this relation reads as follows:

$$\frac{W_{\text{air}}^e}{W_{\text{air}}^m} = 1800 10^7 \sigma/f h_2(R_0)/h_1(R_0). \quad (4.2.9)$$

Under this assumption we consider the relation W^e/W^m at a second radius R

$$W^e/W^m = W_{air}^e/W_{air}^m \left[f/1800 \cdot 10^7 \right] h_1(R)/h_2(R) \quad (4.3)$$

Substituting the expressions W_{air}^e/W_{air}^m (4.2.9) we obtain

$$W^e/W^m = h_1(R) h_2(R_0)/h_2(R) h_1(R_0) = \quad (4.3b)$$

$$= \frac{\left[1 + \sqrt{\frac{10^7}{\sigma f}} \frac{1}{2\pi R_0} \right] \left[1 + \sqrt{\frac{10^7}{\sigma f}} \frac{1}{2\pi R} + \frac{10^7}{\sigma f} \frac{1}{4\pi^2 R^2} + \frac{10^7}{\sigma f} \sqrt{\frac{10^7}{\sigma f}} \frac{1}{16\pi^3 R^3} \right]}{\left[1 + \sqrt{\frac{10^7}{\sigma f}} \frac{1}{2\pi R} \right] \left[1 + \sqrt{\frac{10^7}{\sigma f}} \frac{1}{2\pi R_0} + \frac{10^7}{\sigma f} \frac{1}{4\pi^2 R_0^2} + \frac{10^7}{\sigma f} \sqrt{\frac{10^7}{\sigma f}} \frac{1}{16\pi^3 R_0^3} \right]} \quad (4.3c)$$

For $R \gg \lambda$ the following expression may be written:

$$\frac{W^e}{W^m} \sim \frac{1 + \sqrt{\frac{10^7}{\sigma f}} \frac{1}{2\pi R_0}}{1 + \sqrt{\frac{10^7}{\sigma f}} \frac{1}{2\pi R_0} + \frac{10^7}{\sigma f} \frac{1}{4\pi^2 R_0^2} + \frac{10^7}{\sigma f} \sqrt{\frac{10^7}{\sigma f}} \frac{1}{16\pi^3 R_0^3}}$$

$$= \frac{h_2(R_0)}{h_1(R_0)} < 1 \quad (4.3d)$$

The expression (4.3c) increases as σ increases, its limiting value being

$$\lim_{\sigma \rightarrow \infty} \left(\frac{W_{air}^e}{W_{air}^m} \right) = 1.$$

This shows unambiguously that from a certain $\sigma = \sigma_{min}$ onward and at a given frequency, with $W_{air}^e/W_{air}^m > 1$, the magnetic dipole yields better results. The expression (4.2.9) is larger than unity from the minimum value of f and σ onward:

Table 4.1

f_{min} (cps)	σ_{min} (mhos/m)
10^3	10^{-2}
10^4	$8 \cdot 10^{-3}$
$5 \cdot 10^4$	$6 \cdot 10^{-3}$
10^5	$4 \cdot 10^{-3}$

where the radius R_0 has been put equal to 1 m. Fig. 4.1 and the corresponding table 4.2 show the dependence of W^e/W^m on the frequency in the range $f = 1 - 100$ kc/sec for three different conductivities $\sigma = 10^{-4}$, 10^{-2} and 1 (mhos/m). For the lowest curve, the ratio W_{air}^e/W_{air}^m is of the order of magnitude 10^{-3} , at $\sigma = 10^{-2}$ mhos/m it is 10 and at $\sigma = 1$ it is 10^5 . The top-most curve along which W^e/W^m lies between $5 \cdot 10^{-3}$ and $5 \cdot 10^{-1}$ clearly shows that even though the energy radiation of the electric dipole in air exceeds that of the magnetic dipole by the 10^5 -fold, in a conducting medium it is only a fraction of this value.

Table 4.2

f(cps) σ (mhos/m)	10^{-4}	10^{-2}	1
10^3	$0.79 \cdot 10^{-6}$	$7.8 \cdot 10^{-5}$	$5.9 \cdot 10^{-3}$
$4 \cdot 10^3$	$3.1 \cdot 10^{-6}$	$3.0 \cdot 10^{-4}$	$2.8 \cdot 10^{-2}$
$9 \cdot 10^3$	$7.1 \cdot 10^{-6}$	$6.9 \cdot 10^{-4}$	$5.8 \cdot 10^{-2}$
$16 \cdot 10^3$	$1.2 \cdot 10^{-5}$	$1.2 \cdot 10^{-3}$	$9.5 \cdot 10^{-2}$
$36 \cdot 10^3$	$2.8 \cdot 10^{-5}$	$2.7 \cdot 10^{-3}$	0.18
$64 \cdot 10^3$	$5.4 \cdot 10^{-5}$	$4.8 \cdot 10^{-3}$	0.28
$81 \cdot 10^3$	$6.3 \cdot 10^{-5}$	$5.9 \cdot 10^{-3}$	0.32
$100 \cdot 10^3$	$7.8 \cdot 10^{-5}$	$7.3 \cdot 10^{-3}$	0.30

From all these considerations we may conclude that the magnetic dipole in the VLF region at ϵ and σ values that are of practical importance, has the more favorable conditions for the generation and propagation of electromagnetic fields in a conducting medium.

A somewhat different approach which might give a better explanation of the physical processes, yields the same result by applying the theory of transmission lines. It is well known that the dipole field may be looked upon as being a combined derivative of a scalar potential and of a vector potential A . The divergence equation

$$\text{div } \vec{H} = 0$$

for the electric case yields

$$\vec{H} = \text{curl } \vec{A} \quad \vec{E} = -i\omega\mu \vec{A} - \text{grad } V$$

and $\text{div } \vec{H} = 0$

for the magnetic case $\text{div } \vec{E} = 0$

$$\vec{E} = \text{curl } \vec{\Psi} \quad \vec{H} = -i\omega\epsilon \vec{\Psi} - \text{grad } U$$

In both cases a special direction of the vector potential

$$\vec{A} = (A_r, 0, 0) \quad \vec{\Psi} = (\Psi_r, 0, 0).$$

Substitution in the Maxwell equations now shows that A and V as well as Ψ and U, respectively, are interrelated by the following equations [16].

Electric case:

$$\frac{\partial A}{\partial r} = -i\omega\epsilon V \tag{4.3.1}$$

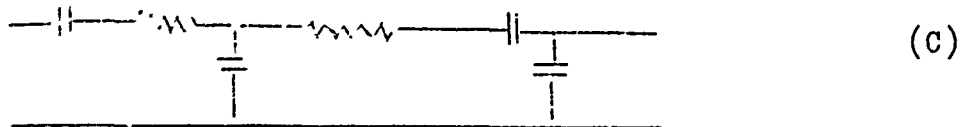
$$\frac{\partial V}{\partial r} = -\left[i\omega\mu + \frac{2}{i\omega\epsilon r^2}\right] A$$

Magnetic case:

$$\frac{\partial \Psi}{\partial r} = -i\omega\mu U \tag{4.3.2}$$

$$\frac{\partial U}{\partial r} = -\left[i\omega\epsilon + \frac{2}{i\omega\mu r^2}\right] \Psi.$$

In vacuo, A and V change with r like the current and voltage of a two-wire cable with a series inductance of $\mu\text{H/m}$, of a series capacitance of $\frac{\epsilon h^2}{2}$ F/m, and of a shunt capacitance of $\epsilon\text{F/m}$.



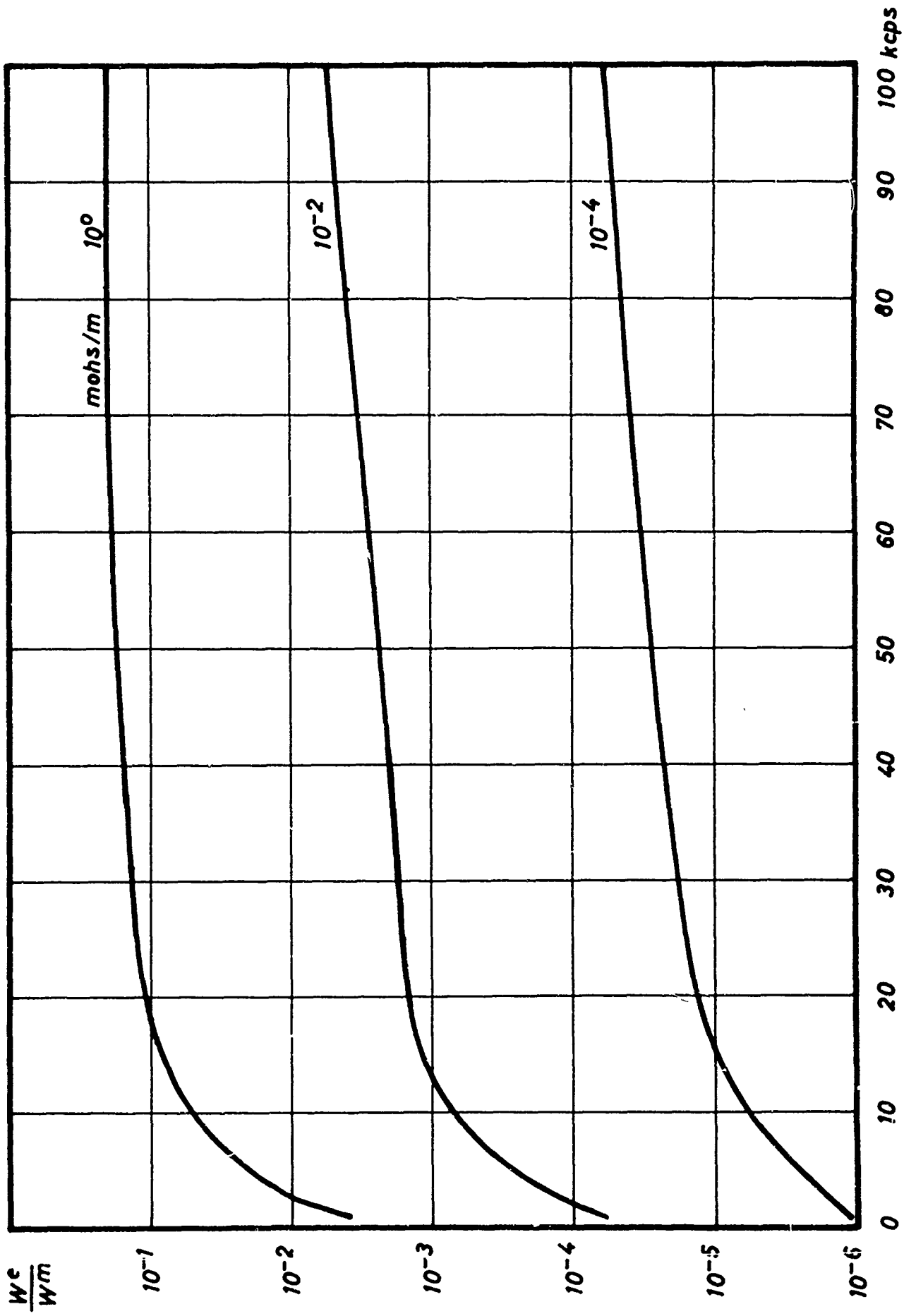


Fig. 4.1

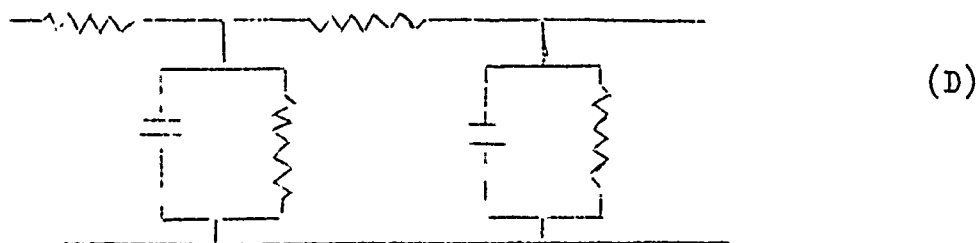
Number of ... Mohs/m

...

...

...

In the magnetic case, Ψ and U behave like current and voltage in a two-wire cable having a series inductance $\mu H/m$ and a shunt inductance of $\frac{\mu r^2}{2}$ H/m and a shunt capacitance $\epsilon F/m$.

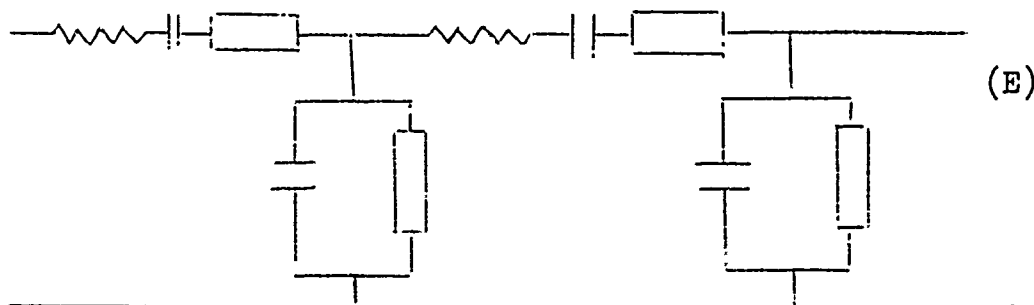


If $i\omega\epsilon^* = i\omega\epsilon + \sigma$ is substituted for $i\omega\epsilon$ in Eq. (4.3.1), then we have

$$\frac{\partial A}{\partial r} = -(i\omega\epsilon + \sigma)V$$

$$\frac{\partial V}{\partial r} = -\left[i\omega\mu + \frac{2\sigma}{(\sigma^2 + \omega^2\epsilon^2)r^2} + \frac{2\epsilon\omega^2}{i\omega(\sigma^2 + \omega^2\epsilon^2)r^2} \right] A \quad (4.3.3)$$

for the electric case. The equivalent-circuit diagram thus is as follows:



It contains an additional series resistance of $\frac{2\sigma}{(\omega^2\epsilon^2 + \sigma^2)r^2}$ $\frac{\Omega}{m}$, the series capacity $\frac{\epsilon r^2}{2}$ thus becomes

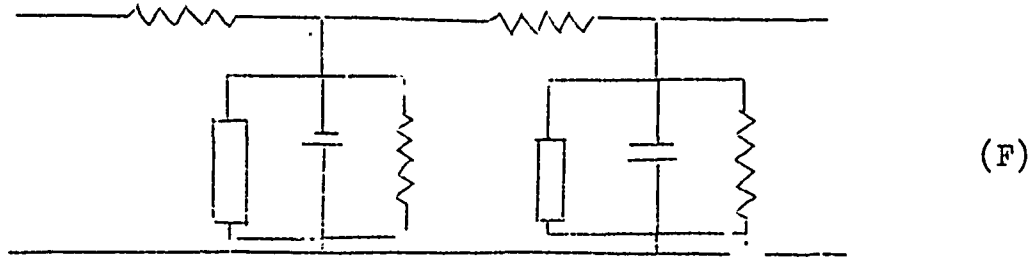
$$\frac{(\omega^2\epsilon^2 + \sigma^2)r^2}{2\epsilon\omega^2} \frac{F}{m},$$

furthermore, an additional shunt resistance $\frac{1}{\sigma} \frac{\Omega}{m}$ is present (in all cases, σ, μ, ϵ is to have the amount of the corresponding physical quantity for reasons of dimensioning, because A and U are only proportional to the current).

In the magnetic case, (4.3.2) is transformed into

$$\frac{\partial \Psi}{\partial r} = -i\omega\mu U \quad \frac{\partial U}{\partial r} = -\left[i\omega\epsilon + \frac{2}{i\omega\mu r^2}\right] \Psi \quad (4.3.4)$$

Equivalent circuit diagram:



The only difference is an additional ohmic loss conductivity σ in the shunt. The comparison of (E) and (F) shows that there exist the resistances $\frac{i\omega\mu r^2}{2}$ and $\frac{2\epsilon\omega^2}{i\omega r^2(\sigma^2 + \omega^2\epsilon^2)}$ without any losses, the former become infinite at infinity (as expected), and the latter disappear (at infinity); furthermore there exists an ohmic resistance $\frac{2\sigma}{r^2(\omega^2\epsilon^2 + \sigma^2)}$ in (E), which is responsible for the high energy loss of an electric dipole, and which disappears only at a large distance so that (E) and (F) there become identical. This is the physical reason for the above result, namely that the magnetic dipole is more suitable for a conducting medium.

REFERENCES

- [1] Second Technical Annual Summary Report: The propagation of VLF waves in solids, 61(052)-490, December 1962
- [2] Third Technical Annual Summary Report: The propagation of VLF waves in solid, 61(052)-490, December 1963
- [3] Scientific Report Nr. 8: Field strength meter for VLF waves (Bitterlich), 61(052)-490, April 1964
- [4] H.v. Suchtelen: Ferroxcibe Aerial Rods. Electronic Application Bulletin Vol. 13 No. 6.
- [5] Scientific Report Nr. 10: Magnetic dipole antennas for receivers (Bitterlich), 61(052)-490, September 1964
- [6] On the propagation of very long electromagnetic (VLF) waves in rock, Thesis by O. Gröbner, Innsbruck University
- [7] Scientific Report Nr. 11: VLF measurements in the mine of Bleiberg (Gröbner), 61(052)-490, October 1964
- [8] Scientific Report Nr. 9: Current distribution of hemispherical electrodes in a homogeneous semispace (Tinhofer), 61(052)-490
- [9] K.W. Wagner, 1913, Zur Theorie der unvollkommenen Dielectric, Annalen der Physik, Band 40, 817 - 855.
- [10] W.A. Yager, 1936, The distribution of relaxation times in typical dielectrics, Physics, v. 7, 434 - 450.
- [11] Scientific Report Nr. 12: Reproducibility of measurements of electric rock parameters on specimens (Wörz), 61(052)-490 November 1964.

- [12] Carson K.H. Tsao, Investigation of electrical characteristics of rock medium on Cape Cod. AFCRS - 64 - 1.
- [13] Carson K.H. Tsao, Investigations of electrical characteristics of rock medium in northern New York State. AFCRL - 64 - 99.
- [14] Modelling studies - subsurface propagation, Final Technical Report, 15 March 1962, 21 R - 10 Contract Nr. AF 30(602)2152.
- [15] Technical Note No. 1 : Modelling studies (Nessler), 1 July 1963, Contract Nr. 61(052)-490.
- [16] R.K. Moore, Effects of a surrounding conducting medium on antenna analysis, I.E.E. E. Transaction on antennas and propagation 1963, Nr. 3.
- [17] Advanced antenna theory, S.A. Schelkuloff, John Wiley and Sons, New York.
- [18] Krajew, Grundlagen der Geoelektrik, VEB Verlag Berlin 1957.

TABLE OF CONTENTS

	page
Preface and contents	I
1. Apparatus	1-1
1.1 Nuvistorized field strength meter E4 for the VLF region	1-1
1.2 Magnetic dipole antennas for receivers	1-7
1.3 Transmitting antenna SA IX at St. Gertraudi	1-12
1.4 Direction-finder antenna	1-14
2. Propagation measurements	2-1
Review	
2.1. Measurements at Bleiberg	2-2
2.2 Near field - far field	2-6
2.3 Measurement of the direction of the magnetic field strength	2-8
2.4 Propagation measurements at St. Gertraudi	2-11
3. Conductivity measurements	3-1
3.1 D-C measurements	3-1
3.2 Measurements with samples	3-13
3.3 Measurements with alternating current in solid rock	3-21
4. Theoretical part	
4.1 Model tests	4-1
4.2 Dipole radiation in conducting media	4-3

Summary

In the present report, different measuring devices, transmitting and receiving antennas (direction-finder antennas) for the VLF region are discussed. The measurements of propagation in inhomogeneous rock are mainly concentrated to the determination of the direction of the field vector at the point of reception. The problem near field - far field of a VLF dipole is also discussed. In order to determine the electrical parameters of rock, comprehensive measurements were conducted in solid rock and in rock samples, furthermore the frequency dependence of σ and ϵ was studied. The influence of the gallery configuration on the result of a σ -measurement was studied in detail. The theoretical part mainly deals with the problems of excitation of a VLF wave in rock, giving a detailed comparison between electrical and magnetic dipoles.

List of coworkers: Dr. W. Bitterlich, contractor
O. Gröbner
O. Wörz
G. Tinhofer
W. Gradl
T. Elster